**Functional thoracic imaging
diagnosis and treatment response in oncology**

Szyszko, Teresa

Awarding institution:
King's College London

FUNCTIONAL THORACIC IMAGING: DIAGNOSIS AND TREATMENT RESPONSE IN ONCOLOGY

Teresa Anna Szyszko

University of London

A thesis submitted for the degree of MD (Res)

2020

Abstract

The aim of the first part of the thesis is to assess if 18F Fluoro-L-Thymidine (FLT) PET-CT molecular imaging (as a marker of proliferation) can predict response to arginine deprivation treatment (ADIPEG20 combined with pemetrexed and cisplatin) earlier than anatomical imaging using CT (RECIST), in mesothelioma (MPM) and non-small cell lung cancer (NSCLC). FLT PET-CT imaging took place in a longitudinal study with scans at baseline (PET1), approximately 24 hours after the first dose ADIPEG20 on day 2 of cycle 1 (PET2); at the end of cycle 1 of ADIPEMCIS (PET3) on day 16; and at the end of treatment (PET4). The baseline and end of treatment scans coincided with CT imaging, however, the interim scans were at different time points in n=10 MPM and n=8 NSCLC. Using end of treatment CT as the gold standard, the response to treatment was greater on PET4 than CT (mean decrease of 36.5% in SUVmax compared to 21.9% decrease in RECIST length). Also, FLT SUVmax treatment response at PET2 predicted end of treatment response on CT results in nearly 2/3 cases, although on ANOVA analysis there is no statistically significant evidence that a decrease in proliferation (SUVmax) precedes a decrease is size (RECIST length).

The aim of the second part of the thesis is to assess tumour heterogeneity changes in arginine deprivation treatment response in MPM using 18F Fluoro-2-deoxy-D Glucose (FDG) PET data from the ADAM trial (scans at baseline and 4 weeks post treatment) to see if texture features of FDG PET predict response better than RECIST. First-order and high-order primary tumour texture features were measured in n=20 patients. PET parameters, overall survival (OS), progression free survival (PFS) and RECIST-based treatment response (CT at 2 months) were tested by Cox and logistic regression analyses. From baseline to 4 weeks post therapy, there was decrease in skewness (mean 0.15 units, p=0.002) and kurtosis (median 0.2 units, p=0.03). None of the parameters at baseline or post therapy were associated with progression on RECIST. In terms of PFS, increase in uniformity was associated with progression (hazard ratio (HR) 2.3, p=0.02); increase in standard deviation (SD) was associated with decreased risk of progression (HR 0.56, p=0.03); and increase in SUVpeak was associated with a decreased risk of progression (HR 0.51, p=0.03). Texture features become more homogeneous after therapy, but this does not translate to improved survival. TLG at baseline was independently prognostic for OS (p=0.006); with additional asoociations with baseline SUVmean (p=0.03), SUVpeak (p=0.04), metabolic tumour volume (MTV) (p=0.01). Texture features are good at predicting the nature of the tumour.

Table of Contents

List of Figures

List of Tables

Acknowledgements

Abbreviations

Abbreviation	Definition
ADAM	ADI-PEG 20 in Patients with Malignant Pleural Mesothelioma
ADI	Arginine deiminase
ADI-PEG 20	Pegylatedargininedeiminase (ADI)
ADIPEMCIS	Arginine deiminase, pemetrexed and cisplatin
AI	Artificial intelligence
ANC	Absolute neutrophil count
ARSAC	Administration of Radioactive Substance Advisory Committee
ASL	Argininosuccinate lyase
ASS1	Argininosuccinate synthetase (also known as ASS)
Barts	St. Bartholomew's Hospital
BSC	Best supportive care
CR	Complete response
CT	Computed tomography
ECOG	Eastern Cooperative Oncology Group
ED	Effective dose
EOT	End-of-treatment
FDG	Fluorodeoxyglucose
FLT	Fluorothymidine
GCP	Good clinical practice
Hb	Haemoglobin
MHRA	Medicines and Healthcare products Regulatory Agency
ML	Machine learning
MPM	Malignant pleural mesothelioma
MRI	Magnetic Resonance Imaging
NSCLC	Non-small cell lung carcinoma
OS	Overall survival
PD	Progressive disease
PET	Positron emission tomography

Abbreviation	Definition (continued)
PFS	Progression free survival
PI	Principle Investigator
PR	Partial response
PS	Performance status
REC	Research Ethics Committee
RECIST	Response Evaluation Criteria in Solid Tumours
ROI	Region of Interest
RR	Response rate
SBRT	Stereotactic body radiation therapy
SD	Stable disease
SOP	Standard operating procedures
SUL	Standardised uptake value corrected for lean body mass
SUV	Standardised uptake value
TRAP	Tumours Requiring Arginine to assess first line ADI-PEG 20 combined with Pemetrexed and Cisplatin
TK	Tyrosine kinase
TS	Thymidylate synthase
TTP	Time to progression
TYMS	Thymidylate synthase (also known as TS)
VOI	Volume of Interest

Publications

Papers

Kamat S, **Szyszko TA,** Subesinghe M, Fischer BM, Chicklore S, Warbey V, Cook JR. The role of new PET tracers for lung cancer. Minerva Pneumologica 2019 March;58(1):16-26

Khadeir R, **Szyszko T**, Szlosarek PW. Optimizing arginine deprivation for hard-to-treat cancers. Oncotarget. 2017 Oct 27;8(57):96468-96469.

Beddowes E, Spicer J, Chan PY, Khadeir R, Corbacho JG, Repana D, Steele JP, Schmid P, **Szyszko T**, Cook G, Diaz M, Feng X, Johnston A, Thomson J, Sheaff M, Wu BW, Bomalaski J, Pacey S, Szlosarek PW. Phase 1 Dose-Escalation Study of Pegylated Arginine Deiminase, Cisplatin, and Pemetrexed in Patients With Argininosuccinate Synthetase 1-Deficient Thoracic Cancers. J Clin Oncol. 2017 Jun 1;35(16):1778-1785

Szlosarek PW, Steele JP, Nolan L, Gilligan D, Taylor P, Spicer J, Lind M, Mitra S, Shamash J, Phillips MM, Luong P, Payne S, Hillman P, Ellis S, **Szyszko T**, Dancey G, Butcher L, Beck S, Avril NE, Thomson J, Johnston A, Tomsa M, Lawrence C, Schmid P, Crook T, Wu BW, Bomalaski JS, Lemoine N, Sheaff MT, Rudd RM, Fennell D, Hackshaw A. Arginine Deprivation With Pegylated Arginine Deiminase in Patients With Argininosuccinate Synthetase 1-Deficient Malignant Pleural Mesothelioma: A Randomized Clinical Trial. JAMA Oncol. 2017 Jan 1;3(1):58-66.

Szyszko TA, Yip C, Szlosarek P, Goh V, Cook GJ. The role of new PET tracers for lung cancer. Lung Cancer. 2016 Apr;94:7-14.

Szlosarek PW, Luong P, Phillips MM, Baccarini M, Stephen E, **Szyszko T**, Sheaff MT, Avril N. Metabolic response to pegylated arginine deiminase in mesothelioma with promoter methylation of argininosuccinate synthetase. J Clin Oncol. 2013 Mar 1;31(7):e111-3.

Published abstracts

Phillips M, **Szyszko T**, Hall P, Rashid S, Khadeir R, Lim L et al. Expansion study of ADIPEG20 PEM CIS in patients with ASS1 deficient NSCLC (TRAP). AACR (American Assoc Cancer Research) IASLC International Joint Conference: Lung Cancer) San Diego, Jan 2018. Poster B33

Szyszko TA, Cook GJR, Bomalaski J, Szlosarek PW. F-18 fluoro-3-deoxy-3-L-fluorothymidine (FLT) PET/CT as an early biomarker of treatment response in Pegylated Arginine Deiminase, Cisplatin, and Pemetrexed in Patients With Argininosuccinate Synthetase 1-Deficient Thoracic (mesothelioma and non-small cell lung) Cancers. BNMS 2017

Phillips M, **Szyszko T**, Hall P, Cook GJR, Khadeir R, Steele J, Spicer JR, Szlosarek PW Expansion study of ADI-PEG 20, pemetrexed and cisplatin in patients with ASS1-deficient malignant pleural mesothelioma (TRAP). ASCO 2017

Sharma N, Farrugia A, Veres L; Preston R, **Szyszko TA**. Established and novel imaging assessment for malignant pleural mesothelioma: from diagnosis to response evaluation in the era of molecular imaging . RSNA 2016

Szyszko TA, Bomalaski JS, Goh V, Barrington SF, Cook GJR, Szlosarek PW; TRAP substudy: assessment of 18-FLT PET/CT to examine tumour proliferation in patients with ASS1-deficient thoracic cancers treated with arginine deiminase (ADI)-PEG20, pemetrexed and cisplatin. EANM 2016

Szlosarek PW, **Szyszko T**, Pacey S, Spicer J, Phillips M, Steele J, et al 18-FLT-PET/CT as an imaging biomarker in patients with ASS1-deficient thoracic cancers treated with ADI-PEG20, pemetrexed and cisplatin. ASCO 2016

Sit C, Green F, Gnanasegaran G , **Szyszko T**. Pictorial atlas of 18F-FDG PET/CT staging in lung cancer. BNMS 2015 P61

Chapter 1 Introduction

1.1 Lung cancer

Lung cancer is a leading cause of cancer-related death. The five-year overall survival for all stages is 15% (1) as most patients present at an advanced stage. However, those with early stage disease can be treated with a potentially curative intent. The majority of patients (80%) are clinically symptomatic and present with cough, haemoptysis, dyspnoea, chest pain or non-resolving pneumonia; some present with features of metastatic disease such as skeletal pain or neurological symptoms, whereas less than 10% are asymptomatic (2).

Lung cancer is classified as either non-small cell lung cancer (NSCLC, accounting for 87%) or small cell lung cancer (SCLC) (3). SCLCs are usually classified as limited disease (tumour and nodal disease, confined to one hemithorax) or extensive disease (including extra-thoracic disease and distant metastases) and the primary tumour may not be visualised as a discrete entity (4). Staging of NSCLC is detailed below.

1.1.1 Staging of NSCLC

Staging of NSCLC is via the AJCC 8th edition (5). T1 tumours are less than 3cm in size. T1a are ≤ 1cm, T1b are >1 cm but ≤ 2 cm, and T1c are > 2cm but ≤ 3cm. T2 tumours are < 5cm. T2a are > 3cm but ≤ 4cm. T2b are > 4cm but ≤ 5cm. T3 are > 5cm but ≤ 7cm. T4 tumours are >7cm or invasive.

The presence of mediastinal lymphadenopathy is important in deciding on surgical options. Hilar nodes are N1. Ipsilateral mediastinal or subcarinal nodes are N2. Contralateral mediastinal, scalene or supraclavicular nodes are N3 and inoperable.

Metastatic disease is classified as M1a for intrathoracic metastases and includes pleural effusion. M1b disease is single-site extra-thoracic disease and M1c relates to multiple sites of extra-thoracic disease most commonly to brain, bone, adrenals and liver.

1.1.2 Imaging of NSCLC

Initial investigation of lung cancer is often with a chest X-ray (CXR), however, although this is useful in providing preliminary confirmation of a tumour, it is inadequate for staging.

Computed tomography (CT) scan of the chest is the main imaging modality in staging lung cancer. Primary lesions demonstrate a wide range of appearances. They may be central or peripheral, smooth or spiculated, solid or cavitating, discrete or invasive. Density is variable. Endobronchial tumour involvement and its distance from the carina are important in deciding a surgical approach. Extent of invasion of the chest wall also affects surgical reconstructive procedures.

The sensitivity of CT for chest wall invasion varies from 38 to 87% and specificity from 40 to 90% (6). Invasion of the pleura is stage T3, however invasion of the great vessels, oesophagus, trachea or vertebral body is stage T4 and makes the tumour inoperable. Useful CT findings include obliteration of the fat plane between the tumour and mediastinum. The diagnostic accuracy for predicting mediastinal invasion on CT is 56 to 89%.

The size of nodes is used to distinguish between benign and malignant nodal disease on CT and commonly a short axis diameter of more than 1cm is considered to be malignant. CT cannot reliably characterise enlarged inflammatory nodes or malignant nodes smaller than 1cm. The sensitivity of CT in evaluating mediastinal nodal disease is 60 to 83% and the specificity is 77 to 82% (7)(8).

Intrathoracic metastases are detected on CT with no additional imaging being required to detect pleural and pericardial effusions or lung nodules. Adrenal metastases can be differentiated from adenomas if the adrenal nodule has a Hounsfield Unit < 10.

Magnetic Resonance Imaging (MRI) has a limited role in staging lung cancer but can be used to determine T stage and shows a wide range of sensitivity (63 to 90%) and specificity (84 to 86%) (9) in determining chest wall invasion. The diagnostic accuracy for predicting mediastinal invasion varies from 50 to 93% on MRI. It is, however, useful in characterising metastases, particularly indeterminate adrenal lesions and superior to CT in the evaluation of brain metastases (10) including detecting brain lesions in asymptomatic patients. It is also useful to diagnose involvement of the brachial plexus or spinal canal.

Positron Emission Tomography (PET) combined with low-dose CT for attenuation correction and anatomical localisation is a molecular imaging technique (PET-CT). Use of PET-CT in thoracic malignancy is discussed in a dedicated section (see section 1.5).

1.2 Mesothelioma

Malignant pleural mesothelioma (MPM) is an uncommon malignancy which arises from the pleura or very occasionally, pericardium or peritoneum. It can invade both visceral and parietal pleura and often extends to adjacent structures. It is associated with prior asbestos exposure (11). Patients usually present with cough, dyspnoea, chest pain, cough, and weight loss.

The prognosis is poor, with a median survival time of 12 months after diagnosis (12). Reduced survival time is associated with intrathoracic lymph node metastases, distant metastatic disease, and extensive pleural involvement (13). MPM has three major subtypes: epithelial is the most common subtype (accounting for 60% MPM); sarcomatoid is the most aggressive (accounting for 10% MPM); biphasic tumours show elements of both epithelial and sarcomatoid subtypes.

1.2.1 Staging of MPM

Staging of MPM is using the AJCC 8th edition (14). T1 tumours are limited to the ipsilateral parietal pleura (including mediastinal and diaphragmatic pleura) with or without involvement of visceral pleura. Survival analysis of the different T categories showed no significant difference in categories T1a and T1b. This has resulted in a collapse of categories T1a and T1b (from the 7th edition) into one category T1 (although tumour thickness is significantly associated with overall survival). T2-4 tumour staging is unchanged from the 7th edition. T2 tumours involve each of the ipsilateral pleural surfaces (parietal, mediastinal, diaphragmatic, and visceral pleura) with at least either involvement of the diaphragmatic muscle or extension into lung parenchyma. T3 tumours are locally advanced but potentially resectable. There is at least involvement of the endothoracic fascia, extension into the mediastinal fat, extension into the soft tissue of the chest wall or non-transmural involvement of the pericardium. With locally advanced tumours, it is important to distinguish between T3 (potentially resectable) and T4 (technically unresectable) disease. T4 tumours have extension to contralateral pleura or peritoneum.

There has been a major revision in nodal staging with the removal of category N3. Both intrapleural and extrapleural (N1 and N2 in the seventh edition) are now combined into a single category N1. Lymph nodes that were previously categorized as N3 are now considered N2. These

include contralateral internal mammary as well as ipsilateral or contralateral supraclavicular lymph nodes and contralateral mediastinal nodes.

M1 disease is any distant metastasis (and no metastases is M0).

1.2.2 Imaging of MPM

CT is the primary imaging modality used for evaluation of MPM. Key CT findings that suggest the presence of MPM include pleural effusion, nodular pleural thickening and interlobar fissure thickening. Growth typically leads to tumoural encasement of the lung with a rind like appearance. Calcified pleural plaques are found at CT in approximately 20% of patients and may become engulfed by the primary tumour. There may be contraction of the affected hemithorax with associated ipsilateral mediastinal shift and elevation of the ipsilateral hemidiaphragm.

The presence of a soft-tissue mass that surrounds more than 50% of the circumference of a vascular structure is strong evidence of invasion. Chest wall involvement may manifest as obliteration of extrapleural fat planes, invasion of intercostal muscles, displacement of ribs, or bone destruction, although, irregularity of the interface between the chest wall and the tumour is not a reliable predictor of chest wall invasion. MPM can extend into the chest wall via needle biopsy and chest tube tracks or surgical scars.

Transdiaphragmatic extension of MPM is suggested by a soft-tissue mass that encases the hemidiaphragm, whereas if there is a clear fat plane between the diaphragm and adjacent abdominal organs and a smooth diaphragmatic contour, this indicates that the tumour is limited to the thorax. Pulmonary metastases can be nodules or masses and rarely diffuse military nodules may be identified (15).

MRI imaging can provide additional staging information in patients with potentially resectable disease. MPM is typically iso- or slightly hyperintense on T1-weighted images and moderately hyperintense on T2-weighted images. It enhances with gadolinium contrast. The superior contrast resolution of MRI imaging can allow improved detection of tumour extension, especially to the chest wall and diaphragm, hence better prediction of overall respectability (15). It is superior to CT in detecting invasion of the diaphragm and invasion of endothoracic fascia or a

single chest wall focus and in most useful in patients with an allergy to iodine contrast (16). FDG PET-CT can be used in the diagnosis and staging of MPM (see section 1.5).

1.3 Arginine auxotrophy in cancer cells, arginosuccinate synthetase (ASS1) and clinical use in cancer therapy

Arginine is a non-essential amino acid which is not required for the growth of most human cells, however it is critical for the growth of human cancers (17). Arginine is involved in multiple diverse aspects of tumour metabolism, including protein synthesis, as well as synthesis of nitric oxide, polyamines, nucleotides, proline and glutamate (Figure 1).

A recognised rate limiting step in arginine synthesis is down regulation of the enzyme arginosuccinate synthetase (ASS1) (part of the urea cycle), which catalyzes the conversion of citrulline and aspartic acid into argininosuccinate, which is then converted into arginine and fumaric acid by argininosuccinate lyase (ASL). This results in dependence on extracellular arginine, due to the inability to synthesise arginine (auxotropy) (17).

Normal cells derived from liver, kidney and testes could grow in medium depleted of arginine but supplemented with citrulline, while tumour cells from these organs could not (18). This implies that certain tumour cells could not re-synthesize arginine from citrulline. It was hypothesised that cells auxotrophic for arginine might lack ASS1 or ASL and subsequently shown that certain cancer cell lines and human cancer tissue specimens lack significant expression of ASS1 (19)(20)(21).

Some tumour cells are auxotrophic for arginine. ASS1 deficiency has been identified across the spectrum of haematological, epithelial and mesenchymal tumours, however regulation and expression of the enzyme displays significant variability and is tissue-specific. ASS1 loss is due partly to epigenetic silencing of the ASS1 promoter. Methylation-dependent silencing of the ASS1 promoter has been identified as a mechanism of gene repression in a subset of ASS1-deficient arginine auxotrophic solid and haematological tumours (22)(23)(24)

Methylation-dependent silencing of the ASS1 promoter reported in mesothelioma and bladder cancer cell lines confers exquisite sensitivity to the arginine-lowering agents, arginine deiminase or arginase. In pancreatic malignancy, there was also no increase in ASS1 (25). In contrast, ASS1 is induced rapidly in tumour cell lines without ASS1 promoter methylation limiting the

applicability of arginine deprivation under these circumstances, particularly as a monotherapy (26).

Argininosuccinate lyase (ASL), which is downstream of ASS1 and converts argininosuccinate into arginine and fumarate, has a secondary role in modulating tumoural arginine auxotrophy and sensitivity to arginine depletors in cancers including glioblastoma multiforme (27). Moreover, while the significance for ASS1 loss in cancer is presently unclear, several groups have revealed an association with worse clinical outcome and shorter metastasis-free survival in ovarian carcinoma, osteosarcoma, lymphoma, bladder cancer and myxofibrosarcoma (23)(28)(24)(29)(30).

There is emerging evidence of resistance to arginine deprivation in cancer. Several mechanisms may reduce the efficacy of arginine depleting enzymes for cancer therapy, including ASS1 upregulation; autophagy; stromal-tumour cell metabolic co-operation; and anti-drug antibodies (for example to ADI-PEG 20). Approaches to overcoming resistance include combining arginine depletors with chemotherapy, human (non-antigenic) arginases, and autophagy modulators such as chloroquine (26).

Arginine is a substrate for a diverse array of metabolic and inflammatory pathways in health and disease. It may be sourced via the cationic amino acid transporter, ASS1, or autophagy. Reprogramming of the arginine metabolome via inactivation or upregulation of ASS1 results in differential effects on tumourigenesis. T cells also need arginine for proliferation, T cell receptor (TCR) expression, and development of memory. While arginine deprivation has been shown to impede proliferation and cell cycle progression of activated T cells, in vitro this effect can be reversed by addition of citrulline (31).

Figure 1. Arginine utilisation in cancer (from Delage et al (24))
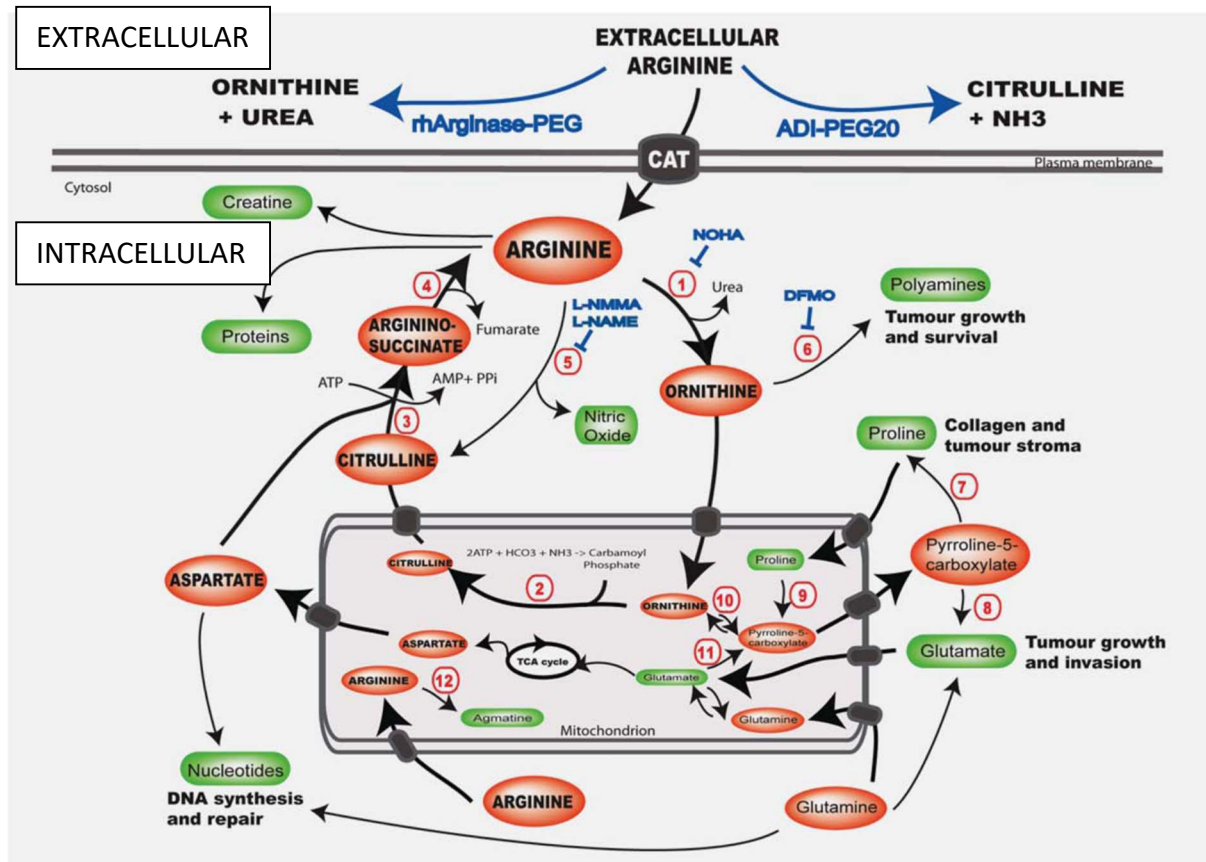
Key enzymes:

1 arginase;

2 ornithine transcarbamylase(OTC);

3 argininosuccinate synthetase (ASS1);

4 argininosuccinate lyase;

5 nitric oxide synthase;

6 ornithine decarboxylase;

7 pyrroline-5-carboxylate reductase;

8 pyrroline-5-carboxylate dehydrogenase;

9 proline oxidase (dehydrogenase);

10 ornithine aminotransferase;

11 pyrroline-5-carboxylate synthase;

12 arginine decarboxylase

1.4 ADI-PEG 20 and clinical cancer therapy

ADI-PEG 20, or Pegargiminase (PEG-arginine deiminase; Polaris Group) is a bacterial enzyme that degrades the amino acid, arginine. The active ingredient is arginine deiminase (ADI), which is formulated with polyethylene glycol (PEG) of 20,000 molecular weight (PEG 20). Investigators reported that certain tumour cell lines could not be maintained in medium contaminated with Mycoplasma species and that the killing of tumour cells under these conditions was associated with arginine depletion (32)(33). Further studies have shown that the depletion of arginine by Mycoplasma was due to the activity of the enzyme arginine deiminase (ADI), which is not present in mammalian cells (34).

As a result of these observations regarding the potential anti-cancer activity of arginine depletion, interest was focused on the development of ADI as a drug. The enzyme was cloned from Mycoplasma hominis, expressed in E. coli and subsequently conjugated to polyethylene glycol (PEG) (35)(36) as the ADI alone can cause severe allergy whereas conjugation with PEG makes this enzyme less antigenic. It was determined that synthesis of pegylated arginine deiminase (ADI-PEG) with PEG of 20,000 molecular weight (mw) via a succinimidyl succinate linker (ADI-PEG 20) provided the optimal combination of enhanced half-life and diminished immunogenicity, as well as ease and yield of manufacture. Hence, ADI-PEG 20 is an arginine lowering drug used in ASS1-negative tumours which has been used in phase I and II trials.

Several monotherapy clinical cancer studies of ADI-PEG 20 revealed safety and promising early activity despite the antigenic properties of a mycoplasma-derived enzyme , including patients with hepatocellular carcinoma (HCC) and melanoma, which showed low toxicity and evidence of efficacy (37) (38). However, a recent phase 3 study of ADI-PEG 20 versus placebo in patients with post-sorafenib relapse did not demonstrate an overall survival benefit in second line setting for HCC.

Post-hoc analyses revealed that ASS1 was upregulated by sorafenib and may have influenced patient outcome (39). In contrast, a modest improvement in progression-free survival in a randomized phase 2 study in patients with ASS1-deficient mesothelioma versus best supportive care alone was reported in the ADAM (ADI-PEG 20 in Patients With Malignant Pleural

Mesothelioma, NCT01279967) trial highlighting a need for patient selection in future studies (40). ASS1 was prognostic with ASS1 deficient disease conferring a worse survival compared to ASS1 proficient disease. Other studies looking at ADI-PEG 20 plus nab-paclitaxel and gemcitabine in patients with advanced pancreatic adenocarcinoma showed therapy was well tolerated (41).

Preliminary results from a phase 1 dose-escalation study of pegylated arginine deiminase, cisplatin, and pemetrexed in patients with argininosuccinate synthetase 1–deficient thoracic cancers (TRAP, NCT02029690) showed target engagement with depletion of arginine was maintained throughout treatment with no dose-limiting toxicities (42) and 100% disease control (78% partial response) in 9 patients. To minimise resistance to ADI PEG 20, this was used in combination with cisplatin and pemetrexed. Cisplatin is a platinum based chemotherapy and pemetrexed is an anti-folate drug which targets folate dependent enzymes, such as thymidylate synthase (TS).

Early phase clinical studies of several non-antigenic pegylated arginases are underway and further testing will reveal how the differential catalysis of arginine into ornithine and urea will impact tumourigenesis (26).

1.5 18F Fluoro-2-deoxy-D Glucose (FDG) PET-CT imaging in thoracic malignancy

FDG positron emission tomography with computed tomography (FDG PET-CT) is regarded as standard of care in the management of NSCLC and SPN. The F18 molecule is a positron-emitter gives rise to high energy photons with 511 keV, from produce the image. The FDG molecule is a glucose analogue which enters cells and remains trapped within the cell. It competes for GLUT receptors with glucose in blood and hence the patient needs to starve for 4-6 hours to maximise FDG uptake. The low dose CT is primarily for attenuation correction of the F18 photons, however, is also useful for anatomical localisation (43).

1.5.1 PET-CT scanner and imaging principles

PET-CT is a scanning technique which incorporates PET (positron emission tomography), where a radioactive molecule (which gives the "image") is labelled with a biological molecule (which determines the distribution) and low dose CT (for attenuation correction of the PET image and anatomical localisation).

Bombarding target material with protons that have been accelerated in a cyclotron produces positron-emitting radionuclides. PET is based on the detection of gamma (γ) photons released from such radionuclides (for example fluorine-18, carbon-11, and oxygen-15). The emitted positrons undergo annihilation with electrons (Figure 2) (44). The photons thus released have energies of 511 keV (0.511 MeV) and are detected by coincidence imaging as they strike scintillation crystals made of bismuth germinate (BGO), lutetium oxyorthosilicate (LSO), or gadolinium silicate (GSO). The value 511 keV represents the energy equivalent of the mass of an electron according to the law of conservation of energy.

Figure 2. Annihilation reaction

Positrons (β+) released from the nucleus annihilate with electrons (β-), releasing two coincidence 511-keV photons (γ), which are detected by scintillation crystals (blue rectangles).

N = neutron,
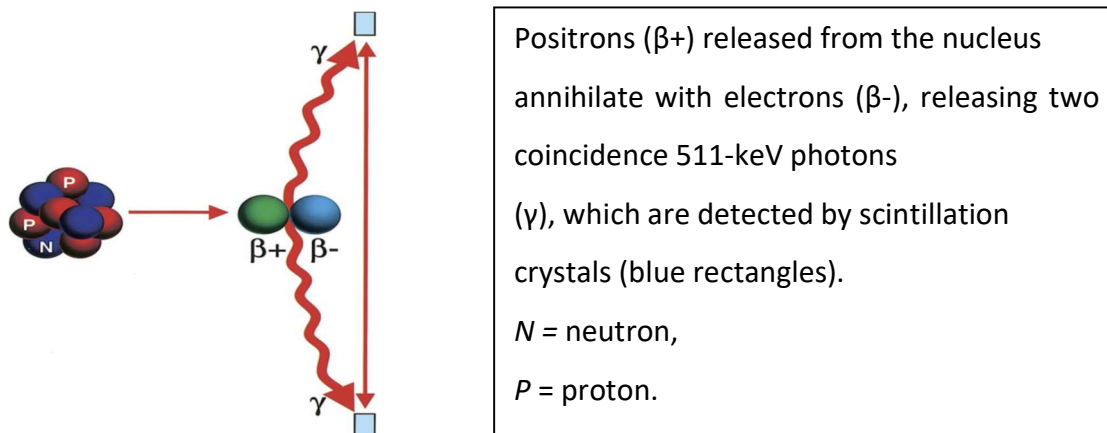
P = proton.

Fluorine- 18 (F-18) is the most commonly used positron emitter in imaging. It is produced by bombarding O-18–enriched water with high-energy protons. Negatively charged hydrogen ions are accelerated in a cyclotron until they gain approximately 8 MeV of energy, then the orbital electrons from the ion are removed. The resultant high-energy positive hydrogen ions (H^+, or proton beam) is directed toward a target chamber that contains the stable O-18–enriched water molecules.

The protons undergo a nuclear reaction to form hydrogen (F-18) fluoride:

H_2(O-18) + H-1 + energy → H_2(F-18).
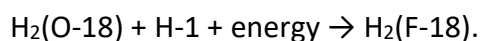
O-18 and F-18 are isobars, so have the same mass number (A= nucleons) but different atomic numbers (Z = 8 for oxygen and 9 for fluorine).

F-18 is an unstable radioisotope and has a half-life of 109 minutes. It decays by beta-plus emission or electron capture and emits a neutrino (ν) and a positron $β^+$:

F-18 → O-18 + $β^+$ + ν
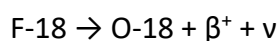
The positron annihilates with an electron to release energy in the form of coincident photons, which move in opposite directions (180 degrees):

$β^+$ + e^- →→→ (annihilation reaction) →→→ 511keV γ + 511keV γ

By changing the target, other positron emitting radionuclides can be produced.

The F-18 is labelled with a biological molecule, most commonly FDG, a glucose analogue in an automated computer controlled radiochemical process. The F-18 FDG thus produced is a sterile, non-pyrogenic, colourless liquid, with residual solvent of less than 0.04% and radioactive purity is greater than 95%. After local quality control procedures, this can be injected into the patient.

When the patient lies on the PET-CT scanner, it is the annihilation gamma photons which are detected by scintillation crystals coupled to photomultiplier tubes (PMTs). These crystals are often composed of bismuth germinate (BGO), cerium doped lutetium oxyorthosilicate (LSO), or cerium-doped gadolinium silicate (GSO), which have very high densities and atomic numbers. An ideal crystal has high stopping power and light output and fast decay time.

The absorption efficiency of BGO crystals is greater than that of LSO crystals due to its higher effective atomic number; however, LSO crystals emit 5 times as much light as BGO crystals, and the decay time for LSO is lower at 40 nsec (compared with 300 nsec for BGO), which enables the necessary counts or scintillation events required for image formation to be shorter with LSO crystals. Each detector is coupled to 4 photomultiplier tubes and they are arranged in a ring geometry with as many as 250 blocks in a ring (Figure 3).

Figure 3. PET-CT ring detector system
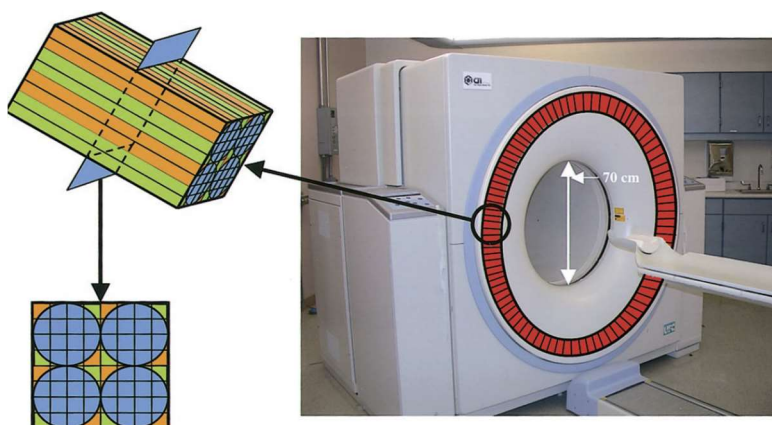
PET-CT scanner shows the PET ring detector system (red ring). There are up to 250 block detectors in the ring. Drawing shows a detector block with 8 x 8 smaller scintillation crystals (green and orange rectangles) linked to four photomultiplier tubes (blue circles).

The 511-keV gamma photons emitted opposite to each other easily penetrate soft tissues. The point of annihilation of a positron is not necessarily equidistant from the detector ring for both annihilation photons; therefore, although two photons may be coincident, they might not be detected at the same time by two detectors (Figure 4). Therefore, photons interacting with detectors within a set time window are considered to be "in coincidence." The window for this coincidence detection is typically 6–12 ns. Photons outside this time window are considered as single events and discarded by the coincidence circuit. As many as 99% of the photons detected may be rejected.

Figure 4. Coincidence imaging
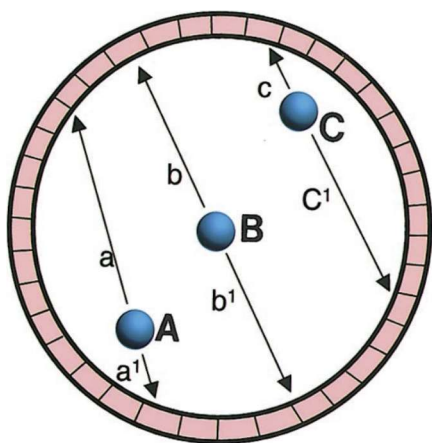
Although the photons emitted by annihilation points *A* and *C* are coincident, the distances that the coincident photons *a* and *a1* and *c* and *c1* will travel before they reach the scintillation crystals are different. There is a predetermined time window within which detected photons are considered to be in coincidence. Therefore, even though photons *a* and *a1* and *c* and *c1* are coincident, they will be electronically rejected as non-coincident. However, the coincident photons from point *B* are likely to reach the scintillation crystals within the time window and will be accepted as coincident.

Time-of-fight (TOF) is a method of measuring distance based on time difference between emission and detection. TOF differences between two photons stopped in two detectors of the PET scanner are used to determine if the photons are in "time coincidence", and, therefore, associated with the annihilation of a positron–electron pair. If the detection time difference between two photons is smaller than a coincidence window (traditionally 4–10 ns), the two events are considered physically associated to the same annihilation event. A line-of-response (LOR) joining the two detectors is drawn, and the source of the positron is assumed to be located in a undetermined position along the line (45). To generate 3D images, coincident LORs are detected and recorded at many angles and tomographic images are generated through filtered back projection or iterative reconstruction. The point of origin of the annihilation event is where these lines intersect. In TOF, for each annihilation event, the actual time difference in arrival time

between two coincident photons is also measured during coincident events to more accurately identify distance from annihilation event to detector. Hence, TPF scanners are characterized by a more accurate measurement of the TOF difference, which allows better localization of the source of annihilation along the LOR.

The PET scanner is located behind the CT scanner and housed in the same extended-length gantry (Figure 5). PET is performed following the CT study without moving the patient. Approximately 6 to 7 bed positions are planned in the three-dimensional acquisition mode for scanning the entire patient 3-4 minutes at each bed position.

Figure 5. PET-CT scanner
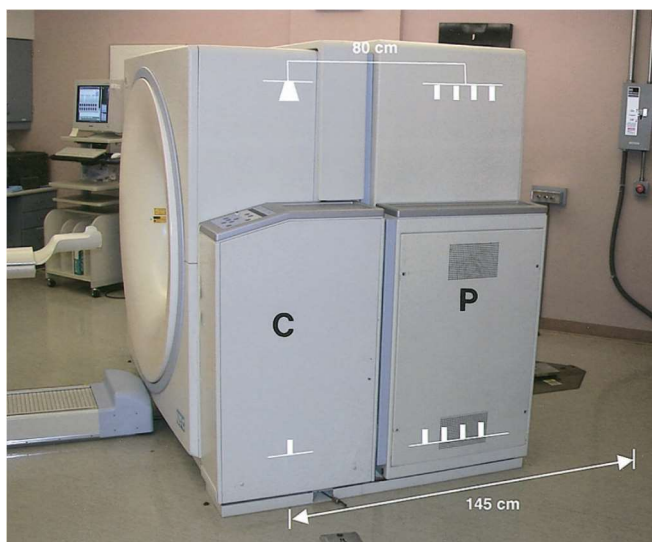
Hybrid PET-CT scanner shows the PET *(P)* and CT *(C)* components.

As gamma photons traverse the patient, they are attenuated. The half value layer of 511keV photons in tissue is 7cm. Therefore, photons originating in the centre of the body are attenuated more than the photons originating at the edge and hence central regions appear relatively less "bright" than peripheries and there appears to be activity in the skin, unless an attenuation correction is performed. Correct factors for attenuation correction of the PET study are obtained from the low dose CT. As the CT is acquired with a much lower energy than the PET, a procedure to convert the measured attenuation coefficients to 511keV is required. The CT attenuation correction (CTAC) is usually accomplished by assuming a simple bilinear relationship between

the CT number in Hounsfield Unit (HU, linearly related to the CT attenuation coefficient) and the 511 keV attenuation coefficient required for PET (46) (Figure 6).

Figure 6. Bilinear scaling function used to convert CT numbers (HUs) to linear attenuation values at 511 keV
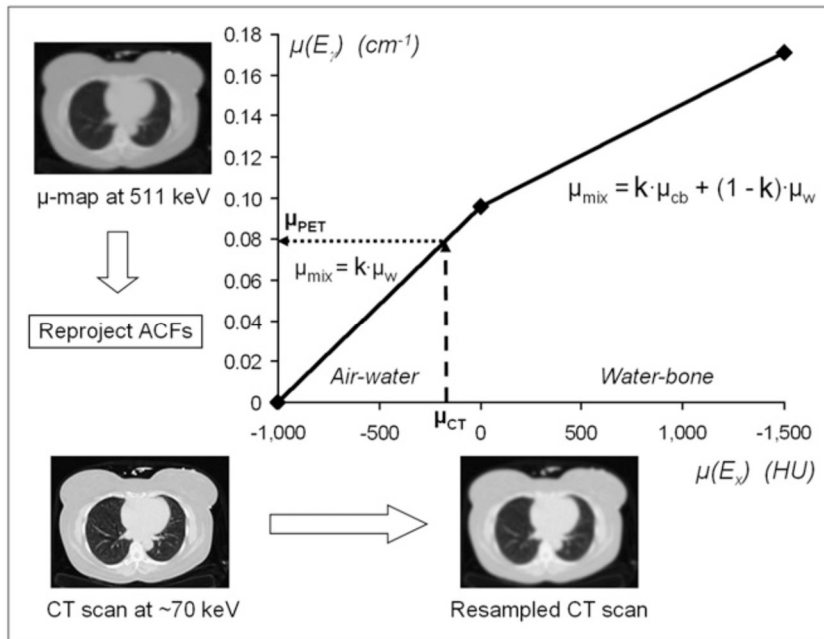
PET images are reconstructed using iterative algorithms, which model the statistical properties of the data, resulting in improved image quality over filtered back projection algorithms (47).

1.5.2 Clinical FDG PET-CT imaging

18F-Fluorodeoxyglucose (FDG) is a glucose analogue which is widely used clinically to evaluate regional glucose metabolism in cancer and yields functional information useful for both diagnosing and staging cancer. The basis for use of FDG PET-CT is the increased glucose consumption by cancer cells compared to normal tissue.

Solitary Pulmonary Nodule

A solitary pulmonary nodule (SPN) is defined as a focal round or oval lung lesion with a diameter smaller than 3 cm, completely surrounded by normal lung tissue, not associated with atelectasis or adenopathy (48). Several studies showed that PET had similar sensitivity (92–95%) but superior specificity (72–83%) as compared to CT (sensitivity 95%; specificity 40%) for the characterization of SPN [146–149] (49)(50)(51)(52), especially in excluding malignancy in small SPNs (<15mm) (53).

Non-Small Cell Lung Cancer

FDG PET-CT is accepted as a standard imaging modality in the initial staging and diagnostic work-up of patients with lung cancer. PET-CT is superior to PET and CT alone in T staging (88% of patients compared to 40% and 58%, respectively) (54).

FDG PET-CT offers an improvement in diagnostic accuracy of imaging mediastinal nodal disease as it can differentiate reactive or inflammatory nodes from metastatic disease and can detect metastases in normal-sized nodes. A meta-analysis on FDG-PET in lung cancer showed a pooled sensitivity of 72% and specificity of 91% for mediastinal nodal disease (55).
In NSCLC, FDG PET-CT has better sensitivity than CT alone in the detection of locoregional disease (most notably mediastinal nodal staging) and distant metastases, including differentiation of equivocal lesions seen on conventional cross-sectional imaging.

The American College of Chest Physicians (ACCP) Clinical Practice Guidelines recommends the use of FDG PET-CT for mediastinal and extra-thoracic staging in patients with clinical stage IB to

IIIB in lung cancer being treated with curative intent and it should be considered in patients with clinical 1A lung cancer being treated with curative intent. Minimally invasive needle techniques to stage the mediastinum have become increasingly accepted and are the tests of first choice to confirm mediastinal disease in accessible lymph node stations (56)

PET-CT can help characterise pleural disease (57). FDG PET-CT performs better than bone scintigraphy in detecting skeletal metastases. A recent meta-analysis shows PET-CT has sensitivity of 92% and specificity of 98% for diagnosing bone metastases (58) This is due to its ability to detect both osteolytic and sclerotic metastases and can detect asymptomatic marrow metastases which can be seen in up to 13% of cases of lung cancer. However, brain metastases are less easily identified due to high background grey matter uptake (43).

The addition of FDG PET-CT reduces the frequency of unnecessary thoracotomies by 20%. A study by Fischer et al. showed that the use of FDG PET-CT for pre-operative staging of NSCLC reduced both the total number of thoracotomies and the number of futile thoracotomies but did not affect overall mortality (59). The impact of PET on staging has shown an upstage in 16-33% and downstage in 6-10% of patients (60). Systematically applied PET scanning has a significant impact on patient management, altering diagnostic or therapeutic interventions in 72.2% of patients, changing staging in 22.2% of patients, and identifying serious unsuspected diagnoses in 4.0% of patients, with potentially life-saving consequences in 2.0% (61).

However, whilst this is a sensitive technique, specificity for characterising lung cancer is limited. Some lung malignancies such as adenocarcinomas in situ, carcinoid and well-differentiated adenocarcinomas may not be as metabolically active as one may expect, yielding a false negative finding (62). False negative findings may also be related to small lesion size although modern PET cameras have a spatial resolution of 5 to 8mm. Thus false negative results may accrue due to low-grade or slow-growing tumours, or small lesions.

False positive results occur in infection and inflammatory processes such as active tuberculosis and sarcoidosis due to overexpression of GLUT1 and GLUT3 transporters in the acute phase of inflammation (63).

Malignant Mesothelioma

The degree of metabolic activity in MPM than is significantly higher than in benign pleural diseases such as inflammatory pleuritis and asbestos-related pleural thickening. PET-CT has increased accuracy in the detection of mediastinal nodal metastases (64), but is also useful in the identification of occult extrathoracic metastases (65). Patients with MPM may have diffuse pleural thickening but only focal areas of malignancy and areas of pleural thickening may not correspond to areas of high metabolic activity, hence PET-CT can guide clinicians to the most appropriate biopsy site, which may not be apparent from CT findings alone. PET-CT may also help predict prognosis in patients with MPM as higher FDG uptake is associated with significantly shorter survival time (66).

In MPM, FDG PET-CT identifies significantly more patients with nodal or distant metastatic disease than CT and hence may contribute to more appropriate selection of patients with MPM for surgery. Elliott et al. found that nodal disease was concordant to surgical histopathology in 38/60 patients (63.3%) on PET-CT, compared to 27/60 (45%) on CT (p = 0.001). Distant metastases were identified uniquely on PET-CT in 8 patients and on CT only in one patient (67). There is limited value in using FDG PET-CT in patients who have undergone prior talc or chemical pleurodesis, as inflammatory response can cause increased avidity in the pleura for prolonged periods of time and can also result in an increase in size of the mediastinal and hilar nodes with increased SUV (68).

Radiotherapy Planning

FDG PET-CT is also increasingly used for radiotherapy planning in patients with NSCLC and is preferable to CT alone. PET-CT planning for target volumes in radiotherapy is different from the treatment volume. The percentage of changes recorded by PET-CT ranges from 27% to 100% and relates to the exclusion of atelectasis or inclusion of PET positive nodes (69).

Treatment Response

The main system for assessing anatomic tumour response is the Response Evaluation Criteria in Solid Tumours (RECIST), which is based on serial measurements using standard imaging techniques such as CT (70). This method relies on changes in tumour size. Two sets of response criteria using PET are currently available to monitor metabolic changes to anti-cancer treatment. The European Organization for Research and Treatment of Cancer (EORTC) criteria, the first metabolic criteria for solid tumours, were published in 2000 (71), and the PET Response Criteria in Solid Tumours (PERCIST) in 2009 (72). Although the two metabolic criteria have quite different approaches, tumour responses between the two criteria showed almost perfect agreement in a pooled analysis of several studies with different types of cancers (73).

Sequential FDG PET imaging has also been investigated as a metric of response to treatment. Increased FDG uptake in tumours is generally correlated positively with the total tumour cell mass, and decrease in FDG uptake with treatment is typically associated with response to therapy (74)(75), not uncommonly preceding a decrease in tumour size (76).

Studies have shown the sensitivity and specificity of PET for assessing histopathological response of NSCLC ranging between 81% and 97% and 64% and 100%, respectively (77). Huang et al. have shown that standardised uptake values (SUV) and metabolic tumour volume (MTV) changes from two serial FDG PET-CT scans before (baseline) and after initial chemoradiotherapy (at approximately 28 days) allow prediction of treatment response in advanced NSCLC (78).

PET-CT may be useful in assessing treatment response, with a partial metabolic response demonstrated at 4 weeks after arginine deprivation treatment in 46% of 39 patients (40). Kanemura et al. found that metabolic response assessment with FDG PET-CT was superior to modified RECIST for the evaluation of response to platinum-based doublet chemotherapy (3 weekly cycles with assessment after 3 cycles)in malignant pleural mesothelioma (79). Similarly, Ceresoli et al. in a study of 20 patients with MPM (mostly treated with pemetrexed and carbo-platin) found that a decrease in metabolic response determined by SUVmax correlated significantly with time to progression and a trend towards longer survival, while response evaluation by CT was not predictive (80). Veit-Haibach et al., however, found that SUVmax was

not predictive of survival (81). Metabolic responses were noted in 46% patients with ASS1 deficient mesothelioma treated with arginine deprivation therapy (27). In the ADAM trial, FDG PET-CT treatment response was assessed using the EORTC criteria. This trial showed that PET-CT may be useful in assessing treatment response, with a partial metabolic response demonstrated at 4 weeks after arginine deprivation treatment in 46% of 39 patients, stable disease in 31%, progression in 15% and mixed response in 8% (40). Participants with partial metabolic response showed a 46% decrease in SUVmax.

FDG PET-CT, however, carries with it challenges in assessing response, notably uptake of the radiotracer into non-malignant inflammatory cells, which can confound assessments of tumour response. In particular, there is significant prolonged FDG uptake post talc pleurodesis.
In addition, "flare" reactions and "stunning" of FDG activity levels by treatment have been described, which make it less than perfect in some instances as a general early metric of tumour response to treatment (82) and increase in FDG uptake post ADI therapy have been demonstrated in melanoma in mouse xenografts. There is also significant prolonged FDG uptake post talc pleurodesis, due to

1.6 18F Fluoro-L-Thymidine (FLT) PET-CT imaging in thoracic malignancy

There is recognition that evaluation of other aspects of abnormal cancer biology in addition to glucose metabolism may be more helpful in characterising tumours and predicting response to novel targeted cancer therapeutics. Therefore, efforts have been made to develop and evaluate new radiopharmaceuticals in order to improve the sensitivity and specificity of PET imaging in lung cancer with regards to characterisation, treatment stratification and therapeutic monitoring.

F-18 fluoro-3-deoxy-3-L-fluorothymidine (18F-FLT) a marker of cellular proliferation and hence used as a proliferation tracer for PET-CT imaging. Thymidine is a native nucleoside, which is used by proliferating cells for DNA synthesis during the S-phase of the cell cycle and a substrate for thymidine kinase (TK), but is not involved in RNA synthesis. There are two main pathways involved in DNA synthesis. The 'salvage' (exogenous) pathway recycles nucleoside precursors from outside the cell, and the 'de-novo' (endogenous) pathway methylates deoxyuridine monophosphate by thymidylate synthetase to thymidine monophosphate (Figure 7). As the precursors of the de-novo pathway (deoxyuridine, uridine and uracil) are also precursors for RNA synthesis, the thymidine salvage pathway is a more specific reflection of DNA synthesis (83).

Figure 7. Thymidine and FLT pathway (from Barwick et al. (85))
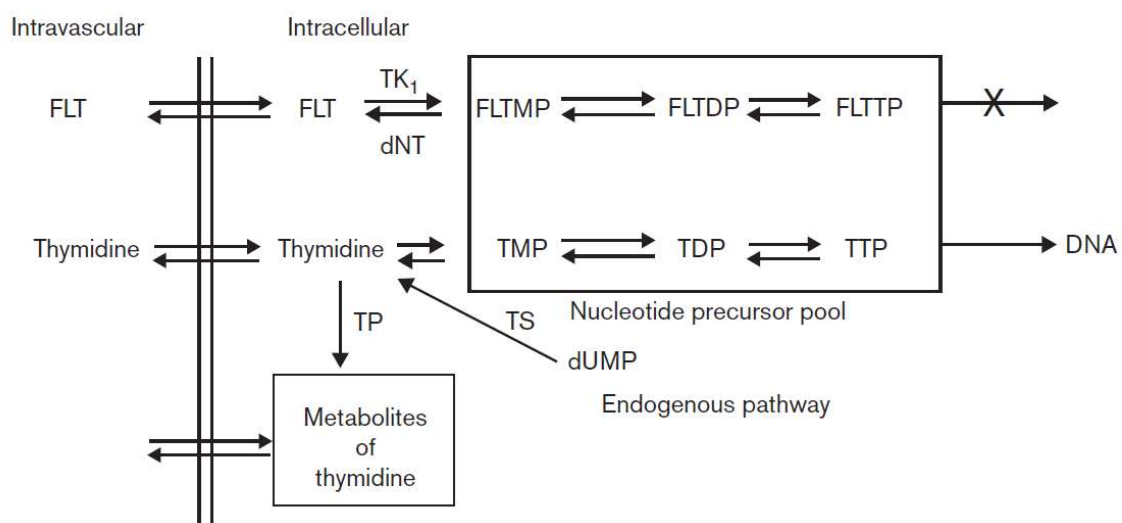
FLT is a thymidine analogue, where 18F replaces the OH group. It follows only the exogenous pathway. It generally enters the cell by Na+-dependent active nucleoside transporters and to a lesser extent by passive diffusion. It follows the salvage pathway of DNA synthesis and, like thymidine, undergoes phosphorylation by thymidine kinase1 (TK1) but it is then trapped intracellularly and not incorporated into DNA. FLT is a selective substrate for TK1 and hence its uptake correlates with the activity of TK1. TK1 is up-regulated during active DNA synthesis, such as in malignant cells, thus FLT uptake is a marker of active DNA synthesis (84). FLT is glucuronidated in the liver and at I hour post administration, 1/3 of FLT injected is diverted to glucuronide.

Most data to date suggest that FLT is not a suitable biomarker for staging of cancers.
FLT shows a lower accumulation in tumours than FDG as it only accumulates in the cells that are in the S phase of growth and demonstrates a low sensitivity for nodal staging
This is because of the rather low fraction of tumour cells that undergo replication at a given time with subsequently relatively low tumour FLT uptake. There is also marked physiological uptake in bone marrow and liver making these tissues difficult to investigate (85). Its uptake in tumour cells, however, directly correlates with histopathological Ki-67 expression in NSCLC (86) and therefore it is a more specific oncological tracer than FDG. Its main role is in evaluating treatment response (87).

Buck et al. compared uptake in lung cancer (NSCLC, SCLC and metastases) using both FDG and FLT and showed that-FLT uptake was related exclusively to malignant tumours; in contrast FDG uptake was seen in 4/8 benign lesions (88). Buck et al. also found that the sensitivity of FLT for nodal staging was unacceptably low (53%), but as there was no physiological tracer accumulation in the brain, it could be a suitable radiotracer for investigating brain metastases (86) and suggested that FLT may be the superior tracer for assessment of therapy response and outcome. In a similar study in 31 patients with NSCLC, Yang et al. reported that the sensitivities of FLT and FDG for primary lesions were 74% and 94%, respectively (p=0.003) and FDG was more sensitive in regional nodal staging (89). Tian et al. studied dual tracer imaging of pulmonary nodules with FLT and FDG in 55 patients and found this to be better than either tracer alone (90). Each patient was imaged twice using FDG and FLT within 7 days. The order of 18F-FDG or 18F-FLT scanning of each patient was determined randomly by a binary code produced by a computer. Within 7 days,

the whole procedure was repeated using the alternative radiopharmaceutical. The uptake of a lesion was also scored qualitatively ranging from no uptake to very high uptake. The sensitivity and specificity of FDG were 87.5% and 58.97% and for FLT 68.75% and 76.92%, respectively. The combination of dual-tracer PET-CT improved the sensitivity and specificity up to 100% and 89.74%. Sohn et al. studied gefitinib (an EGFR tyrosine kinase inhibitor) response in patients with advanced adenocarcinoma of the lung measuring changes in FLT uptake and found that activity on day 7 differed significantly between responders and non-responders (91). Trigonis et al. found that in patients with NSCLC treated with radiotherapy and imaged with FLT, that radiotherapy induced an early significant decrease in tracer uptake, after 5-11 treatment fractions (92).

1.6.1 Rationale for use of FLT

Recent preclinical work (30) has identified that ADI-PEG 20 affects both pathways of sourcing thymidine: in addition to suppression of the endogenous de novo thymidylate biosynthesis pathway (with a resulting increase in glutamine), ADI-PEG 20 also downregulates the salvage pathway with reduced thymidine uptake linked to a reduction in the level of TK1 (rather than an increased level as one would expect if just the de novo pathway was involved, i.e. 5FU, a pure TS inhibitor). ADI is selective, as it does not affect all amino acids. Xenograft studies have confirmed that ADI-PEG 20 therapy lowers FLT tumoural levels thereby providing a rationale for measuring tumour proliferation with FLT PET-CT imaging in patients.

FLT therefore may be a more robust biomarker of early ADI-PEG 20 activity than measurement of tumour metabolism with FDG PET-CT, which yields an increased signal in some ADI-treated tumours due to enhanced glucose uptake via suppression of phosphatase and tensin homolog (PTEN) and activation of PI3K signalling (93). Interestingly, they also showed that FLT was not useful for melanomas, implying that the ASS1-negative cell type of origin is very important when evaluating PET tracers in the context of arginine deprivation (94). ADI-PEG 20 suppresses TS and dihydrofplate reductase (DHFR) protein (in mesothelioma and bladder cancer cells) and sensitises ASS1-negative bladder cancer (and mesothelioma) cells to the cytotoxic effects of pemetrexed. In addition, ADI-PEG 20 blocks thymidine uptake linked to reduced TK1protein, which is detectable using FLT PET-CT (in bladder cancers and mesothelioma, but not in melanoma cells) (30).

ASS1 is expressed constitutively (i.e. unstimulated or basal conditions) at high levels in most tissues, except within lymphoid tissue and bone marrow. However, once arginine is removed, it is hypothesised that lymphoid tissue and bone marrow upregulate ASS1 to make arginine for cell proliferation. This then results in upregulation of TK1 and hence increased FLT uptake (24). Arginine (and hence ASS1) is important for BM/lymphoid derived cell proliferation.

Work with FLT to assess treatment response of NSCLC and mesothelioma with ADI-PEG20 in combination with cisplatin and pemetrexed is encouraging and has shown a significant decrease in tracer uptake at the end of treatment, consistent with human tumour xenograft studies of ADI-PEG20 and the known pharmacology of arginine depletion in ASS1-deficient tumours suggesting that measuring changes in proliferation with FLT are likely to be more specific than non-specific downstream effects of FDG (30). Pemetrexed, is an antifolate agent and antifolates target folate dependent enzymes, such as thymidylate synthase (TS), which are specific for the endogenous pathway. In particular, 5 fluorouracil, have been shown to increase FLT uptake post therapy as part of the salvage response to TS inhibition.

Potential problems with using FLT in imaging treatment response include:
1) high physiological uptake in liver and bone marrow;
2) exogenous pathway only;
3) potential "flare" from increased dependence on exogenous thymidine following anti-folate therapy;
4) potential increase in unconjugated FLT in plasma (as some chemotherapy agents deplete glucouronidate and hence less FLT is conjugated with resultant increase in FLT plasma fraction).

The preclinical data suggests that FLT PET-CT, as a marker of proliferation, may be a better biomarker of treatment response than FDG PET in arginine deprivation therapy in thoracic malignancy and hence provides rationale for why further evaluation is required. The overall goal is to improve response assessment using new techniques.

1.7 Quantifying tumour heterogeneity using radiomics

Radiomics, or texture analysis, is the "comprehensive quantification of tumour phenotypes by applying a large number of quantitative image features" (95). Texture analysis is a tool for assessing intratumoural heterogeneity and refers to mathematical methods which are applied to describe relationships between grey-level intensity in pixels or voxels and their position within an image. Texture parameters can be measured on standard clinical imaging protocols using post processing techniques, most commonly using a statistics based model (96), based on spatial distribution of pixel or voxel values calculating local features at each pixel in an image and deriving parameters from the distribution of local features. The statistical methods are categorized as first-order (one voxel); second-order (two voxel); and high-order (three or more voxel) statistics (97).

First-order texture features describe global textural features relating to grey-level frequency distribution within a region of interest and are based on histogram analysis. They include mean, minimum and maximum intensity (SUVmean, SUVmin, SUVmax), standard deviation, skewness (asymmetry of the histogram) and kurtosis (peak of the histogram), first order uniformity (regularity) and first order entropy (randomness of grey level voxel intensities within an image) (98).

They do not convey spatial information within the tumour as the above properties are calculated using individual voxel values, ignoring the spatial relationships between voxels. This group also includes metabolic tumour volume (MTV) and total lesion glycolysis (TLG = SUVmean x MTV).

Second-order (in plane) features describe local texture features and are calculated using e.g. spatial grey-level dependence (GLDM) or co-occurrence matrices (GLCM) and determine how often a pixel of intensity finds itself within a certain relationship with another pixel of intensity. These include second order entropy (randomness of the matrix) and uniformity (orderliness/homogeneity; not to be confused with first-order entropy and uniformity), contrast (local variation), homogeneity, dissimilarity (difference between elements in the matrix) and correlation (grey level linear dependencies).

High-order (multiplane) parameters are calculated e.g. using neighbourhood grey-tone (intensity) difference matrices (NGTDM) or grey- level size-zone matrices (GLSZM) and describe local features based on differences between each voxel and its neighbouring voxels in adjacent planes. These include coarseness (granularity); contrast (dynamic range of intensity levels and the level of local intensity variation) and busyness (rate of intensity change within an image) (97). Figure 8 illustrates the differences between these different order statistics. Table 1 (below) lists the parameters we have evaluated in this thesis.

Figure 8. Four simulations of different intensity variations (from Chicklore et al.(97))
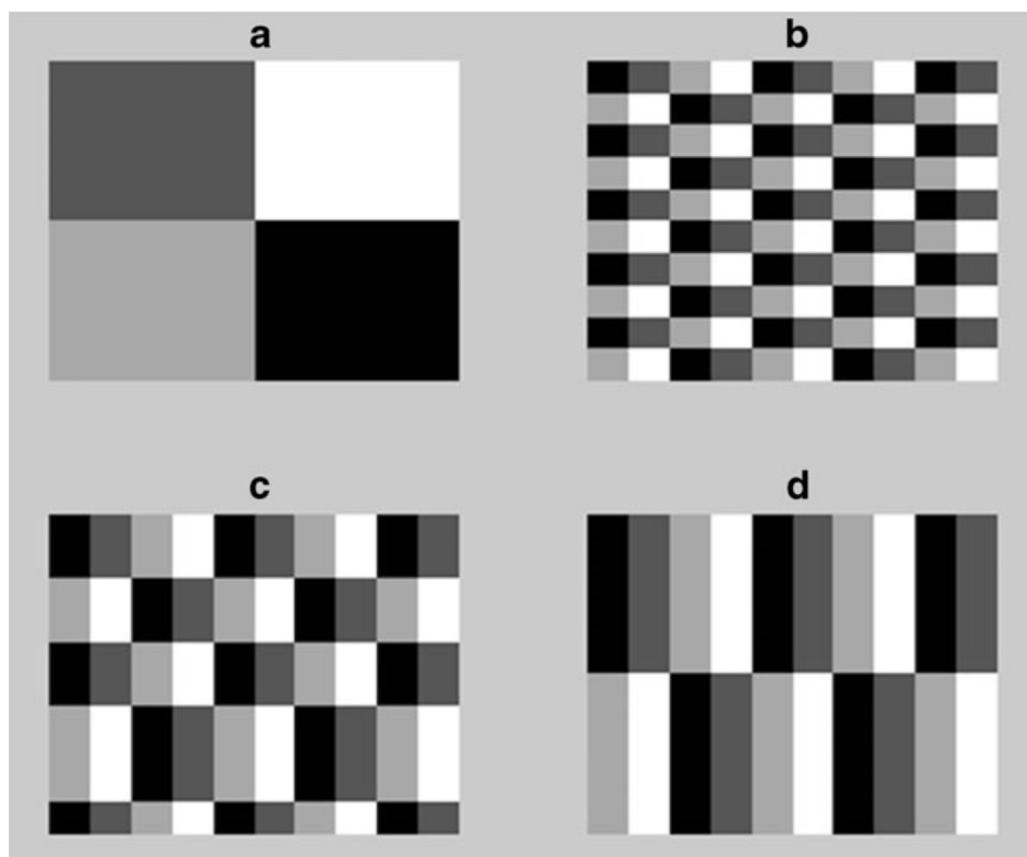
First order parameters are the same for all four cases.

Second-order features (which are derived from grey-level co-occurrence matrix with offset[1.0]) will be different for "a" compared to "b", "c" and "d", but the latter three will be the same.

High-order features (derived from neighbourhood grey time difference matrices or grey-level size-zone matrices) will be different for all four cases.

Table 1. Common heterogeneity parameters (from Cook et al.(98))

Parameter	Order	Description
SUVmax	First	Voxel with highest intensity
SUVmean	First	Average of all pixel intensities
SUVpeak	First	Maximum average SUV within a 1 cm ^{3} spherical volume
MTV	First	Metabolic tumour volume
TLG	First	Total lesional glycolysis = MTV x SUV mean
Standard deviation	First	Positive square root of variance (variance= variability that utilizes all data; average of the squared differences between each data value and the mean)
Skewness	First	Measure of asymmetry and deviation from a normal distribution. Skewness >0: right skewed, most values concentrated on the left of the mean. Skewness <0: left skewed, most values concentrated on the right of the mean. Skewness = 0: symmetrical distribution around the mean
Kurtosis	First	Describes ''peaked-ness'' of a distribution Kurtosis >3: sharper peak than a normal distribution, with values concentrated around the mean and thicker tails; this means high probability for extreme values; Kurtosis <3: flatter than a normal distribution with a wider peak; the probability for extreme values is less than for a normal distribution, and the values are spread more widely around the mean; Kurtosis = 3: normal distribution
Entropy	First	Measures texture randomness or irregularity
Uniformity	First	Measure regularity. Sum of squared elements in the ROI

Contrast	High	This value increases with the amount of local variation in intensity. An image is said to have a high level of contrast if areas of different intensity levels are clearly visible. Thus, a high contrast means that the intensity difference between neighbouring regions is large. This is usually the case when the dynamic range of the grey scale is large or stretched
Coarseness	High	Based on differences between each voxel and the neighbouring voxels in adjacent image planes, it measures the granularity within an image; described as the most fundamental property of texture.
Busyness	High	A busy texture is one in which there are rapid changes in intensity from one pixel to its neighbour; that is the spatial frequency of intensity changes is very high. A higher value of busyness would tend to emphasise the frequency of spatial changes in intensity values
Complexity	High	A texture has high complexity if the information content is high and there are many grey values present. Complexity is the sum of pairs of normalised differences between intensity values.

1.7.1 Radiomics in thoracic malignancy

Radiomics has shown potential in a number of tasks such as classifying lung lesions into benign or malignant , differentiating between primary and metastatic lesions, predicting survival and response to treatment, thus showing promise towards personalized therapy in oncology (93)(98). Measurement of heterogeneity within medical images may reflect the underlying biologic environment and genetic heterogeneity within a tumour, allowing prediction of changes before and during treatment (99). Beyond the relatively simple measurements of tumour uptake or size, there is increasing recognition that measurement of the spatial heterogeneity of FDG PET image characteristics can give predictive information on baseline, pretherapy, imaging in several solid tumours (100). CT and MRI imaging have high spatial resolution, allowing texture analysis in small volume tumours. However, the poorer spatial resolution of PET imaging (pixel sizes up to 5mm) limits the size of tumours which can be assessed (due to requirement of a reasonable number of adjacent pixels to be present to measure some of the texture features) (97).

In NSCLC, first-order heterogeneity parameters on FDG PET, including SUV intensity-volume histograms, have been described as predictive for radiation therapy response (101) and pre-therapy high order heterogeneity features (coarseness, contrast, and busyness) are associated with non-response to chemoradiotherapy by RECIST and with poorer prognosis (100). A study looking at heterogeneity features on FDG PET in NSCLC treated with erlotinib, a tyrosine kinase inhibitor (TKI), showed that response to treatment is associated with reduced heterogeneity on FDG PET and changes in first-order entropy are independently associated with overall survival and treatment response) (102). Histopathological mean tumour-cell density (MCD) and histopathological lacunarity are associated with several commonly used FDG PET-derived indices including SUV-lacunarity, metabolically active tumour volume, SUVmean, entropy, skewness, and kurtosis, which may explain the biological basis of FDG PET heterogeneity in non-small-cell lung cancer(103).

A recent study by Bianconi et al. found significant associations between PET features, CT features, and histological type in NSCLC and concluded that texture analysis on PET-CT shows potential to differentiate between histological types in patients with non-small-cell lung cancer. Intra-PET analysis identified a strong positive correlation between the radiotracer uptake

(SUVmax, SUVmean) and its degree of variability/disorder throughout the lesion. Conversely, there was a strong negative correlation between the uptake (SUVmax, SUVmean) and its degree of uniformity. There was a positive moderate correlation between MTV and radiotracer uptake (SUVmax, SUVmean). Inter (PET-CT) correlation analysis identified a very strong positive correlation between the volume of the lesion on CT and MTV, a moderate positive correlation between average tissue density (CTmean) and radiotracer uptake (SUVmax, SUVmean), and between kurtosis on CT and MTV. Squamous cell carcinomas had larger volume higher uptake, stronger PET variability and lower uniformity than the other subtypes. By contrast, adenocarcinomas exhibited significantly lower uptake, lower variability and higher uniformity than the other subtypes (104).

1.7.2 Rationale for further investigation

There is very little published data in MPM to determine if there is any role for textural analysis in FDG PET in MPM. The only published study to date shows that FDG PET-CT parameters that take into account functional volume (MTV, TLG) show significant associations with survival in patients with MPM before adjusting for histological subtype and are worthy of further evaluation (105).

1.8 Thesis Aims and Hypothesis

1.8.1 Thesis aims:

To assess tumour proliferation (with FLT PET-CT) as a marker of early treatment response in thoracic malignancy (MPM and NSCLC) using arginine deprivation therapy (ADI-PEG 20 combined with pemetrexed and cisplatin), as part of TRAP trial substudy.

To assess tumour heterogeneity changes in arginine deprivation treatment response in MPM using FDG PET data from the ADAM trial with scans at baseline and 4 weeks post treatment.

1.8.2 Scientific hypotheses:

FLT PET-CT molecular imaging can predict response to arginine deprivation treatment (EORTC) earlier than anatomical imaging using CT in NSCLC and MPM (RECIST).

Texture features of FDG PET-CT predict responders and non-responders to arginine deprivation treatment better than CT in MPM (and hence superior to RECIST, currently considered to be the gold standard) and are prognostic.

Chapter 2 TRAP Substudy

2.1 Methodology

TRAP was a phase 1 study (NCT02029690) in subjects with Tumours Requiring Arginine to assess first line ADI-PEG 20 combined with Pemetrexed and Cisplatin (ADIPEMCIS) chemotherapy. Informed consent was obtained for inclusion in the FLT PET-CT imaging substudy of this trial, in patients with thoracic malignancy (MPM and NSCLC). I was Co-Principle Investigator for this substudy, responsible for the PET imaging protocol, supervising and overseeing the PET studies, ensuring the PET studies were performed in accordance with the protocol and good clinical practice (GCP). Approvals were obtained from Leeds East REC (14/YH/0090), MHRA and ARSAC before study initiation.

2.1.1 Participants

Inclusion criteria

Patients with histologically proven ASS1-deficient MPM and NSCLC (defined as >50% ASS1 loss) recruited into the phase 1 dose-expansion imaging substudy were chemotherapy naive, had an expected survival of at least 3 months, were over 18 years of age, ECOG performance status (PS) 0-1 with adequate haematological (Hb > 9.0g/dL; absolute neutrophil count (ANC) > 1,500/μL; platelets > 75,000/μL), hepatic and renal function.

Exclusion criteria

These included toxic manifestations of previous treatments, brain and spinal cord metastases, serologically positive for human immunodeficiency virus (HIV), serious infection, therapeutic anticoagulation, pregnancy, ECOG PS >2, seizures and allergy to pegylated compounds or platinum salts.

2.1.2 Treatment

Patients received the maximum tolerated dose derived from the dose-escalation study: weekly ADI-PEG 20 (36 mg/m^2 I.M.) with standard doses of pemetrexed (500 mg/m^2 I.V.) and cisplatin (75 mg/m^2 I.V.), both given every 21 days (42). Subjects with MPM received up to a maximum of 6 cycles of treatment every 3 weeks (i.e. up to 18 weeks). Patients achieving stable disease or better could continue ADI-PEG 20 monotherapy until disease progression or withdrawal. Subjects with NSCLC received up to a maximum of 4 cycles of treatment every 3 weeks. Subjects were free to discontinue the study at any time, for any reason, and without prejudice to further treatment.

2.1.3 Imaging and Analysis

Computed Tomography (CT)

CT imaging was performed as part of routine clinical care: at baseline (CT1), after 2 cycles of treatment (at approximately 6 weeks, CT2) and end of treatment (@18 weeks for MPM and 12 weeks for NSCLC, CT4). In MPM, subjects had an additional clinical CT scan after 4 cycles (CT3).

CT Image Acquisition

Diagnostic CTs were acquired as standard of care on a Definition AS 64 slice CT scanner (Siemens Healthcare, Erlangen, Germany) at St. Bartholomew's Hospital. IV contrast-enhanced CT scans obtained with a minimum slice thickness of 3–5 mm were available for review. Each patient received 80–100 mL of IV iodinated contrast medium (iodixanol 300 or iohexol 300) injected at a rate of 2–3 mL/s, and scanning began after a delay of 20-25 seconds for arterial and 75–90 seconds after injection for the portovenous phase imaging.

CT Image Analysis

CT response was assessed by an experienced chest radiologist (SE) using RECIST 1.1 (NSCLC) (70) (Table 2) and modified RECIST (MPM) criteria (106). For modified RECIST, the tumour thickness perpendicular to the chest wall or mediastinum is measured in two positions at three separate levels on transverse cuts of CT scan. The sum of the six measurements is defined as a pleural unidimensional measure. Complete response (CR) is defined as the disappearance of all target lesions with no evidence of tumour elsewhere; partial response (PR) is defined as at least a 30% reduction in the total tumour measurement; progressive disease (PD) is defined as an increase of at least 20% in the total tumour measurement over the nadir (lowest) measurement, or the appearance of one or more new lesions. Patients with stable disease (SD) were those who fulfilled the criteria for neither PR nor PD.

Table 2. Response assessment of CT imaging on RECIST 1.1 criteria

Complete Response (CR):	Disappearance of all target lesions. Any pathological lymph nodes (whether target or non-target) must have reduction in short axis to < 10 mm.
Partial Response (PR):	At least a 30% decrease in the sum of the diameters of target lesions, taking as reference the baseline sum diameters.
Progressive Disease (PD):	At least a 20% increase in the sum of the diameters of target lesions, taking as reference the smallest sum on study (this includes the baseline sum if that is the smallest on study). In addition to the relative increase of 20%, the sum must also demonstrate an absolute increase of at least 5 mm. The appearance of one or more new lesions is also considered progression.
Stable Disease (SD):	Neither sufficient shrinkage to qualify for PR nor sufficient increase to qualify for PD, taking as reference the smallest sum diameters on study.

FLT PET-CT

FLT PET-CT imaging took place in a longitudinal study with scans at baseline (PET1), approximately 24 hours after the first dose ADI-PEG20 on day 2 of cycle 1 (PET2); at the end of cycle 1 of ADIPEMCIS therapy (PET3) on day 16 (2 weeks); and at the end of treatment (PET4 at day 120 (18 weeks) for MPM and at day 80 (12 weeks) for NSCLC). The baseline and end of treatment scans coincided with CT imaging, however, the interim scans were at different time points (Figures 9 and 10).

Baseline PET-CT imaging was performed in a total of 22 patients, however 4 patients were subsequently excluded due to deterioration in performance status. Ten patients with histologically proven advanced MPM (mean age 69 +/- 7.6 years) and 8 patients with non-squamous NSCLC (mean age 58 +/- 8.4 years) proceeded to further PET imaging. There was slight variation in the timing of PET scan 2 between groups due to a change in FLT tracer availability and scheduling: for the NSCLC group, this took place around at 28-29hrs post ADI-PEG20, rather than exactly 24hrs, while in the MPM group, this took place at 22-24 hrs.

Figure 9. Imaging schedule in MPM patients
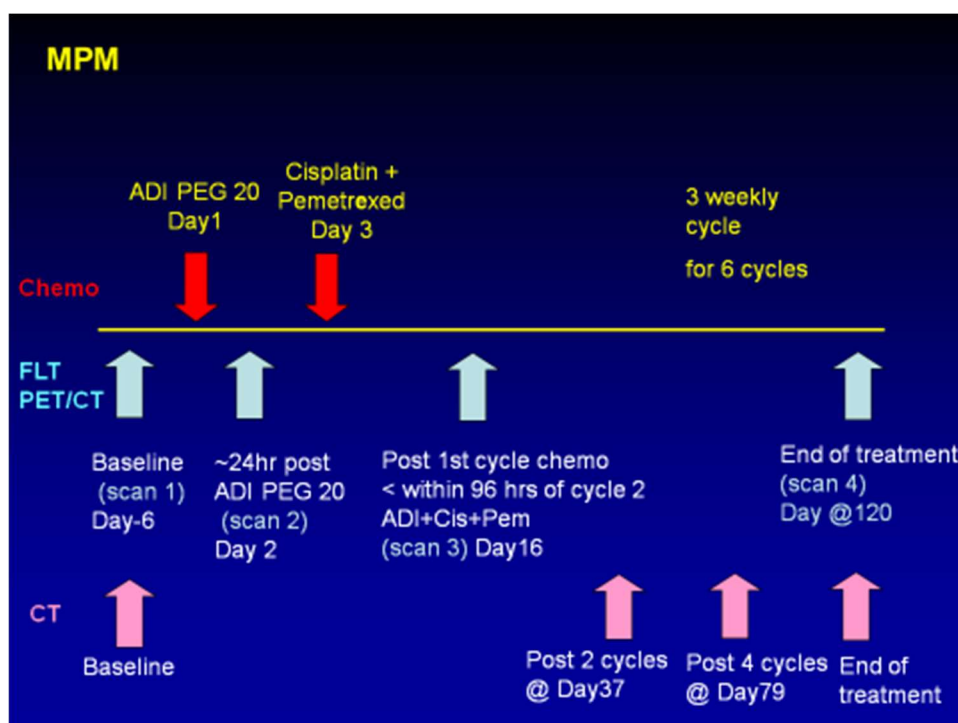
Figure 10. Imaging schedule in NSCLC patients
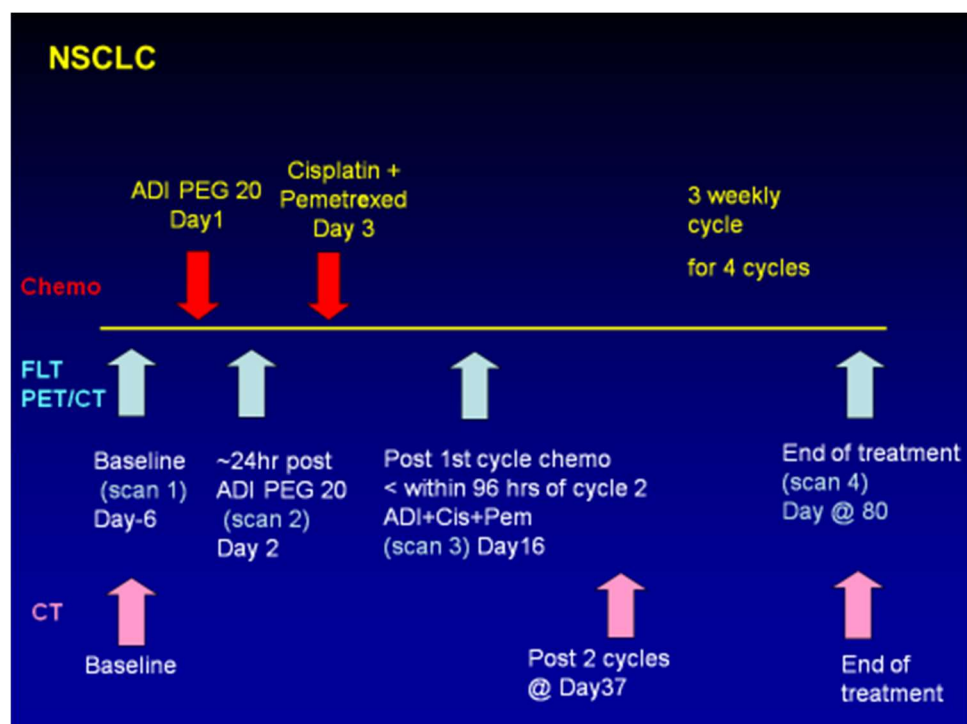
PET-CT Image Acquisition

A mean administered activity of 244 +/- 6.3 MBq of FLT was injected IV in patients who were well hydrated. The PET emission acquisition was started 60 ± 5 minutes after the FLT administration. All PET-CT images were acquired on a GE Discovery 710 PET-CT scanner (GE Healthcare, Chicago, USA). Patients were positioned in the scanner with their arms raised and each scan covered the skull base to the bottom of the liver (covered in 4 to 5 bed positions), with an axial field of view of 14.9 cm and an 11- slice overlap. All PET data were acquired in 3D time-of-flight (TOF) acquisitions, according to local protocols. A low-dose CT scan (140 kV, 10 mA, 0.5 s rotation time, 40 mm collimation) was performed at the start in order to provide attenuation correction and anatomical localisation. The length of scan was 4 minutes per bed position. The PET data was corrected for dead time, scatter, randoms and attenuation using standard algorithms provided by the scanner manufacturer. Images were reconstructed using iterative reconstruction with time-of-flight (reconstruction parameters: 2 iterations, 24 subsets, Gaussian post filter with 6.4mm FWHM, 4mm voxels). Both attenuation-corrected and non attenuation-corrected PET

images were reconstructed. The response scans were all performed at the same time +/- 5 mins after injection as the baseline scan.

PET-CT Imaging Analysis

As there are no guidelines for the use of FLT in response measurement, I used an adaption of the EORTC criteria developed for FDG (71). These have previously been used (for FDG) in the ADAM trial which investigated arginine deprivation therapy with ADI-PEG20 monotherapy in MPM (40). Volumes of interest (VOI)s were drawn manually (TS) using Hermes Gold 3 (Sweden) software within the primary tumour at baseline and then subsequent scans. The maximum standardized uptake value (SUVmax) is widely used as a semiquantitative measure of FDG uptake ((107); I note that strictly it is per cm^3 but it is assumed that soft tissue is equivalent to water, so 1 g/cm^3) .

$$SUV = \frac{tracer\ uptake\ (MBq/mL)}{administered\ activity(MBq)\ /\ patient\ weight(kg) x 1000}$$

There is no true "gold standard" for evaluating treatment response and in the absence of a biochemical parameter, we used the end of treatment diagnostic CT (CT4) as the best surrogate to define end of treatment response. As an initial analysis, we compared the PET-CT studies at all time points (PET 2, 3 and 4) with this, to assess if the early PET-CT studies were able to predict end of treatment response and if FLT PET-CT could be an early biomarker of treatment response.

Treatment response based on percentage change in FLT SUVmax between baseline, early and late FLT PET-CT scans was previously published by Scheffler et al. (108), hence we used the change in SUVmax from baseline in the analysis of the PET data. A partial response (PR) required a 15% reduction in values; progressive disease (PD) was taken to be a 25% increase and stable disease (SD) was taken to be everything in between. As a further step, we also looked at all PET parameters to see if response on PET2, PET3 and PET4 was concordant with response to treatment at CT4.

In a secondary analysis, the effect of scan timepoint was assessed by comparing treatment response at an "early" timepoint for PET (change in SUVmax, from baseline, after one cycle of

therapy) and CT (change in RECIST length, from baseline after 2 cycles of therapy); and at a "late" timepoint, namely end of treatment, namely PET4 and CT4. We looked at effects of timepoint ("early", "EOT"), modality (PET, CT) and patient group (MPM, NSCLC). PET response was measured using SUVmax and CT using RECIST length.

As a tertiary analysis of treatment response, we evaluated additional PET parameters, other than SUVmax, including SUVmean and SUVpeak as well as maximum, mean and peak SUVs adjusted for lean body mass (SULmax, SULmean, SULpeak), to see if these were better markers of treatment response compared to SUVmax. PERCIST measurements (72) were also attempted (these use standardized uptake values normalized by lean body mass, so SUL rather than SUV), but not used. It was difficult to delineate pleural MPM tumoural uptake adjacent to the ribs on FLT PET-CT (as both demonstrate increased tracer uptake); there was high background hepatic uptake on FLT PET-CT (in PERCIST criteria, the tumour uptake should be higher than background activity); we even attempted to use mediastinal blood pool (MBP) activity (which was low on FLT), instead of liver, but again tumour distribution was difficult to assess separate to this, due to proximity of tumour in mediastinum.

We did also attempt to look at survival data (as a surrogate marker of treatment response) and plot Kaplan Meier charts looking at progressors and non-progressors as well as responders and non-responders. However, as there was only one case in several of the datasets, hence unreliable.

Scanner stability and background checks

Scanner stability was assessed using the daily QC phantom SUVmean measurements from March 2015 until mid July 2016 (during which time the majority of FLT scans had taken place).

Measurements of background FLT uptake in bone marrow (in the L1 vertebral body) and other background regions (liver, mediastinal blood pool and erector spinae muscle) were measured by placing regions of interest (ROIs) in these areas over sequential scans. Ratios of bone marrow/MBP and bone marrow/liver were also calculated. These provided surrogate data for stability. See **Appendix A**

2.1.4 Statistical analysis

Statistical analysis was performed using SPSS (IBM SPSS Statistics for Windows, Version 24.0. Armonk, NY: IBM Corp). A test for normality (Shapiro-Wilk) showed no significant deviation from normality in each PET parameter and so parametric statistical tests were used.

A primary analysis was undertaken using a 2-way repeated measures linear mixed effects ANOVA model to look at treatment response at various "time points" on PET scan (PET2, PET3, PET4), measured as change in SUVmax from baseline to that timepoint compared to treatment response on CT (measured as change in RECIST length from baseline to CT4); and assuming that the RECIST change is the gold standard. An additional analysis of the effect of "group" compared responses in the MPM and NSCLC groups. Post-hoc pairwise tests were used to further investigate significant main effects or interactions.

No statistical analysis was used in assessment of concordance of treatment response using EORTC criteria (PR, SD and PD) on PET2, PET 3 and PET4 with CT4.

A secondary analysis looking at the effects of scan timepoint ("early", "EOT"), modality (PET, CT) and patient group (MPM, NSCLC) on change from baseline was investigated using a 3-way repeated measures ANOVA executed as a linear mixed effects model using SPSS. Post-hoc pairwise tests were used to further investigate significant main effects or interactions. PET response was measured using SUVmax and CT using RECIST length.

A tertiary analysis was undertaken again with post-hoc pairwise comparisons in a 3-way repeated measures ANOVA model using a linear mixed effect model in SPSS (as with the secondary analysis) but this time all 8 PET parameters (SUV measures) were included.

No statistical analysis was used in comparison of treatment response rate on FLT PET-CT using EORTC criteria (PR, SD and PD) at PET 2, 3 and 4 and RECIST response on CT after 2 cycles of therapy (CT2) and at end of treatment (CT4).

2.2 Results

2.2.1 Demographics

Demographic data is as per Table 3 below.

Table 3 Demographic data in TRAP substudy

TRAP Demographic data for MPM n=10			TRAP Demographic data for NSCLC n=8	
Age mean (range)/yrs			**Age** mean (range)/yrs	
all patients	69 (58-82)		all patients	58 (39-65)
women	69		women	61 (56-64)
men	69 (58-82)		men	56 (39-65)
Gender			**Gender**	
no of female	1		no of female	4
no of male	9		no of male	4
ASS1% mean (range)			**ASS1%** mean (range)	
all patients	79 (51-100)		all patients	82 (55-100)
women	80		women	81 (55-100)
men	79 (51-100)		men	82 (70-98)

In the MPM group, there were 5 patients with biphasic MPM; 4 with sarcomatoid MPM, the most aggressive subtype (one of which was desmoplastic) and one patient had epithelioid MPM (least proliferative). In the NSCLC group, all were adenocarcinomas (some poorly differentiated). 1.4

In the MPM group, median progression free survival was 5.4 months (range 1.4 – 12.2 months) and median overall survival was 11.4 months (range 2.8-23.1 months). In the NSCLC group, median progression free survival was 5.2 months (range 2.3 – 10.6 months) and median overall survival was 9.0 months (range 2.3-18.8 months).

For radiation exposure calculations - see **Appendix B.**

2.2.2 Response compared to end of treatment CT as "gold standard"

ANOVA

A primary analysis using a 2-way repeated measures linear mixed effects ANOVA model in the combined dataset (all subjects) comparing the treatment response on PET (measured using change in SUVmax from baseline to that timepoint) at different timepoints (PET2, PET3 and PET4) with response on CT at end of treatment (measured as change in RECIST length from baseline to CT4), revealed a significant fixed effect, $p < 0.001$ and hence "real" difference between CT4 and PET.

A more detailed analysis using post-hoc pairwise comparison (Table 4) found a mean reduction of RECIST length from baseline to CT4 of 21.9%; which is a significantly greater reduction than the decrease in SUVmax from baseline to PET2 which was only 2.1%, ($p=0.03$); and greater than the change in SUVmax from baseline to PET 3 (where SUVmax increased by 3.2%, $p=0.006$). However, the mean reduction in SUVmax from baseline to PET4 is 36.5% (which is even greater than the corresponding reduction on CT) and which is also significantly greater than the decrease in SUVmax from baseline to PET2 (2.1%, $p<0.001$) and baseline to PET 3 (increase of 3.2%, $p<0.001$). Hence treatment response changes at PET4 are not clearly demonstrated at a statistically significant level on the earlier PETs (PET2 and PET3).

This ANOVA model also looked for a difference in treatment response between the MPM and NSCLC groups, but found no significant difference in response between the groups ($p=0.65$). Similarly, interaction of image session and group was not significant ($p=0.07$).

Table 4. Image session effects in all patients (18 total; 10 MPM and 8 NSCLC)

Estimates					
ImageSession	Mean Change within Image session (*)	Std. Error	df	95% Confidence Interval	
				Lower Bound	Upper Bound
==CT4==	==-21.933==	7.075	47.515	-36.163	-7.703
PET2	-2.103	7.226	48.931	-16.625	12.419
PET3	3.193	6.933	46.831	-10.756	17.143
==PET4==	==-36.502==	7.730	50.303	-52.025	-20.979

Pairwise Comparisons							
Image Session 1	Image Session 2	Mean Difference btw Image Sessions	Std. Error	df	Sig.	95% Confidence Interval for Difference[c]	
						Lower Bound	Upper Bound
CT4	PET2	-19.831	8.954	40.588	==.032==	-37.920	-1.741
	PET3	-25.126	8.618	38.194	==.006==	-42.570	-7.682
	PET4	14.568	9.234	38.972	.123	-4.109	33.246
PET2	PET3	-5.296	8.832	40.068	.552	-23.145	12.553
PET3	PET4	34.399	9.515	41.978	==.001==	15.197	53.601
	PET4	39.695	9.163	39.346	==.000==	21.167	58.223

(*) CT4- mean change in RECIST length from baseline to CT4
PET2, PET3, PET4 – mean change in SUVmax from baseline

Concordance of treatment response on PET and CT in terms of PR, SD and PD

As a further step in the initial analysis, we also looked at treatment response in terms of PR, SD and PD on PET2, PET3 and PET4 and compared with response to treatment on CT4. For PET, we looked at all parameters (not just SUVmax). However, the most reliable PET parameter was found to be SUVmax, as it was concordant with CT4 in 62% at PET2 and PET4 (Table 5); demonstrating PR, SD or PD in agreement with CT4. In MPM cases alone, this increased to 71% at PET2, but was less concordant with the NSCLC cases (although still 50%).

Table 5. Treatment response on FLT PET-CT in terms of PR, SD and PD concordance with CT4

	All data agreement with CT4			MPM agreement with CT4			NSCLC agreement with CT4		
	PET2	PET3	PET4	PET2	PET3	PET4	PET2	PET3	PET4
SUVmax	8/13 (62%)	7/16 (44%)	8/13 (62%)	5/7 (71%)	3/9 (33%)	4/7 (57%)	3/6 (50%)	4/7 (57%)	4/6 (67%)
SUVmean	4/13 (31%)	6/16 (38%)	6/13 (46%)	1/7 (14%)	3/9 (33%)	2/7 (29%)	3/6 (50%)	3/7 (43%)	4/6 (67%)
SUVpeak	6/13 (46%)	6/16 (38%)	7/13 (54%)	3/7 (43%)	2/9 (22%)	3/7 (43%)	3/6 (50%)	4/7 (57%)	4/6 (67%)
SULmax	7/13 (54%)	5/19 (31%)	8/13 (62%)	4/7 (57%)	2/9 (22%)	4/7 (57%)	3/6 (50%)	3/7 (43%)	4/6 (67%)
SULmean	5/13 (38%)	5/19 (31%)	6/13 (46%)	3/7 (43%)	3/9 (33%)	2/7 (29%)	2/6 (33%)	2/7 (29%)	4/6 (67%)
SUL peak	6/13 (46%)	5/19 (31%)	7/13 (54%)	3/7 (43%)	2/9 (22%)	3/7 (43%)	3/6 (50%)	3/7 (43%)	4/6 (67%)

Other PET parameters were less concordant with CT4. SUL measurements are of uncertain significance (FDG does not go into fat and hence can exclude for normalisation, but this may not be true for FLT).

Looking at the data in more depth and subdividing into PR, SD and PD on CT4 (Table 6), we found that in cases with PR at CT4, there was good agreement with PET4 as they agreed in 83% cases (as also demonstrated on the ANOVA analysis). Looking at the MPM cases alone, this agreement increased to 100% at PET4 (in NSCLC it was 75%). All PET parameters showed a similar response. In SD cases, there was good early agreement with 100% agreement with SUVmax at PET2 and CT4, suggesting that early FLT PET-CT is as good as CT in predicting stable disease. In PD cases, agreement was poor, but there were very few cases.

Table 6 Treatment response on FLT PET-CT in agreement with CT4 divided into PR, SD and PD

	PR at CT4 (all)			PR at CT4 (MPM only)			PR at CT4 (NSCLC only)		
	PET2	PET3	PET4	PET2	PET3	PET4	PET2	PET3	PET4
SUVmax	2/6 (33%)	2/7 (29%)	5/6 (83%)	1/2 (50%)	1/3 (33%)	2/2 (100%)	1/4 (25%)	1/4 (25%)	3/4 (75%)
SUVmean	1/6 (17%)	2/7 (29%)	5/6 (83%)	0/2 (0%)	1/3 (33%)	2/2 (100%)	1/4 (25%)	1/4 (25%)	3/4 (75%)
SUVpeak	2/6 (33%)	3/7 (43%)	5/6 (83%)	1/2 (50%)	1/3 (33%)	2/2 (100%)	1/4 (25%)	2/4 (50%)	3/4 (75%)
SULmax	2/6 (33%)	1/7 (14%)	5/6 (83%)	1/2 (50%)	1/3 (33%)	2/2 (100%)	1/4 (25%)	0/4 (0%)	3/4 (75%)
SULmean	2/6 (33%)	2/7 (29%)	5/6 (83%)	1/2 (50%)	1/3 (33%)	2/2 (100%)	1/4 (25%)	1/4 (25%)	3/4 (75%)
SULpeak	2/6 (33%)	2/7 (29%)	5/6 (83%)	1/2 (50%)	1/3 (33%)	2/2 (100%)	1/4 (25%)	1/4 (25%)	3/4 (75%)
	SD at CT4 (all)			SD at CT4 (MPM only)			SD at CT4 (NSCLC only)		
	PET2	PET3	PET4	PET2	PET3	PET4	PET2	PET3	PET4
SUVmax	5/5 (100%)	5/6 (83%)	3/5 (60%)	3/3 (100%)	2/3 (67%)	2/3 (67%)	2/2 (100%)	3/3 (100%	1/2 (50%)
SUVmean	3/5 (60%)	4/6 (67%)	1/5 (20%)	1/3 (33%)	2/3 (67%)	0/3 (0%)	2/2 (100%)	2/3 (67%)	1/2 (50%)
SUVpeak	4/5 (80%)	3/6 (50%)	2/5 (40%)	2/3 (67%)	1/3 (33%)	1/3 (33%)	2/2 (100%)	2/3 (67%)	1/2 (50%)
SULmax	4/5 (80%)	4/6 (67%)	3/5 (60%)	2/3 (67%)	1/3 (33%)	2/3 (67%)	2/2 (100%)	3/3 (100%	1/2 (50%)
SULmean	3/5 (60%)	4/6 (67%)	1/5 (20%)	2/3 (67%)	2/3 (67%)	0/3 (0%)	1/2 (50%)	2/3 (67%)	1/2 (50%)
SULpeak	4/5 (80%)	3/6 (50%)	2/5 (40%)	2/3 (67%)	1/3 (33%)	1/3 (33%)	2/2 (100%)	2/3 (67%)	1/2 (50%)
	PD at CT4 (all)			PD at CT4 (MPM only)			no PD NSCLC		
	PET2	PET3	PET4	PET2	PET3	PET4			
SUVmax	1/2 (50%)	0/3 (0%)	0/2 (0%)	1/2 (50%)	0/3 (0%)	0/2 (0%)			
SUVmean	0/2 (0%)	0/3 (0%)	0/2 (0%)	0/2 (0%)	0/3 (0%)	0/2 (0%)			
SUVpeak	0/2 (0%)	1/3 (33%)	0/2 (0%)	0/2 (0%)	1/3 (33%)	0/2 (0%)			
SULmax	1/2 (50%)	0/3 (0%)	0/2 (0%)	1/2 (50%)	0/3 (0%)	0/2 (0%)			
SULmean	0/2 (0%)	0/3 (0%)	0/2 (0%)	0/2 (0%)	0/3 (0%)	0/2 (0%)			
SULpeak	0/2 (0%)	0/3 (0%)	0/2 (0%)	0/2 (0%)	0/3 (0%)	0/2 (0%)			

In terms of clinical outcomes in treatment response, it is important to know if the patient is progressing on treatment (so that it can be changed), hence progression and non-progression dichotomy is important for clinical management decisions. Therefore, we also grouped together the non-progressors (NP=PR+SD) and reanalysed (Table 7). In MPM non progressors, FLT SUVmax at PET 2 and PET 4 is concordant with CT4 in 80%; in NSCLC PET 4 is concordant with

CT4 in 67%, suggesting that in MPM, early FLT PET can predict early response to treatment better than in NSCLC.

Table 7. Response on FLT PET-CT agreement with CT4 in PD and non-progressors (NP= SD+PR)

	NP at CT4			NP at CT4 (MPM only)			NP at CT4 (NSCLC only)		
	PET2	PET3	PET4	scan2	scan3	scan4	scan2	scan3	scan4
SUVmax	7/11 (64%)	6/13 (46%)	8/11 (72%)	4/5 (80%)	3/6 (50%)	4/5 (80%)	3/6 (50%)	4/7 (57%)	4/6 (67%)
SUVmean	4/11 (36%)	6/13 (46%)	6/11 (55%)	1/5 (20%)	3/6 (50%)	2/5 (40%)	3/6 (50%)	3/7 (43%)	4/6 (67%)
SUVpeak	6/11 (55%)	6/13 (46%)	7/11 (64%)	3/5 (60%)	2/6 (33%)	3/5 (60%)	3/6 (50%)	4/7 (57%)	4/6 (67%)
SULmax	6/11 (55%)	5/13 (38%)	8/11 (73%)	3/5 (60%)	2/6 (33%)	4/5 (80%)	3/6 (50%)	3/7 (43%)	4/6 (67%)
SULmean	5/11 (45%)	5/13 (38%)	6/11 (55%)	3/5 (60%)	3/6 (50%)	2/5 (40%)	2/6 (33%)	2/7 (29%)	4/6 (67%)
SULpeak	6/11 (55%)	5/13 (38%)	7/11 (64%)	3/5 (60%)	2/6 (33%)	3/5 (60%)	2/6 (33%)	3/7 (43%)	4/6 (67%)
	PD at CT4			PD at CT4 (MPM only)			no PD NSCLC		
	scan2	scan3	scan4	scan2	scan3	scan4			
SUVmax	1/2 (50%)	0/3 (0%)	0/2 (0%)	1/2 (50%)	0/3 (0%)	0/2 (0%)			
SUVmean	0/2 (0%)	0/3 (0%)	0/2 (0%)	0/2 (0%)	0/3 (0%)	0/3 (0%)			
SUVpeak	0/2 (0%)	1/3 (33%)	0/2 (0%)	0/2 (0%)	1/3 (33%)	0/2 (0%)			
SULmax	1/2 (50%)	0/3 (0%)	0/2 (0%)	1/2 (50%)	0/3 (0%)	0/2 (0%)			
SULmean	0/2 (0%)	0/3 (0%)	0/2 (0%)	0/2 (0%)	0/3 (0%)	0/2 (0%)			
SULpeak	0/2 (0%)	0/3 (0%)	0/2 (0%)	0/2 (0%)	0/3 (0%)	0/2 (0%)			

In phase 1 trials, subdividing into responders and non-responders (NR=SD+PD) (Table 8) is a more relevant dichotomisation, as here you are looking for drug effect. In non-responders, PET 2 is concordant with CT4 in 86% overall, in 80% MPM and all NSCLC cases. In responders, PET 4 is concordant with CT4 in 83% overall, in all MPM cases and in 75% of responders NSCLC. However, as seen on the ANOVA analysis, these effects are not statistically significant.

Table 8. Response on FLT PET-CT agreement with CT4 in PR and non responders (NR= SD + PD)

	PR at CT4			PR at CT4 (MPM only)			PR at CT4 (NSCLC only)		
	scan2	scan3	scan4	scan2	scan3	scan4	scan2	scan3	scan4
SUVmax	2/6 (33%)	2/7 (29%)	5/6 (83%)	1/2 (50%)	1/3 (33%)	2/2 (100%)	1/4 (25%)	1/4 (25%)	3/4 (75%)
SUVmean	1/6 (17%)	2/7 (29%)	5/6 (83%)	0/2 (0%)	1/3 (33%)	2/2 (100%)	1/4 (25%)	1/4 (25%)	3/4 (75%)
SUVpeak	2/6 (33%)	3/7 (43%)	5/6 (83%)	1/2 (50%)	1/3 (33%)	2/2 (100%)	1/4 (25%)	2/4 (50%)	3/4 (75%)
SULmax	2/6 (33%)	1/7 (14%)	5/6 (83%)	1/2 (50%)	1/3 (33%)	2/2 (100%)	1/4 (25%)	0/4 (0%)	3/4 (75%)
SULmean	2/6 (33%)	2/7 (29%)	5/6 (83%)	1/2 (50%)	1/3 (33%)	2/2 (100%)	1/4 (25%)	1/4 (25%)	3/4 (75%)
SULpeak	2/6 (33%)	2/7 (29%)	5/6 (83%)	1/2 (50%)	1/3 (33%)	2/2 (100%)	1/4 (25%)	1/4 (25%)	3/4 (75%)

	NR at CT4			NR at CT4 (MPM only)			NR at CT4 (NSCLC only)		
	scan2	scan3	scan4	scan2	scan3	scan4	scan2	scan3	scan4
SUVmax	6/7 (86%)	5/9 (56%)	3/7 (43%)	4/5 (80%)	2/6 (33%)	2/5 (40%)	2/2 (100%)	3/3 (100%)	1/2 (50%)
SUVmean	3/7 (43%)	4/9 (44%)	1/7 (14%)	1/5 (20%)	2/6 (33%)	0/5 (0%)	2/2 (100%)	2/3 (67%)	1/2 (50%)
SUVpeak	4/7 (57%)	4/9 (44%)	2/7 (29%)	2/5 (40%)	2/6 (33%)	1/5 (20%)	2/2 (100%)	2/3 (67%)	1/2 (50%)
SULmax	5/7 (71%)	4/9 (44%)	3/7 (43%)	3/5 (60%)	1/6 (17%)	2/5 (40%)	2/2 (100%)	3/3 (100%)	1/2 (50%)
SULmean	6/7 (86%)	5/9 (56%)	3/7 (43%)	4/5 (80%)	2/6 (33%)	2/5 (40%)	2/2 (100%)	3/3 (100%)	1/2 (50%)
SULpeak	4/7 (57%)	3/9 (33%)	2/7 (29%)	2/5 (40%)	1/6 (17%)	1/5 (20%)	2/2 (100%)	2/3 (67%)	1/2 (50%)

To summarise this section, ANOVA analysis reveals that in the combined dataset (all subjects), response to treatment demonstrated on CT4 in terms of change from baseline (21.9% decrease in RECIST length), is also seen in PET4 and the change is even greater on PET (mean decrease of 36.5% in SUVmax); however, these treatment response changes are not clearly demonstrated at a statistically significant level on the earlier PETs.

However, FLT SUVmax treatment response on early PET (PET2) in terms of PR, SD and PD can predict end of treatment response on RECIST (using CT4 as gold standard) in more than 50% of cases (62% cases overall) and better in MPM (71%) than NSCLC (50%). In cases of PR, there was also good agreement in PET4 with CT4 with (83% overall, 100% in MPM and 75% in NSCLC).

2.2.3 Comparison of early and end of treatment PET and CT measures

ANOVA

The initial analysis assumed CT4 as the "gold standard" in the comparison of ADIPEMCIS treatment response on PET and CT. However, as there is no imaging gold standard, we considered other endpoints such as overall survival (OS) and progression free survival (PFS); unfortunately, the sample size was considered too small. Therefore, as a secondary analysis, we looked at the concordance and discordance of the PET and CT data at different timepoints, namely "early" (PET 3 and CT2) and "end of treatment (EOT)" or "late" (PET4 and CT4), under the hypothesis that decreased proliferation is highly suggestive of drug effect and precedes any change in size. PET3 and CT2 were at slightly different timepoints (PET3 after one cycle of treatment, with CT2 after 2 cycles). PET4 and CT4 were both at the end of treatment, at approximately 18 weeks for MPM and 12 weeks for NSCLC.

This secondary analysis ANOVA assumes the data is normally distributed so this assumption was explored using the Shapiro-Wilks test and no significant deviation from normality was found.

The 3-way ANOVA results showing main effects of time, modality and group and their 2-way and 3-way interactions is shown in Table 9.

Table 9. Summary ANOVA table

Effect	F ratio	Significance
Time	14.804	< 0.001
Group	.011	.918
Modality	.130	.720
Time * Group	.116	.736
Time * Modality	7.530	.009
Group * Modality	11.088	.002
Time * Group * Modality	.111	.740

Effect of Time

Significant main effects were only revealed for time (p<0.001), with EOT having a larger negative change (reduction in value) than early scans: -28.2% compared to -5.5% respectively (see Table 10). The estimated confidence intervals suggest the EOT scans showed a real change while the early scans did not.

Hence the primary observation from this analysis is that the EOT scan time point revealed a significantly negative change, which was not observed in (and was significantly different to) the early time point.

Table 10. Post-hoc means & differences between time points in all patients (18 total; 10 MPM and 8 NSCLC)

Estimates					
Time	Mean Change from Baseline to Timepoint (*)	Std. Error	df	95% Confidence Interval	
				Lower Bound	Upper Bound
Early	-5.503	5.926	23.229	-17.754	6.749
EOT	-28.156	6.305	27.044	-41.091	-15.221

Pairwise Comparisons						
Time	Time	Mean Difference in time	Std. Error	df	Sig.	95% Confidence Interval for Difference	
						Lower Bound	Upper Bound
Early	EOT	22.654	5.888	41.436	<0.001	10.767	34.540

(*) Early- mean change in RECIST length from baseline to CT2 and SUVmax from baseline to PET3;
EOT- mean change in RECIST length from baseline to CT4 and SUVmax from baseline to PET4.

2-way Interaction between Time and Modality

A significant 2-way interaction was found between time and modality (p = 0.009). Table 11 shows the estimated means and differences between time & modality. This interaction effect appears to be driven by a difference between the modality only in the early scans with CT2 showing a significantly greater change than PET3 (-14.6% vs 3.6%, p = 0.026).

Hence CT scans appear to show a significant decrease at the early scan which is not observable in the PET scan, therefore, a decrease in size (RECIST length) appears to precede a decrease in proliferation (SUVmax), which does not support our hypothesis. However, it is important to note that PET3 at 2 weeks (after one cycle), preceded CT2 (after 2 cycles) by 3 weeks and it is possible that the changes on CT may not have been observed if the early CT had been performed at the earlier PET 3 time-point, namely at 2 weeks.

At the EOT timepoint, post hoc analysis revealed a significant decrease in both CT and PET measures (consistent with the primary observation), but no statistically difference between modalities (p=0.115).

Table 11. Post-hoc means & differences of time and modality (p=0.009)

Estimates						
Time	Modality	Mean Change in Image Session and Timepoint (*)	Std. Error	df	95% Confidence Interval	
					Lower Bound	Upper Bound
Early	CT2	-14.588	6.998	38.903	-28.743	-.433
	PET3	3.582	7.227	40.576	-11.017	18.182
EOT	CT4	-21.182	7.355	41.757	-36.027	-6.337
	PET4	-35.131	7.934	46.913	-51.092	-19.169

Pairwise Comparisons							
Time	Modality	Modality	Mean Difference in Modalities	Std. Error	df	Sig.	95% Confidence Interval for Difference[c]
							Lower Bound	Upper Bound
Early	CT2	PET3	-18.170*	7.869	40.968	.026	-34.063	-2.277
EOT	CT4	PET4	13.949	8.665	40.746	.115	-3.553	31.450

(*) Early CT2- mean change in RECIST length from baseline to CT2;
Early PET3- mean change in SUVmax from baseline to PET3;
EOT CT4- mean change in RECIST length from baseline to CT4;
EOT PET4 – mean change in SUVmax from baseline to PET4.

2-way Interaction between Group and Modality

A significant 2-way interaction was found between and group and modality (p = 0.002). Table 12 shows the estimated means & differences between group & modality. Here, it appears in the MPM group, PET scans show a significant decrease in proliferation compared to CT (-26.1% vs -8.7% respectively, p = 0.031). Conversely, in the NSCLC group change in CT measures were more negative than PET (-27.1% vs -5.5%, p = 0.018). The significant interaction of modality and group appears to be driven by changes in PET measures in the MDM group, and conversely by CT measures in the NSCLC group.

Table 12. Post-hoc means & differences of group and modality (p=0.002)

Estimates						
Group	Modality	Mean Change in Modality Measure (*)	Std. Error	df	95% Confidence Interval	
					Lower Bound	Upper Bound
MPM	CT	-8.704	7.927	23.590	-25.080	7.671
	SUVmax	-26.081	8.240	26.580	-43.001	-9.162
NSCLC	CT	-27.066	8.915	23.765	-45.475	-8.656
	SUVmax	-5.467	9.402	26.559	-24.774	13.840

Pairwise Comparisons							
Measure 1 (RECIST length)	Measure 2 (SUV max)	Mean Difference in Measures	Std. Error	df	Sig.	95% Confidence Interval for Difference[c]	
						Lower Bound	Upper Bound
CT	SUVmax	17.377[*]	7.753	40.506	.031	1.714	33.040
CT	SUVmax	-21.599[*]	8.769	41.113	.018	-39.307	-3.891

(*) CT modality measure is RECIST length; PET modality measure is SUVmax

Despite the overlap of main effects in 2-way interactions, 3-way interactions were not observed to be significant and a strong consistent message across the board is less obvious. The higher p-

values in the post-hoc pairwise comparisons may not survive stricter multiple comparison corrections and reflect this.

Correlation of PET parameters

In a tertiary analysis, the 3-way ANOVA model was repeated using a linear mixed effect model in SPSS as with the secondary analysis, however all 8 SUV measures were included. Not surprisingly, the SUV measures all show strong ($r > 0.8$) and highly significant ($p < 0.001$) correlation coefficients with each other (Table 13).

Table 13. Percentage change in all PET parameters

Overall response on PET								
	PR			**SD**			**PD**		
	PET2	**PET3**	**PET4**	**PET2**	**PET3**	**PET4**	**PET2**	**PET3**	**PET4**
SUV max	20%	24%	69%	67%	65%	31%	13%	12%	0%
SUV mean	13%	18%	77%	73%	65%	15%	13%	18%	8%
SUV peak	20%	35%	77%	73%	35%	23%	7%	29%	0%
SUL max	20%	18%	69%	67%	65%	31%	13%	18%	0%
SUL mean	20%	12%	77%	67%	71%	15%	13%	18%	8%
SUL peak	20%	29%	77%	20%	29%	77%	7%	29%	0%

MPM response on PET								
	PR			**SD**			**PD**		
	PET2	**PET3**	**PET4**	**PET2**	**PET3**	**PET4**	**PET2**	**PET3**	**PET4**
SUV max	25%	30%	71%	63%	60%	29%	13%	10%	0%
SUV mean	13%	20%	86%	63%	70%	0%	25%	10%	14%
SUV peak	25%	40%	86%	63%	30%	14%	13%	30%	0%
SUL max	25%	30%	71%	50%	50%	29%	25%	20%	0%
SUL mean	13%	20%	86%	63%	70%	0%	25%	10%	14%
SUL peak	25%	40%	86%	63%	30%	14%	13%	30%	0%

NSCLC response on PET								
	PR			**SD**			**PD**		
	PET2	**PET3**	**PET4**	**PET2**	**PET3**	**PET4**	**PET2**	**PET3**	**PET4**
SUV max	14%	14%	67%	71%	71%	33%	14%	14%	0%
SUV mean	14%	14%	67%	86%	57%	33%	0%	29%	0%
SUV peak	14%	29%	67%	86%	43%	33%	0%	29%	0%
SUL max	14%	0%	67%	86%	86%	33%	0%	14%	0%
SUL mean	29%	0%	67%	71%	71%	33%	0%	29%	0%
SUL peak	14%	14%	67%	86%	57%	33%	0%	29%	0%

2.2.4 Response rate assessment on PET and CT

A change in SUVmax from baseline was used to assess treatment response on FLT PET-CT using EORTC criteria for PR, SD and PD at timepoints PET2,3 and 4; and this was compared to RECIST response on CT at the same/similar timepoints(CT3 after 2 cycles and CT4 at EOT).

In patients with MPM (all subtypes included), the PR rate (number of subjects demonstrating PR out of total number of subjects with PET scan at that particular time-point) was 25% at PET2; increased to 30% at PET3 and increased further to 71% at PET4 (Table 14, Figures 11, 17, 18). The PR rate on CT was lower at 33% at the end of treatment (Figure 12). This is in line with the ANOVA result above.

Table 14. MPM: Response on FLT PET-CT and CT

	MPM response on PET				MPM response on CT		
	PET2	PET3	PET4	No early CT	CT3	CT4
PR	2/8 (25%)	3/10 (30%)	5/7 (71%)		2/10 (20%)	3/9 (33%)
SD	5/8 (62.5%)	6/10 (60%)	2/7 (29%)		7/10 (70%)	3/9 (33%)
PD	1/8 (12.5%)	1/10 (10%)	0 (0%)		1/10 (10%)	3/9 (33%)
total	8	10	7		10	9

Figure 11. MPM response on FLT PET-CT in n=10 patients
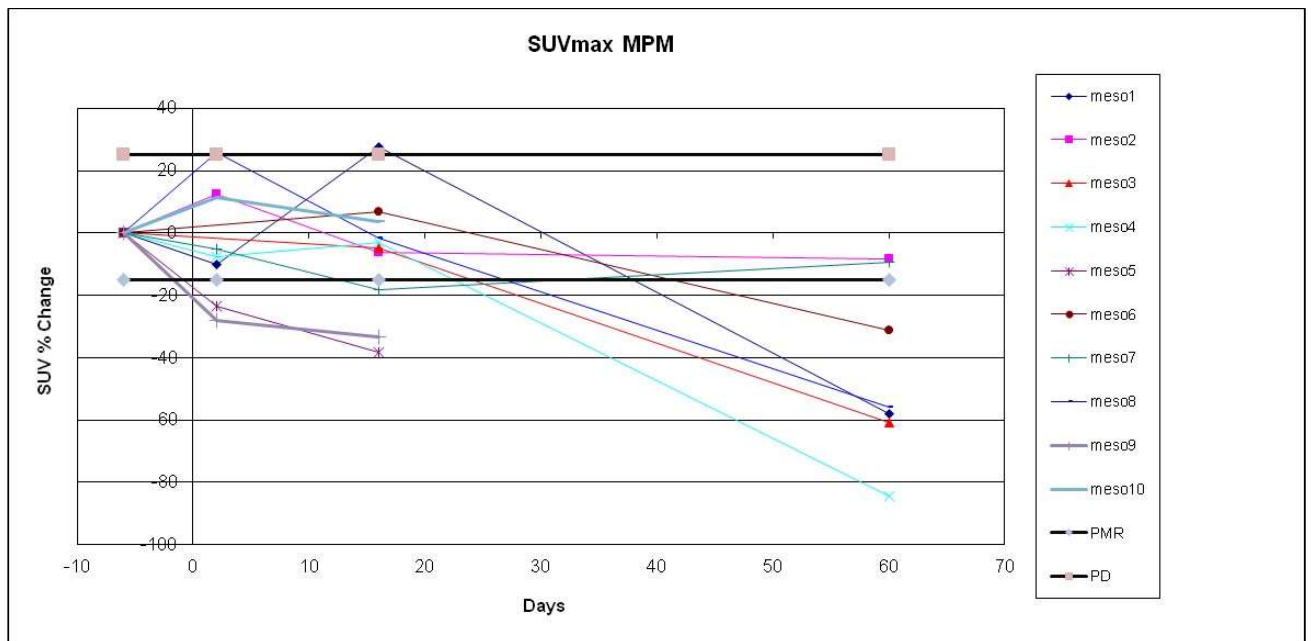
Figure 12. MPM response on CT in n=10 patients
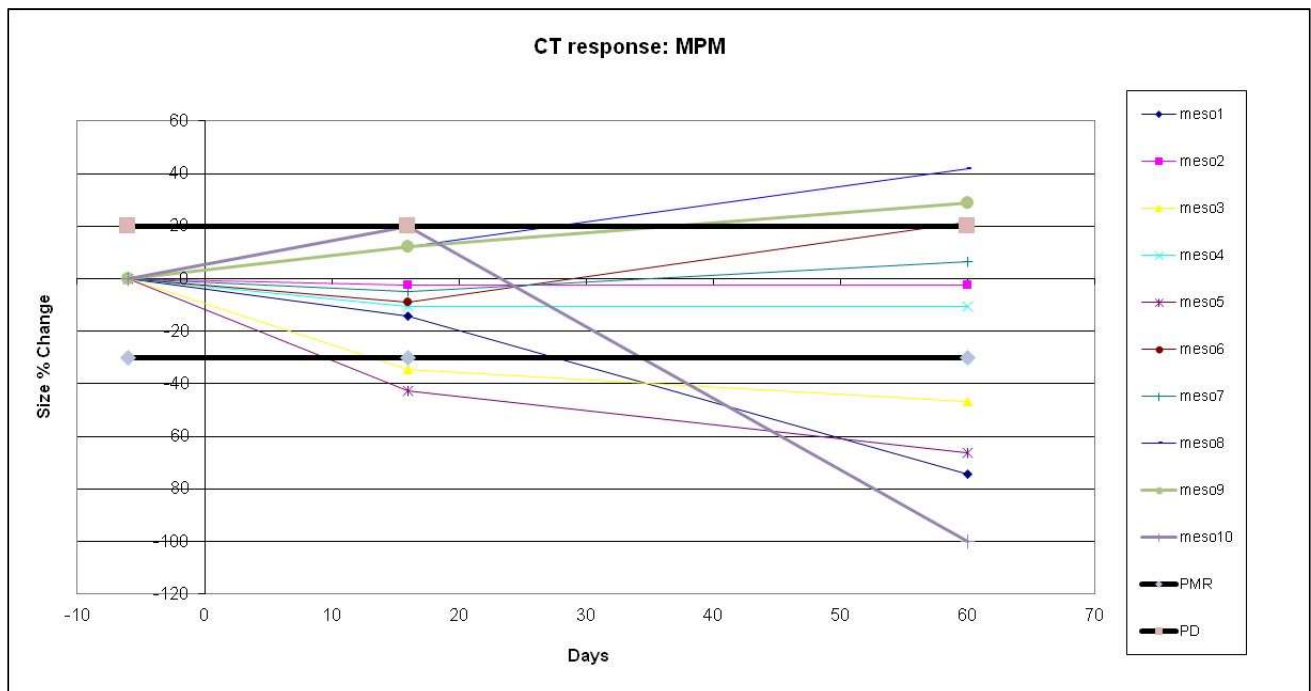
In NSCLC subjects, the PR rate on PET was 14% at PET2 and PET3, but increased to 67 % at PET4 (Table 15, Figure 13). The PR rate on CT was slightly lower at 57% at the end of treatment (Figure 14).

Table 15. NSCLC: Response on FLT PET-CT and CT

	NSCLC response on PET			NSCLC response on CT		
	PET2	PET3	PET4	No early CT	CT3	CT4
PR	1/7 (14%)	1/7 (14%)	4/6 (67%)		2/8 (25%)	4/7 (57%)
SD	5/7 (71%)	5/7 (71%)	2/6 (33%)		6/8 (75%)	3/7 (43%)
PD	1/7 (14%)	1/7 (14%)	0 (0%)		0 (0%)	0 (0%)
total	7	7	6		8	7

Figure 13. NSCLC response on FLT PET-CT in n=8 patients
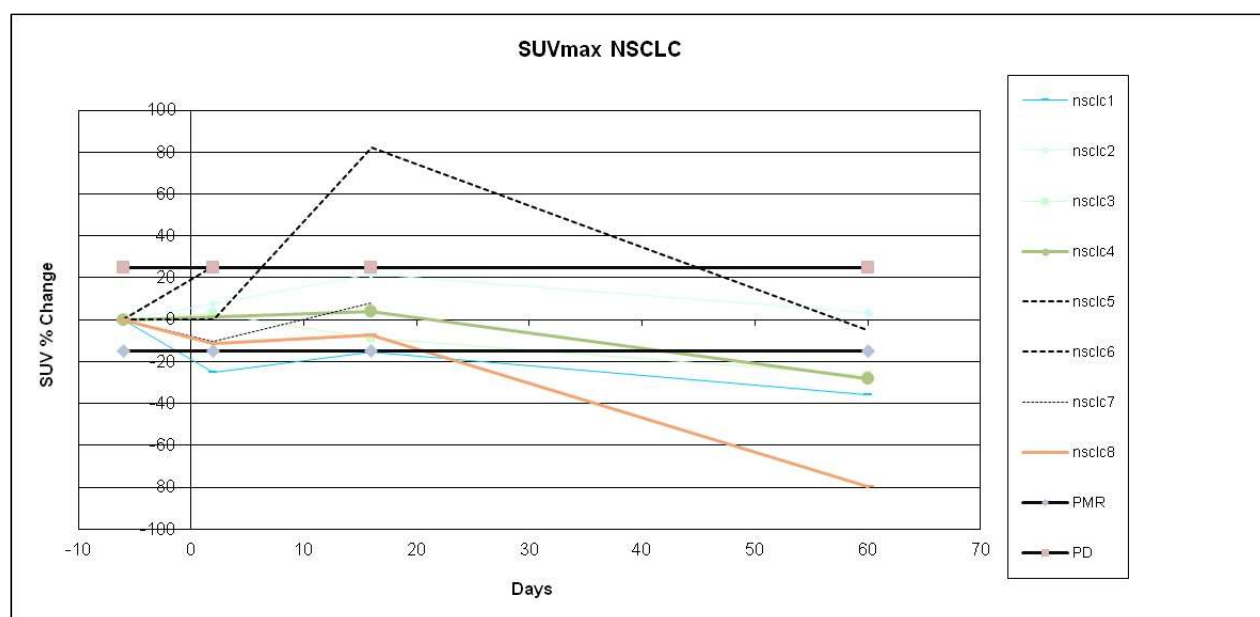
Figure 14. NSCLC response on CT in n=8 patients
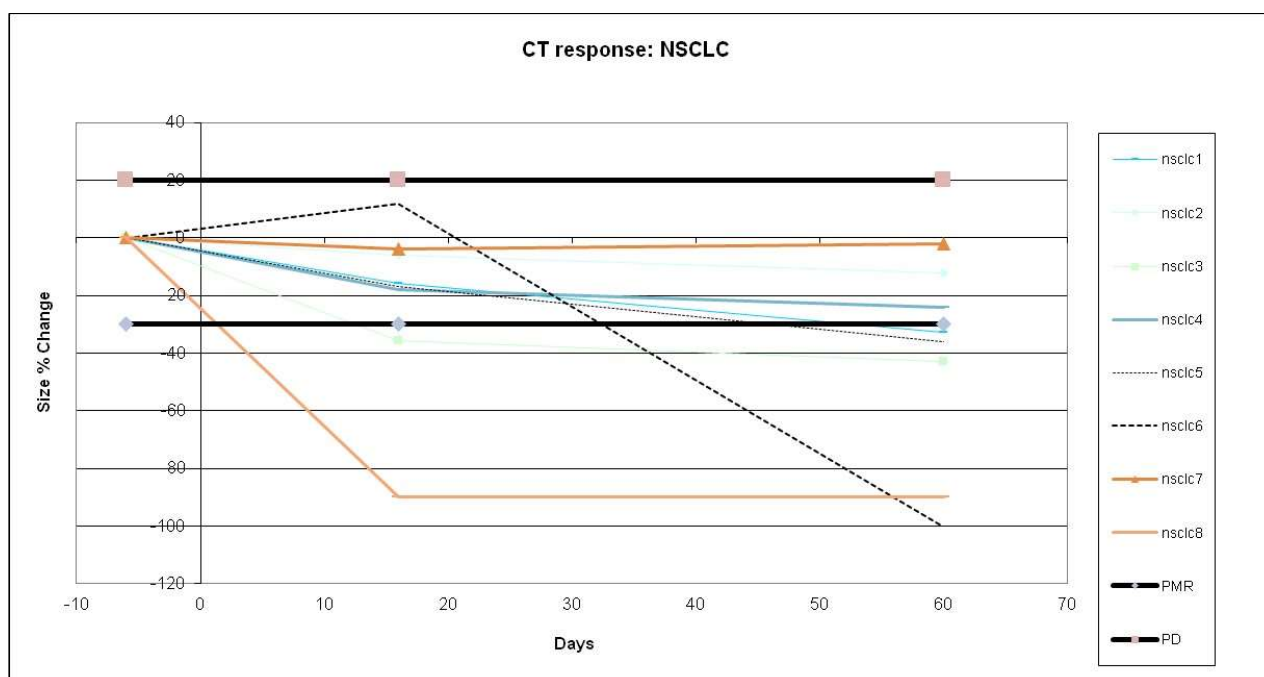
When considering combined MPM and NSCLC data, the PR rate overall was 20% at PET2; increased to 24% at PET3 and increased again to 69% at PET4 (Table 16, Figure 15). The PR rate on CT was lower at 44% at the end of treatment (Figure 16). The early CT (at approximately 5 weeks), demonstrates stable disease in the majority of cases in all groups, namely 70%, 75% and 73% in MPM, NSCLC and combined data, respectively.

Table 16. Combined (MPM+ NSCLC): Response on FLT PET-CT and CT

	Overall response on PET				Overall response on CT		
	PET2	PET3	PET4		No early CT	CT3	CT4
PR	3/15 (20%)	4/17 (24%)	9/13 (69%)			4/18 (22%)	7/16 (44%)
SD	10/15 (67%)	11/17 (65%)	4/13 (31%)			13/18 (72%)	6/16 (38%)
PD	2/15 (13%)	2/17 (12%)	0 (0%)			1/18 (6%)	3/16 (19%)
total	15	17	13			18	16

Figure 15. Combined data response on FLT PET-CT in n=18 patients

Figure 15. Combined data response on FLT PET-CT in n=18 patients

Figure 16. Combined response on CT in n=18 patients
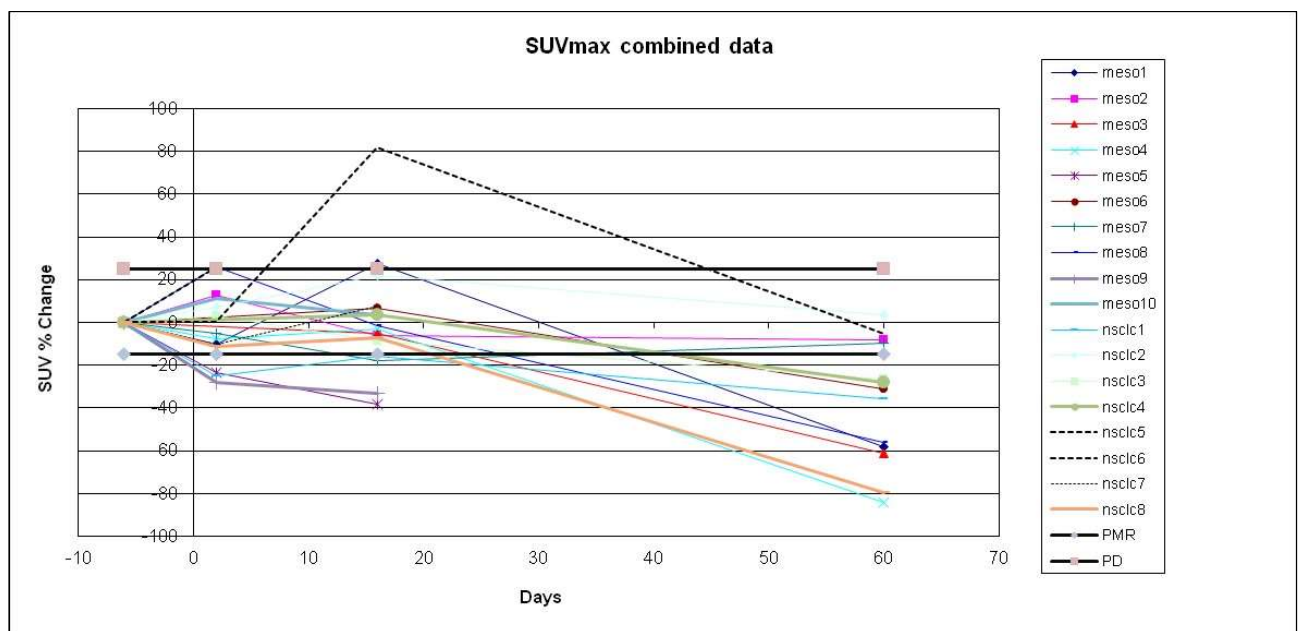
Figure 16. Combined response on CT in n=18 patients
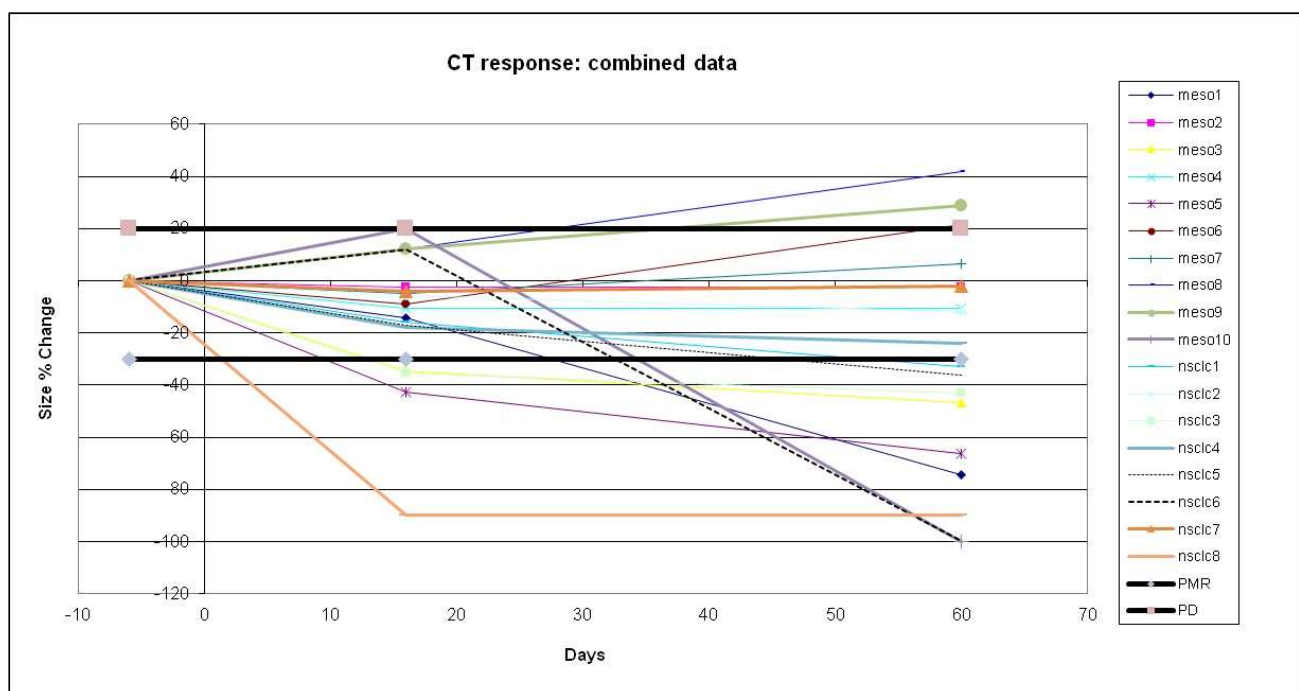
FLT PET-CT proliferation imaging showed greater treatment response to ADIPEMCIS therapy than CT at end of treatment (so appears to be a biomarker for end of treatment response).

Figure 17. FLT PET-CT in epithelioid MPM

a) baseline SUVmax = 9.4; (b) post ADI-PEG20 at 24hrs, the SUVmax reduces to 8.9 (5% reduction hence SD); (c) post cycle 1 of combined therapy, the SUVmax decreases further to 7.7 (18% reduction from baseline hence PR); however at (d) end of treatment, the SUVmax increases minimally to 8.5 (10% reduction from baseline hence SD). CT also showed overall SD at end of treatment (although at this slice visually there appears to be a PR, the average of 3 measurements revealed a 7% increase in RECIST length at end of treatment).
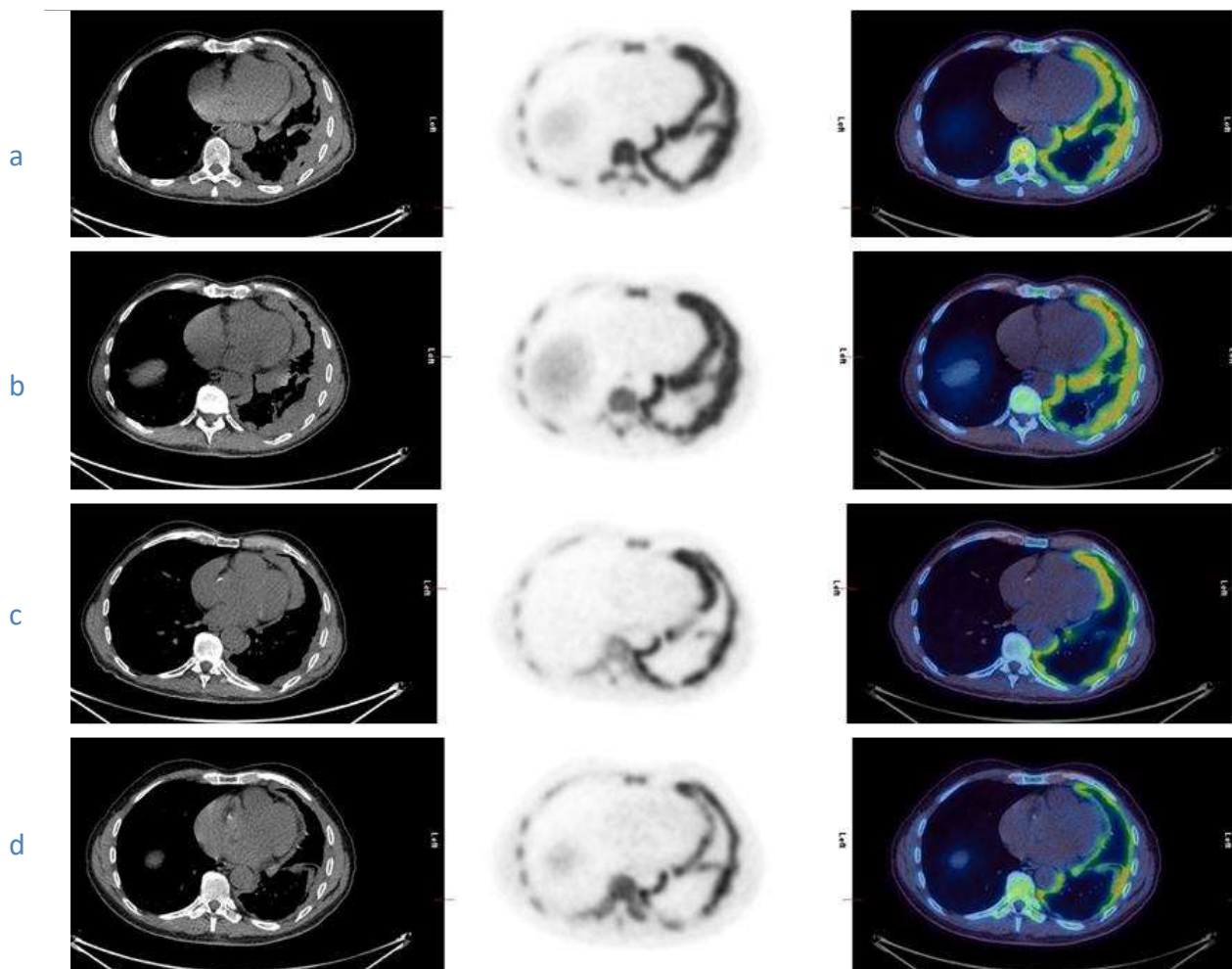
Figure 18. FLT PET-CT in biphasic MPM

a) baseline SUVmax=6.4; (b) post ADI-PEG20 at 24hrs, the SUVmax reduces to 5.9 (8% reduction hence SD); (c) post cycle 1 of combined therapy, the SUVmax increased minimally to 6.2 (maintained SD); however at (d) end of treatment, the SUVmax decreases significantly to 1.0 (84% reduction from baseline hence PR). CT overall showed SD (although again visually there appears to be PR at this slice, an average of 3 measurements revealed a 10% decrease in RECIST length at end of treatment).
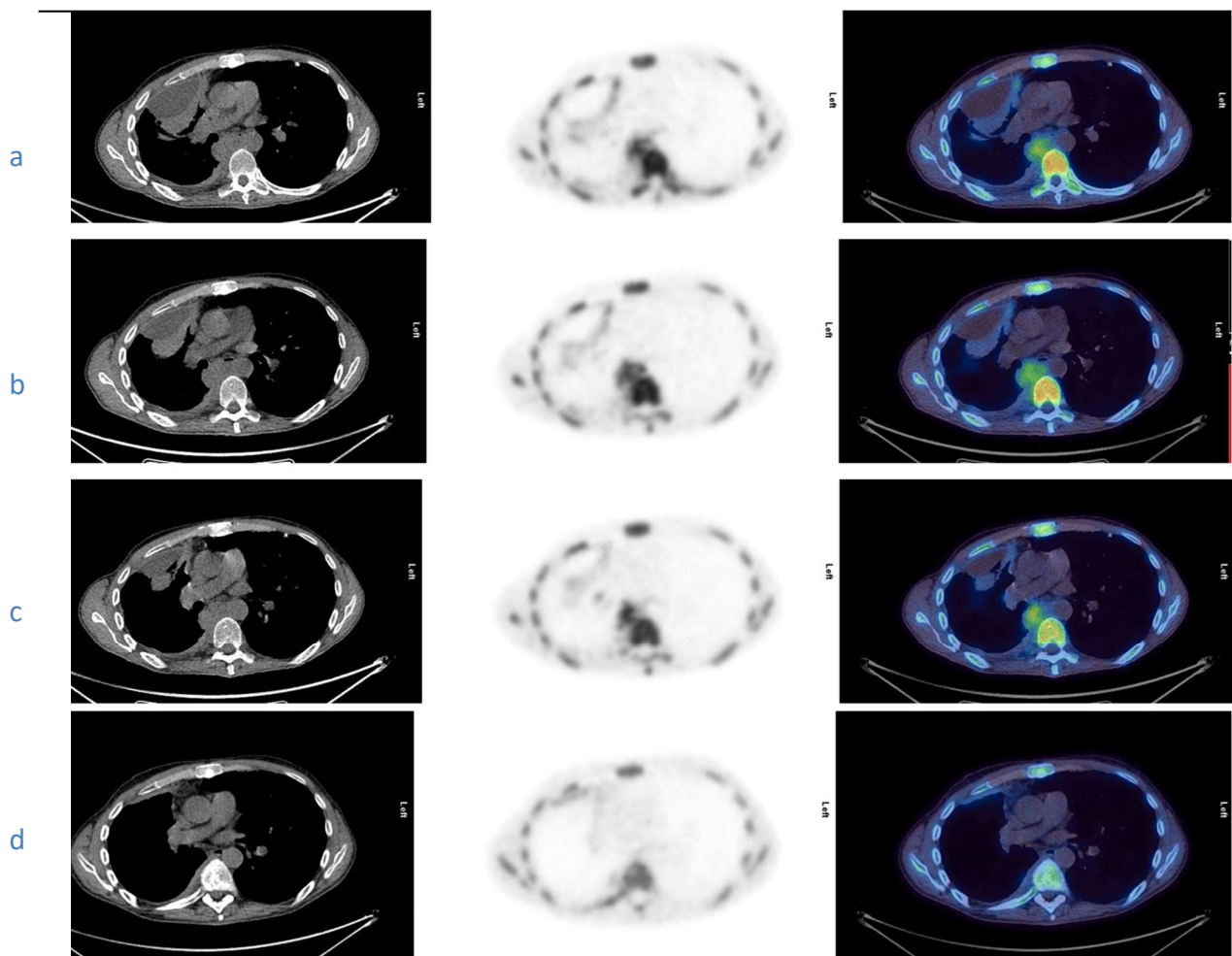
Figure 19. FLT PET-CT in NSCLC

(a) baseline where primary lesion has SUVmax=6.4; (b) post ADI-PEG20 at 24hrs, the SUVmax reduces to 4.8 (25% reduction hence PR); (c) post cycle 1 of combined therapy, the SUVmax increases slightly to 5.4; however at (d) end of treatment, the SUVmax decreases further to 4.1 (36% reduction from baseline) and hence PR is maintained. CT also shows a PR at end of treatment with a 33% reduction in size.
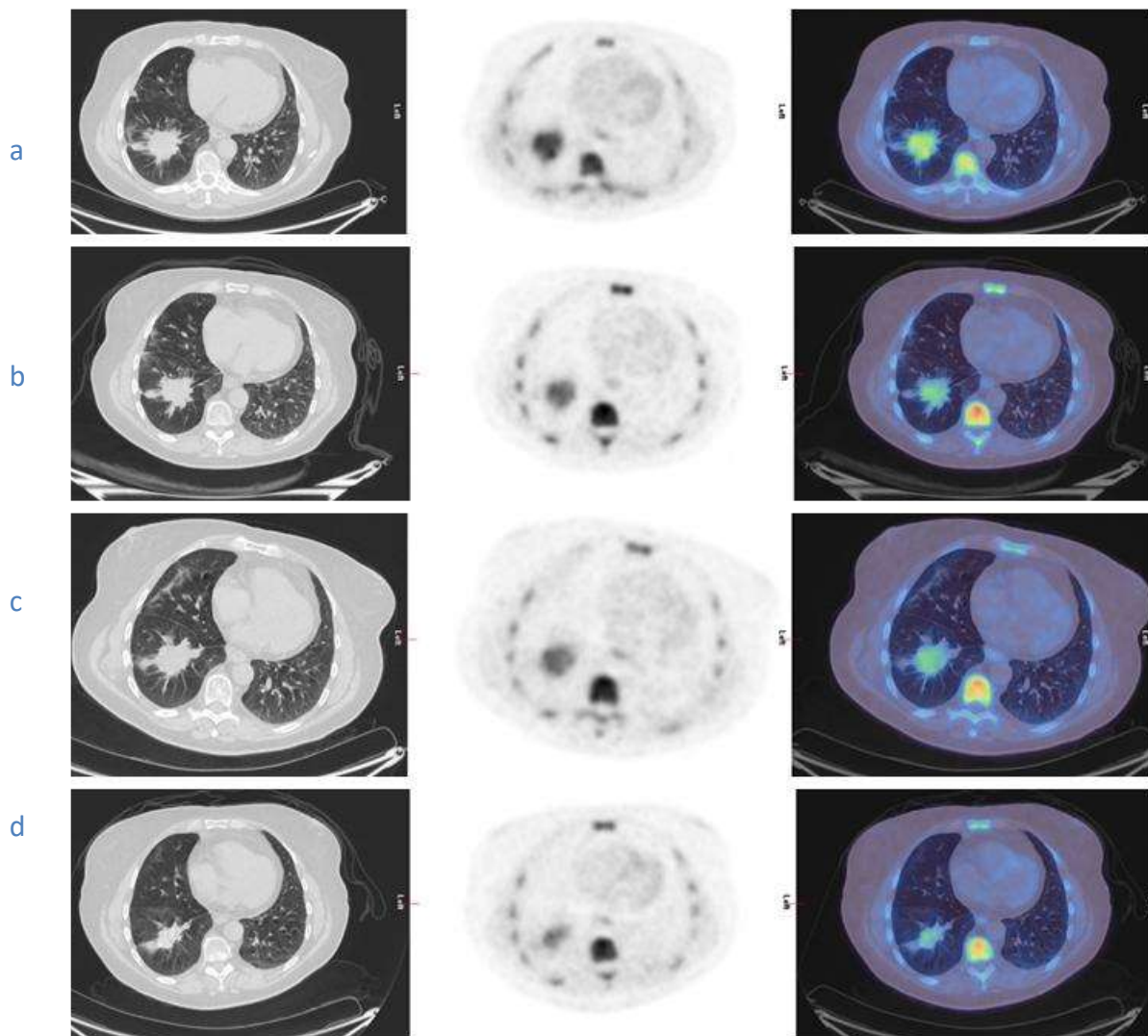
2.2.5 Summary of results

The main findings from our study are:

ANOVA analysis (using CT4 as the gold standard) revealed that response to treatment was greater on PET4 (mean decrease of 36.5% in SUVmax), than CT4 (21.9% decrease in RECIST length); however, these response changes are not clearly demonstrated on the earlier PETs.

FLT PET-CT SUVmax treatment response at PET2 in terms of PR, SD and PD can predict end of treatment response on RECIST (using CT4 as gold standard) in nearly 2/3 of cases (62% cases overall) and better in MPM (71%) than NSCLC (50%), however the SUVmax reduction from baseline to PET2 is not statistically significant and there is no difference between the MPM and NSCLC groups.

In cases of PR, there is good agreement in PET4 with CT4 with (83% overall, 100% in MPM and 75% in NSCLC); and no significant difference between CT and SUVmax at the end of treatment.

At the early imaging time point (post 1 cycle on PET3 and 2 cycles on CT), there is a statistically significant difference (p =0.026) in the way CT and SUVmax measures behave, with the greater decrease seen in RECIST length on CT than SUVmax on PET. At the EOT timepoint, there is a significant decrease in both CT and PET measures, but no statistically difference between modalities (p=0.115). Hence changes in proliferation do not precede changes in size, as at no earlier timepoint is there are a significant difference between RECIST length and SUVmax reduction. The MPM group shows predominantly decrease in SUVmax (26%, p=0.031) whereas the NSCLC group show decrease mainly in RECIST length (27%, p=0.018), irrespective of time.

All PET parameters show strong correlation (r >0.8) which is highly significant (p < 0.001). SUVmax was the most reliable, as it was concordant with CT4 in 62% at PET2 and PET4.

FLT PET-CT proliferation imaging showed greater treatment response to ADIPEMCIS therapy than CT at end of treatment (so appears to be a biomarker for end of treatment response).

2.3 Discussion

TRAP was the first study in humans of FLT PET evaluating the response of MPM and NSCLC to systemic treatment using arginine deprivation with ADI-PEG20 alone and in combination with chemotherapy.

This study shows that FLT PET is at least as good as CT in demonstrating treatment response, at end of treatment. FLT is known to be a biomarker of cellular proliferation and advantages of FLT over FDG in monitoring treatment response have been described. Buck et al. assessed the correlation between FLT uptake and lung tumour proliferation and concluded FLT uptake correlated well with Ki-67 staining in malignant primary lung tumours (88). Other studies in lung cancer have shown conflicting results on the relationship between Ki-67 and FLT uptake, with some studies confirming a good correlation and others presenting negative results. A study looking at change in FLT SUVmax between baseline and 7 days after the start of gefitinib therapy in patients with adenocarcinoma of the lung found that responders (as defined on CT evaluation at 6 weeks) had a significantly different change in SUVmax than non-responders ($-36.0 \pm 15.4\%$ versus $10.1 \pm 19.5\%$, respectively; $p < 0.001$)(91).

We did not directly compare FDG and FLT PET in this study, however, this has been evaluated in other studies. In one study in NSCLC patients who underwent EGFR kinase inhibitor treatment found that change in FDG SULpeak from baseline to 3 weeks post-treatment was significantly better than change in FLT SULpeak at predicting overall survival and progression-free survival (109). Interestingly, Everitt et al. evaluated differential FDG and FLT uptake on serial PET-CT imaging before and during definitive chemoradiation for NSCLC and found that FLT PET-CT was a more sensitive tracer of early treatment response (weeks 2 and 4) than FDG PET-CT (110). Tian et al. (90), found that in 55 patients with pulmonary nodules who underwent FDG and FLT PET within 7 days, the sensitivity and specificity for FDG was 87.5% and 58.9% and 68.7% and 76.9% for FLT. The combination of the two improved sensitivity to 100% and specificity to 89.7%.

We found that a very early scan at 24 hours after ADI therapy is able to predict end of treatment RECIST response in 62% of cases. In a study looking at FLT PET-CT in pemetrexed therapy in

NSCLC, a non-systematic reduction in FLT uptake was observed 4 hours after pemetrexed administration. However, the association between FLT uptake and treatment response was not significant (111). A very recent publication, looking at early response assessment to targeted therapy using FLT in lung cancer, showed early response demonstrated at 4 weeks and in one case at 9 days (112).

We evaluated multiple PET parameters, including maximum standard uptake value adjusted for lean body mass, SULmax, as this had been evaluated in a prior study by Crandall et al. (82) and is consistent with PERCIST criteria evaluation. We found good correlation between all parameters (r >0.8, p <0.001), but used SUVmax in the majority of our study as this parameter showed most consistent overall agreement with end of treatment CT and can predict end of treatment response (on RECIST) in more than 50% of cases (62% cases overall) although better in MPM (71%) than NSCLC (50%).

Crandall had looked at percentage change in FLT and FDG uptake (as measured by SULmax,) between baseline and after one cycle of chemotherapy in NSCLC patients categorised by RECIST 1.1 CT as responders or non-responders after two cycles of therapy (docetaxel + cisplatin). Post cycle one, non-responders had mean SULmax increases of 7.0 and 3.4% for FDG and FLT, respectively. Responders had mean decreases of 44.8 and 32.0% in FDG and FLT SULmax, respectively. Post cycle one, primary tumour FDG SUL values were significantly lower in responders than in non-responders (P = 0.016), but primary tumour FLT SUL values did not differ significantly between these groups. The study concluded that fractional decrease in FDG SULmax from baseline to post-cycle 1 imaging was significantly different between anatomic responders and non-responders (also seen in the ADAM study, but using SUVmax), while percentage changes in FLT SULmax were not significantly different between these groups over the same period of time. PERCIST measurements on FLT PET-CT use SUL parameters, however, although we attempted to use these, we found it difficult to accurately delineate pleural MPM tumoural uptake (as explained in "methods" section); hence, we did not use PERCIST criteria.

Our hypothesis does not hold as a decrease in proliferation does not seem to precede a change in size. Nevertheless, treatment response was correctly predicted at 24 hours in 62% cases. Also, it is important to note that the "early" PET at 2 weeks, preceded the "early" CT by 2-3 weeks and

it is possible that the changes on CT may not have been observed if the early CT had been performed at an earlier time-point, namely at 2 weeks. Early phase combination trials of ADI-PEG20 with chemotherapy are reporting increased efficacy, and sustained arginine depletion with reduced immunogenicity of ADI-PEG 20 (42). In thoracic cancers this multimodality strategy has instigated the phase 2/3 ATOMIC-meso trial of pemetrexed and cisplatin with or without ADI-PEG 20 focusing on chemorefractory (non-epithelioid) MPMs.

Recent and as yet unpublished work by Szlosarek et al from an expansion group of the TRAP study of n=31 participants (primarily looking at safety and resistance) showed disease control rate of 93.5% and partial response 35.5% at 18 weeks. Post ADI therapy biopsies from 6 participants who had progressed showed that there were 4 mechanisms of resistance, which could help explain our findings. Firstly there was patchy tumoural re-expression of ASS1 (thus recycling of citrulline to arginine); autophagy (degradation and recycling of cellular components; increased tumour associated macrophages which were significant (p=0.02) in ASS1 tumour areas; and changes in the tumour microenvironment, including increased tumoural programmed death ligand 1 (PD-L1) expression.

2.3.1 Limitations

We do not have FLT test retest data in this study, but we have assumed that this is similar to published literature (113) (*test-retest* r ≥ 0.97 on serial baseline scans in a study on breast cancer).

A major limitation of our study is that there is no biochemical marker to act as the gold standard and we are relying on RECIST data, as there was no better surrogate marker of response available. However, RECIST response looks at changes in size, whereas FLT PET-CT looks at changes in proliferation. The number of patients is also too small to reliably compare to OS or PFS.

These patients are typically unwell symptomatically due to the significant burden of disease and thus difficult to recruit. This was a longitudinal study and a number of patients were unable to complete the full imaging protocol due to morbidity. Tracer production and quality control was also an issue and the availability of tracer only once a week meant that there was little flexibility. A change in day of production of tracer halfway through the study meant that the patients were needing ADI-PEG20 administration on a Sunday. Also, the cohorts for EORTC and RECIST assessment had early imaging at different time points.

2.3.2 Conclusion

The TRAP substudy shows that early FLT PET-CT (at 24 hours post ADI therapy) is predictive of the end of treatment CT results in nearly 2/3 cases and FLT PET-CT does provide evidence of response to ADI therapy in ASS1-deficient thoracic tumours which appears higher than the RECIST 1.1 response rate at the end of treatment. This study therefore provides molecular validation for arginine deprivation with ADI-PEG20 in targeting thymidine uptake as a treatment for ASS1-deficient thoracic tumours, however, decrease in proliferation does not seem to precede a change in size.

Chapter 3 ADAM Substudy

3.1 Methodology

ADAM was a phase 2 clinical trial (NCT01279967) of ADI-PEG 20 and best supportive care vs best supportive care alone in patients with malignant pleural mesothelioma (ADAM). Written informed consent for each patient and ethical approval for the study was obtained (09/H1102/107) as well as approvals from MHRA and ARSAC. I was a co-Investigator in this study responsible for supervising and overseeing the PET studies, ensuring the PET studies were performed in accordance with the protocol and good clinical practice (GCP). I also was the central reviewer of all PET-CT studies performed at several sites in the UK.

3.1.1 Participants

From March 2011 to June 2013, 86 patients at 6 centres, with histologically proven advanced ASS1-deficient MPM (defined as >50% ASS1 loss) and measurable disease by modified Response Evaluation Criteria in Solid Tumours (RECIST) criteria were recruited into the phase 2 randomised, non-blinded trial to receive a weekly intramuscular injection of ADI-PEG20 (36.8 mg/m2) for up to 6 months (cycles) into the buttock plus best supportive care (BSC), or BSC alone. Randomization was performed at a Trials Centre, where a computer program allocated patients to the respective arms of the study. In our substudy, we analysed textural features in 20 patients who had received ADI-PEG 20 treatment at a single institution (St. Bartholomew's Hospital, Barts).

Inclusion criteria

Inclusion criteria included life expectancy of at least 3 months, over 18 years of age, Eastern Cooperative Oncology Group (ECOG) performance status (PS) 0-1 with adequate haematological, hepatic and renal function.

Exclusion criteria

Patients with surgically resectable disease, recurrent pleural effusion (not pleurodesed), receipt of extensive radiation (hemi-thorax) therapy within 6 weeks before enrolment, brain and spinal cord metastases, uncontrolled or severe heart disease, pregnancy, seizures and allergy to pegylated compounds.

3.1.2 Imaging and Analysis

Computed Tomography (CT)

CT imaging was performed as part of routine clinical care and performed at baseline and at the end of month 2, 4, 6 and end of treatment. Progression free survival (PFS) and overall survival (OS) were also recorded.

CT Image Acquisition

Diagnostic CTs were acquired as standard of care on a Definition AS 64 slice CT scanner (Siemens Healthcare, Erlangen, Germany) at St. Bartholomew's Hospital. IV contrast-enhanced CT scans obtained with a minimum slice thickness of 3–5 mm were available for review. Each patient received 80–100 mL of IV iodinated contrast medium (iodixanol 300 or iohexol 300) injected at a rate of 2–3 mL/s, and scanning began after a delay of 20-25 seconds for arterial and 75–90 seconds after injection for the portovenous phase imaging.

CT Image Analysis

CT response was assessed by an experienced radiology (SE) at St Bartholomew's hospital using modified RECIST (MPM) criteria (Byrne et al). Uni-dimensional measurements of tumour thickness perpendicular to the chest wall were measured at 2 sites at 3 different levels on CT scan, at least 1 cm apart. At reassessment, pleural thickness was measured at the same position and level. Nodes were not measured. Uni-dimensional measurements are added to produce the total tumour measurement, so the sum of 6 pleural thickness measurements = one univariate diameter. Complete response (CR) was defined as the disappearance of all target lesions with no evidence of tumour elsewhere, and PR was defined as at least a 30% reduction in the total tumour measurement. Progressive disease (PD) was defined as an increase of at least 20% in the total tumour measurement over the nadir (lowest) measurement, or the appearance of one or more new lesions. Patients with stable disease (SD) were those who fulfilled the criteria for neither PR nor PD.

PET-CT imaging

As part of the translational component of this study, patients receiving ADI-PEG 20 underwent a FDG PET-CT scan at baseline and at approximately 4 weeks. A subset of 20 patients who had received ADI-PEG 20 treatment at a single institution (St. Bartholomew's Hospital, Barts) had textural features of the FDG PET data analysed. The low dose CT was not assessed as tumour delineation was suboptimal and prior studies have assessed texture features using diagnostic CT.

PET-CT Imaging Acquisition

The subset of patients from Barts were injected with 347 (+/-20) MBq FDG. All patients fasted for 6 h and the uptake time was 60 min. All data were acquired on a Philips Gemini TF LSO64 system with 3-dimensional time-of-flight (TOF) PET scanner together with a 16-slice Brilliance CT scanner (Philips Healthcare, Best, the Netherlands). Patients were imaged supine from skull base to upper thighs with arms raised above head to avoid attenuation artefacts. A low dose CT scan was acquired first (parameters: 40 mAs, 140 kV, 0.5 s per tube rotation) with a slice thickness of 5 mm, a scan length of approximately 900mm and data acquisition time of 22.5 s. The CT scan was acquired during free breathing. This was immediately followed by PET acquisition with a 3 min per bed position (6–7 bed positions) and 7-slice overlap in 3D reconstruction mode (matrix size 128×128). The acquisition time was approximately 30–40 min. The CT data were used for attenuation correction and localization. Iterative reconstruction with ordered-subset expectation maximisation (OSEM)(ordered subset expectation maximisation; 33 subsets, three iterations, no filters) for 3D PET was used to reconstruct the PET raw data.

PET-CT Image Analysis

Images were transferred to a HERMES workstation (Hermes Medical Solution, London, UK) for reporting. Volumes of interest (VOIs) of the primary tumour on FDG PET images were manually selected. Nodal disease was not included in this analysis.

Calculation of the textural features was performed by using in-house software implemented with MATLAB (MathWorks, Natick, Massachusetts). Voxel values within the tumour VOI were resampled to yield 64 discrete bins. A selection of parameters were chosen, as detailed in Table 1 (introduction). These specific parameters were chosen as they had been examined in a previously published study looking at NSCLC (100) and are a small subset of available texture parameters (98).

3.1.3 Statistical analysis

Statistical analyses were performed by an experienced statistician (P.B).

Changes in features with treatment from baseline to 4 weeks were assessed using a one sample t-test (as data followed a normal distribution (except for uniformity, coarseness, TLG and kurtosis). Associations of texture features with treatment response based on modified RECIST response (at 2 months) and PFS and OS were assessed using Cox regression models. Associations of texture features with metabolic tumour volume were assessed using Pearson correlation.

Analyses were performed for the texture variables at baseline, 4 weeks post treatment and also for the percentage change in values from baseline to 4 weeks, except in skewness and kurtosis, where the raw change in scores was examined.

Tumour response to ADI- PEG 20 was defined according to the modified RECIST criteria by an independent radiologist (S.E) who was blinded to the PET results. Patients were then dichotomized into progressors (PD) and non-progressors (SD, PR and CR) on the basis of these criteria. Response according to contrast-enhanced CT findings was used in preference to a PET-based response to provide a measurement independent of the PET studies.

The analyses were performed in two stages. Firstly, the separate association between each variable and each outcome was examined separately in a series of univariable analyses.
The second stage of the analysis examined the joint association of the variables in a multivariable analysis. Before this stage of the analysis, the collinearity between the texture variables was examined using variance inflation factors (which occurs when two, or more, factors are strongly associated with each other). To avoid potential problems in regression analysis where collinearity was detected, one of the variables was excluded from the multivariable analyses. A backwards selection was performed to retain only the significant variables in the final mode (omitting non-significant variables, one at a time, until all remaining variables are significant). Apart from the univariable analyses, $p < 0.05$ was considered to indicate a statistically significant difference.

3.2 Results

3.2.1 Demographics

There were 20 patients in this dataset; 17 of whom were male (Table 17). They were all non sarcomatoid mesothelioma (MPM) cases on histology and ASS1 levels were above 50%.

Table 17. Demographic data in subset of ADAM study (n=20)

Age mean (range) /yrs	
all patients	64 (54-77)
Women	62 (59-67)
Men	65 (54-77)
Gender	
no of female	3
no of male	17
Histology	
no of MPM sarcomatoid	0
no of MPM non sarcomatoid	20
ASS1%	
all patients	64 (50-100)
Women	53 (50-60)

The actual post ADI therapy FDG PET-CT scans were performed after a mean of 23 days (+/- 6.2) and hence slightly earlier than 4 weeks. RECIST measurements were performed on diagnostic CTs at 2 months post therapy.

3.2.2 Changes with treatment from baseline to 4 weeks

Baseline, 4-week values and percentage change for all measured parameters are summarised in Table 18. Most data values were normally distributed and hence were summarised by the mean and standard deviation (SD). Uniformity, coarseness, TLG and kurtosis were not normally distributed and hence median and inter-quartile ranges were used. The fourth column shows the mean percentage change between time points, along with a corresponding confidence interval. The exception is for two parameters (skewness and kurtosis) where the absolute change was preferred, when again the average change is shown with a corresponding confidence interval.

Table 18. Baseline, 4-week values and percentage change for all measured parameters

Parameter	Baseline	4 weeks	% change Mean (95% CI)	P-value
SUVmax	8.5 ± 2.5	8.0 ± 2.5	-6 (-12, 0)	0.05
SUVmean	3.3 ± 1.1	3.4 ± 1.3	1 (-5, 6)	0.85
SUVpeak	6.8 ± 2.0	6.5 ± 2.1	-4 (-10, 2)	0.18
MTV	587 ± 338	592 ± 361	-2 (-8, 4)	0.51
TLG	1457 [839, 3568]	1730 [805, 3488]	1 (-8, 10)	0.84
Standard deviation	1.4 ± 0.5	1.3 ± 0.5	-5 (-12, 1)	0.12
Skewness	0.57 ± 0.50	0.41 ± 0.48	-0.15(-0.24, -0.07)	**0.002**
Kurtosis	0.11 [-0.39, 1.15]	-0.19 [-0.41, 0.47]	-0.20 (-0.38, 0.00)	**0.03**
Entropy	2.4 ± 0.5	2.3 ± 0.5	-4 (-8, 1)	0.11
Uniformity	0.027 [0.024, 0.032]	0.027 [0.024, 0.029]	-3 (-9, 2)	0.19
Contrast	0.12 ± 0.06	0.12 ± 0.05	12 (-6, 31)	0.17
Coarseness (x10^{-4})	0.8 [0.3, 4.6]	0.9 [0.3, 3.8]	2 (-12, 16)	0.76
Busyness	13.8 ± 9.9	12.5 ± 10.3	-9 (-21, 3)	0.14
Complexity	2462 ± 350	2492 ± 392	2 (-3, 6)	0.52

Summary statistics for table 18 are: mean (± Standard Deviation), or median [inter-quartile range].

There was a significant decrease in skewness and kurtosis between baseline and 4 weeks post therapy (for both of these parameters, the raw change in scores was examined rather than the percentage change) with a mean reduction of 0.15 units for skewness, and a median reduction of 0.2 units for kurtosis (Figures 20 and 21).

Figure 20. Changes in histograms demonstrating changes in skewness and kurtosis in a responder

Baseline
Skewness: 0.57
Kurtosis: 0.11
Mean SUV 2.38

4 weeks post treatment
Skewness: 0.41
Kurtosis: -0.19
Mean SUV 2.05
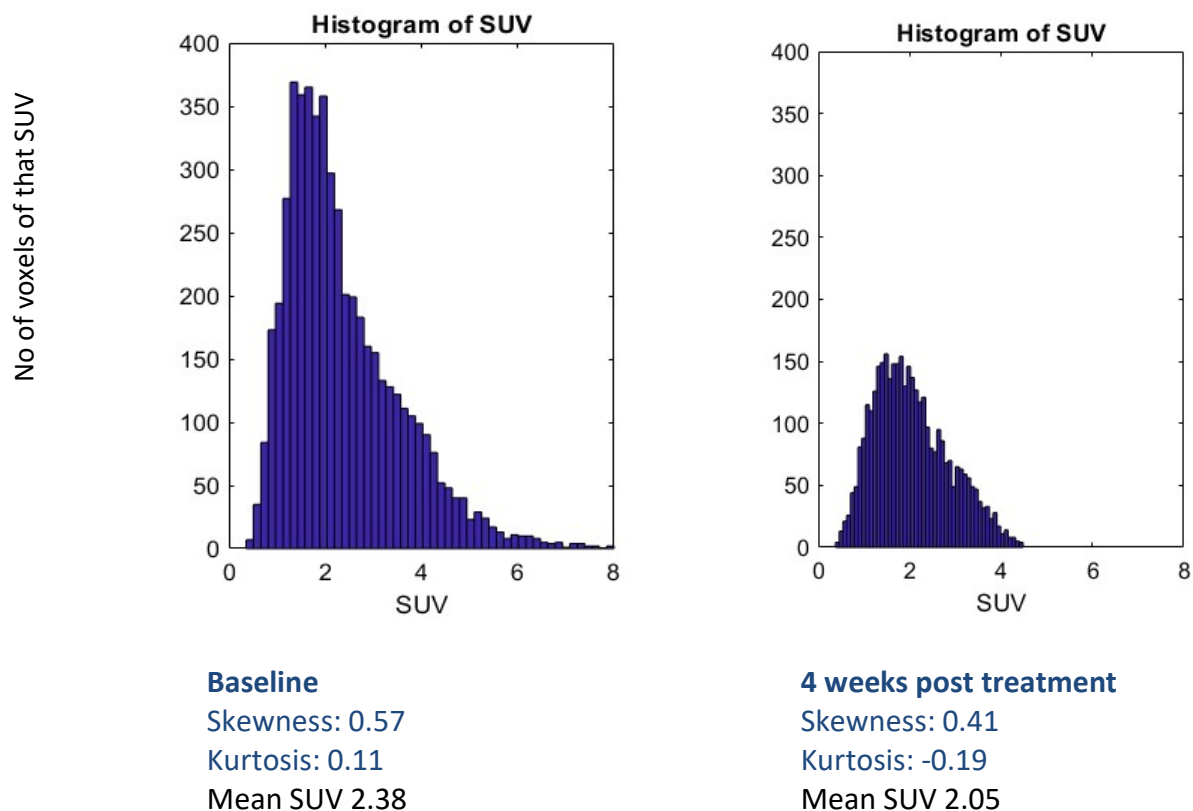
There is a reduction in skewness, but this remains >0 so although values are right skewed, and most values concentrated on the left of the mean, this is less marked at 4 weeks than at baseline (appears more symmetrically distributed at 4 weeks than baseline). There is a decrease in kurtosis from 0.11 at baseline to -0.19 at 4 weeks, so curve becomes less peaked (flat topped). The tails are thinner with fewer, or less extreme outliers than standard normal distribution.

Figure 21. Change in skewness and kurtosis in the same patient as Figure 20
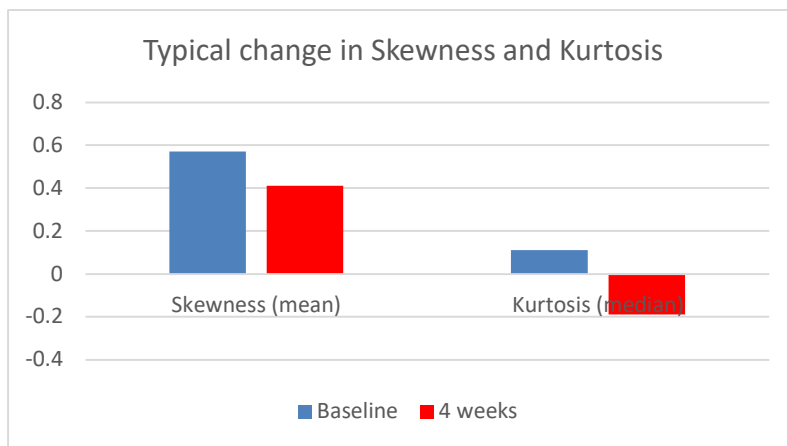
There was also slight evidence that SUVmax values decreased over time, although this difference was only of borderline statistical significance (p=0.05). None of the other parameters were found to significantly change from baseline to 4 weeks. Some of the typical changes on other texture parameters are shown below (Figure 22).

Figure 22. Changes in other texture parameters
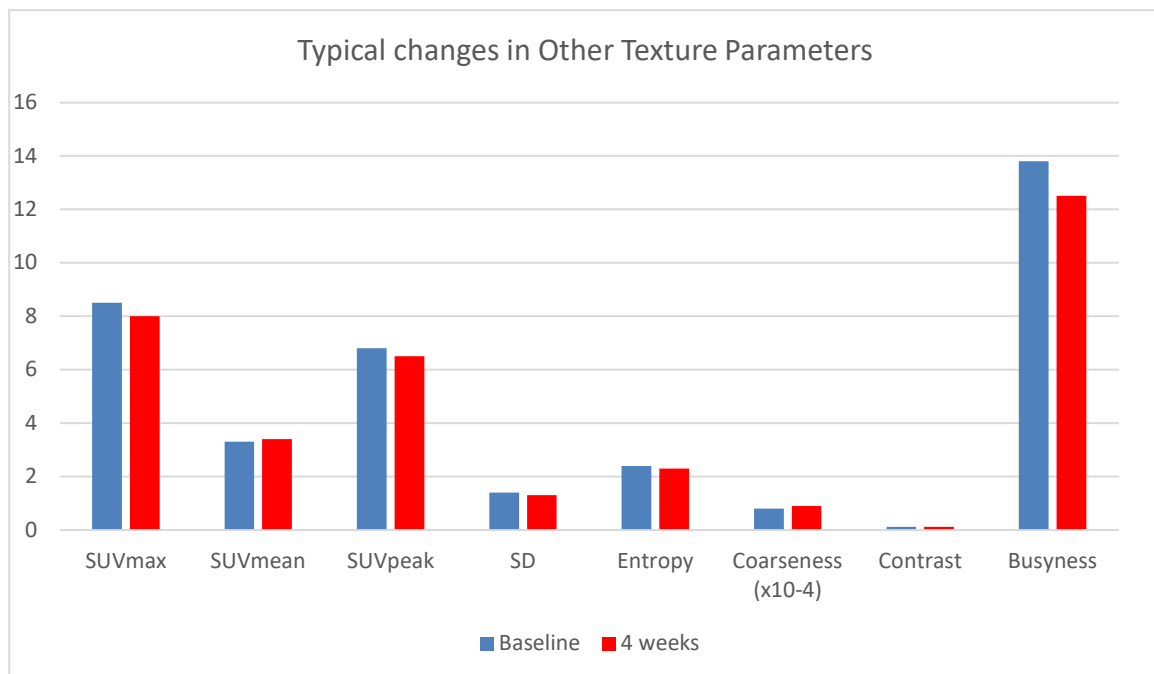
3.2.3 Associations with treatment response and progression based on RECIST

According to CT RECIST, at 2 months, 9 participants progressed and 11 did not progress. Those patients who progressed had a median PFS and OS of 2 months and 18.5 months, respectively; whereas those who did not progress had a median PFS and OS of 4.2 months and 20.8 months, respectively.

An initial set of analyses compared the differences in each parameter between patients who progressed and those who did not. Analyses were made for the parameters at baseline (Table 19); 4 weeks (Table 20) and percentage (or absolute) change (Table 21). The data for the majority of the parameters was normally distributed, except as previously, uniformity, coarseness, TLG and kurtosis. The results indicate that none of the PET parameters at baseline, 4 weeks or percentage change were associated with progression according to RECIST criteria. Therefore, no further analyses were undertaken.

Table 19 Comparison of parameters at baseline on RECIST in participants who progressed and did not progress.

Parameter	Participants who did not Progress = SD + PR n=11	Participants who Progressed = PD n=9	P-value
SUVmax	9.0 ± 3.1	7.8 ± 1.2	0.29
SUVmean	3.3 ± 1.3	3.4 ± 0.9	0.98
SUVpeak	7.2 ± 2.6	6.3 ± 1.1	0.36
MTV	606 ± 357	563 ± 332	0.79
TLG	1552 [789, 043]	998 [961, 3742]	0.85
Standard deviation	1.5 ± 0.6	1.2 ± 0.3	0.32
Skewness	0.66 ± 0.54	0.45 ± 0.47	0.36
Kurtosis	0.07 [-0.39, 1.25]	0.15 [-0.38, 0.52]	0.79
Entropy	2.5 ± 0.6	2.4 ± 0.2	0.62

Uniformity	0.027 [0.024, 0.037]	0.027 [0.025, 0.031]	0.97
Contrast	0.12 ± 0.08	0.11 ± 0.04	0.69
Coarseness (x10^{-4})	0.7 [0.3, 6.1]	1.0 [0.3, 2.8]	0.85
Busyness	15.8 ± 10.8	11.5 ± 8.8	0.35
Complexity	2427 ± 392	2503 ± 309	0.64

Summary statistics are: mean ± Standard Deviation, or median [inter-quartile range]

Table 20. Comparison of parameters at 4 weeks in RECIST in participants who progressed and did not progress.

Parameter	Participants who did not Progress = SD + PR n=11	Participants who Progressed = PD n=9	P-value
SUVmax	8.5 ± 2.9	7.3 ± 1.8	0.28
SUVmean	3.3 ± 1.4	3.4 ± 1.2	0.93
SUVpeak	7.0 ± 2.6	5.9 ± 1.3	0.29
MTV	628 ± 392	548 ± 337	0.63
TLG	1817 [774, 3555]	1035 [897, 3281]	0.85
Standard deviation	1.4 ± 0.6	1.2 ± 0.3	0.27
Skewness	0.52 ± 0.50	0.27 ± 0.46	0.25
Kurtosis	0.16 [-0.44, 0.59]	-0.25 [-0.38, 0.09]	0.57
Entropy	2.4 ± 0.6	2.2 ± 0.3	0.45
Uniformity	0.026 [0.022, 0.035]	0.027 [0.026, 0.028]	0.97
Contrast	0.12 ± 0.06	0.12 ± 0.03	0.85
Coarseness (x10^{-4})	0.8 [0.3, 4.9]	1.5 [0.3, 3.5]	0.97
Busyness	15.7 ± 11.1	8.7 ± 8.3	0.14
Complexity	2426 ± 458	2573 ± 300	0.42

Summary statistics are: mean ± Standard Deviation, or median [inter-quartile range]

Table 21. Comparison of percentage change from baseline to 4 weeks on RECIST in participants who progressed and did not progress.

Parameter	Participants who did not Progress = SD + PR n=11	Participants who Progressed = PD n=9	P-value
SUVmax	-5 ± 10	-7 ± 16	0.83
SUVmean	1 ± 12	1 ± 13	0.99
SUVpeak	-3 ± 12	-6 ± 15	0.66
MTV	-1 ± 11	-3 ± 15	0.64
TLG	0 ± 17	2 ± 24	0.84
Standard deviation	-4 ± 14	-6 ± 15	0.81
Skewness (*)	-0.14 ± 0.15	-0.17 ± 0.23	0.67
Kurtosis (*)	-0.25 [-0.42, 0.02]	-0.09 [-0.29, 0.00]	0.85
Entropy	-2 ± 10	-5 ± 9	0.56
Uniformity	-3 ± 10	-4 ± 14	0.93
Contrast	9 ± 32	17 ± 48	0.67
Coarseness	-2 ± 36	6 ± 21	0.55
Busyness	-5 ± 13	-14 ± 36	0.43
Complexity	0 ± 7	4 ± 14	0.40

Summary statistics are: mean ± standard deviation, or median [inter-quartile range]

(*) Figures for raw change, not percentage change

.

3.2.4 Association with progression free survival

Median PFS overall was 3.6 months (mean 5 months), with no survivors at the time of analysis. The length of time to progression is shown graphically in the Kaplan-Meier plot in Figure 23 and differences in PFS in Figure 24. Looking at participants who progressed on RECIST (with median PFS 2 months) and those who did not progress on RECIST (with median PFS 4.2 months), there was a statistically significant difference in PFS (p=0.015).

Figure 23. Kaplan-Meier plot of progression free survival in all patients
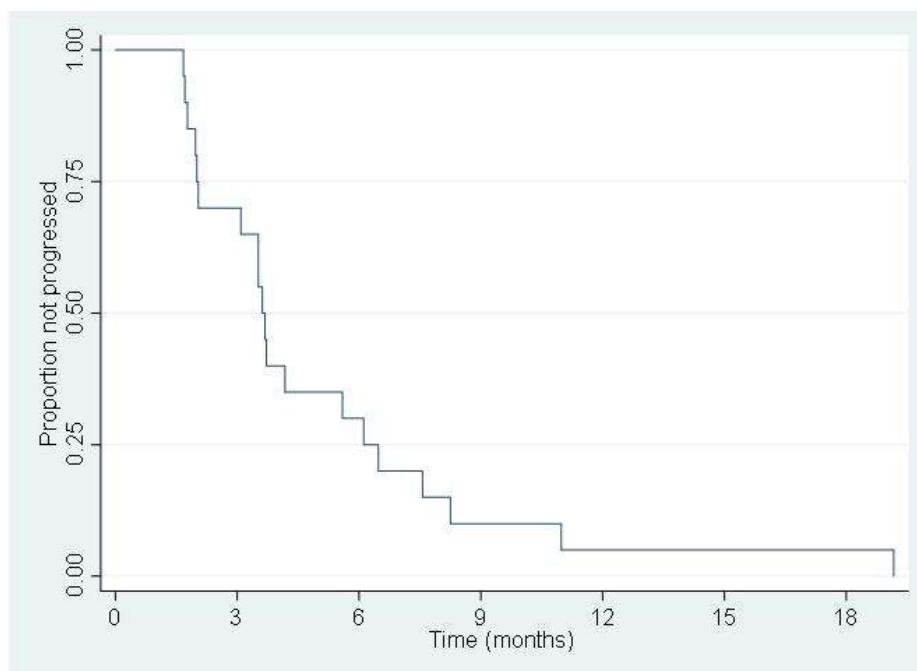
Figure 24. Kaplan-Meier plot of progression free survival on RECIST in participants who progressed and did not progress. (p=0.015)
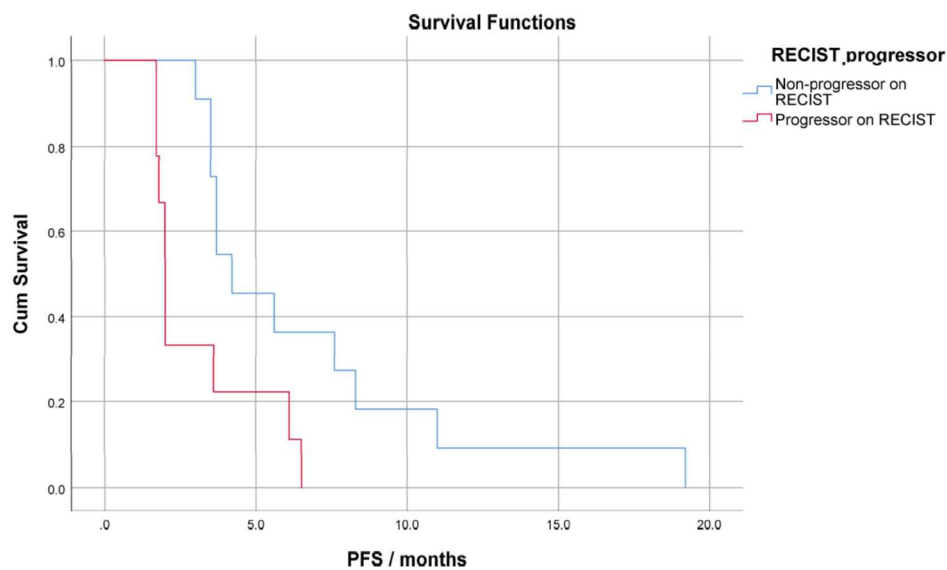
Factors associated with PFS were examined and summarised in Table 22 below. Initially a separate association of each texture variable was examined. Analyses were performed for the values at baseline, 4 weeks and also for the percentage (or absolute) change from baseline to four weeks. The figures reported are the hazard ratios (HR), and corresponding confidence intervals. Due to the different scales for each parameter, hazard ratios are given for a one standard-deviation increase in each variable. This indicates the relative change in the risk of progression at any time as each texture parameter increases by 1 SD. P values indicating the significance of the results are shown in the final column.

A hazard ration > 1.0 suggests the treatment group has shorter survival. A hazard ratio < 1.0 suggests that it is less likely.

Table 22. Univariable analyses for progression free survival

Timepoint	Parameter	Hazard Ratio (95% CI) [*]	P-value
Baseline	SUVmax	1.03 (0.65, 1.61)	0.91
	SUVmean	1.54 (0.92, 2.58)	0.1
	SUVpeak	1.13 (0.70, 1.82)	0.63
	MTV	1.20 (0.75, 1.93)	0.44
	TLG	1.32 (0.84, 2.07)	0.23
	Standard deviation	1.18 (0.72, 1.93)	0.5
	Skewness	0.61 (0.32, 1.19)	0.15
	Kurtosis	0.79 (0.47, 1.31)	0.35
	Entropy	1.16 (0.70, 1.95)	0.57
	Uniformity	0.78 (0.47, 1.29)	0.33
	Contrast	1.23 (0.80, 1.92)	0.35
	Coarseness	1.16 (0.73, 1.85)	0.54
	Busyness	0.91 (0.56, 1.49)	0.7
	Complexity	1.23 (0.78, 1.94)	0.38
4 weeks	SUVmax	0.97 (0.59, 1.60)	0.92
	SUVmean	1.45 (0.83, 2.56)	0.19
	SUVpeak	0.99 (0.59, 1.67)	0.98
	MTV	1.17 (0.73, 1.86)	0.52
	TLG	1.32 (0.83, 2.11)	0.24
	Standard deviation	0.96 (0.58, 1.59)	0.88
	Skewness	0.56 (0.26, 1.18)	0.13
	Kurtosis	0.92 (0.56, 1.49)	0.73
	Entropy	0.93 (0.55, 1.56)	0.78
	Uniformity	0.94 (0.62, 1.44)	0.78
	Contrast	1.03 (0.68, 1.56)	0.89
	Coarseness	1.12 (0.70, 1.79)	0.64
	Busyness	0.83 (0.50, 1.37)	0.47
	Complexity	1.03 (0.68, 1.56)	0.88
% change baseline to 4 weeks	SUVmax	0.79 (0.46, 1.33)	0.37
	SUVmean	0.76 (0.46, 1.27)	0.29
	SUVpeak	0.71 (0.44, 1.16)	0.17
	MTV	1.14 (0.64, 2.01)	0.66
	TLG	0.89 (0.51, 1.56)	0.68
	Standard deviation	0.56 (0.34, 0.94)	**0.03**
Change baseline to 4 week	Skewness	1.03 (0.62, 1.73)	0.91
Change baseline to 4 week	Kurtosis	1.59 (0.86, 2.97)	0.14
% change baseline to 4 weeks	Entropy	0.65 (0.41, 1.03)	0.07
	Uniformity	2.30 (1.13, 4.67)	**0.02**
	Contrast	0.73 (0.36, 1.51)	0.4
	Coarseness	0.93 (0.52, 1.66)	0.81
	Busyness	0.86 (0.42, 1.80)	0.7
	Complexity	0.71 (0.38, 1.32)	0.28

The results suggested that there was no strong evidence that any of the texture parameters at baseline or at 4 weeks were associated with progression.

The analyses for the change in values from baseline to four weeks suggested that an increase in SD was associated with a decreased risk in progression (HR 0.56); conversely a decrease in SD was associated with increased risk of progression (as increase in S D results in a lower risk).

Increase in uniformity (or lesser decrease) was significantly associated with progression (HR 2.3), hence that texture features become more homogeneous after ADI therapy, but patients have reduced PFS (which is contrary to previously published literature with other treatments in other tumour types). 11/20 patients had talc pleurodesis and 5/20 had calcified pleural plaques. These are not expected to have had an effect on PET texture features, as would not change with therapy.

Multi-variable analysis found collinearity between entropy and SD. Although SD was found to be the most significant factor in the univariable analysis, this variable was excluded and entropy was included in the multivariable analysis, as entropy was regarded as the most clinically useful variable with more previous evidence in the literature of utility. A backwards selection procedure was performed to retain only variables found to have some relationship with time to progression. Uniformity, which had been significant in the univariable analysis, was not longer significant in the multi-variable analysis for PFS. The final model is summarised in Table 23.

Table 23. Multi-variable analyses for progression free survival

| Timepoint	Parameter	Hazard Ratio (95% CI) [*]	P-value
Baseline	SUVmean	1.58 (0.98, 2.56)	0.06
Change to 4 weeks	SUVpeak [+]	0.51 (0.28, 0.94)	0.03
	Kurtosis [++]	1.96 (1.01, 3.79)	0.05

(*) Hazard ratios are reported for a one standard deviation increase in each parameter

(+) Percentage change in values

(++) Raw change in values

The main finding was that a greater percentage increase in SUVpeak was associated with a HR of 0.51 (decreased risk); hence reduction in SUVpeak from baseline to 4 weeks was associated with a greater risk of progression (one SD reduction in this variable was associated with a doubling of the risk of progression, p=0.03), suggesting that the SUV post treatment reduces and hence the treatment is having a pharmacological effect, however, this does not translate into improved survival. This is an unexpected finding. A Kaplan-Meier plot of the dichotomised data around the median value reveals p=0.67, hence this was not significant (Figure 25).

Figure 25. Kaplan-Meier plot of progression free survival above and below median SUVpeak % change from baseline to 4 weeks (p=0.67)
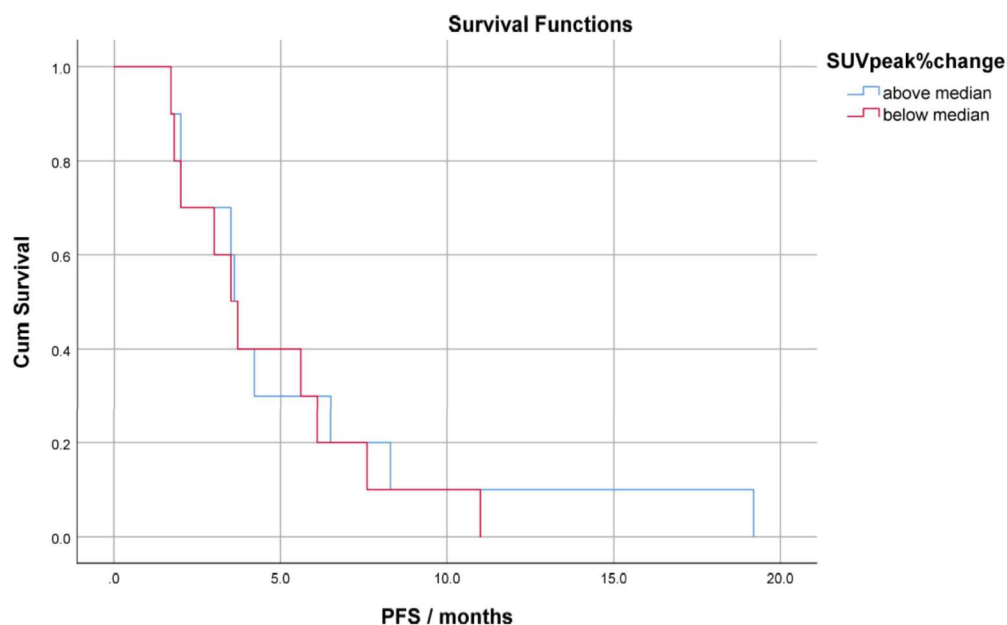
There were two further findings of borderline significance: one that higher baseline values of SUVmean were associated with an increased progression risk (a one SD increase in this variable was associated with a 58% increase in the risk of progression at any time); also that an increase in kurtosis from baseline to 4 weeks post therapy was associated with increased PFS (one SD increase in kurtosis was associated with an almost doubling of the risk). Kaplan-Meier plot of the dichotomised data around the median values for baseline SUVmean and change in kurtosis were p=0.12 and p=0.14, respectively, hence also not significant (Figures 26 and 27). After adjusting for these variables, there was no longer any significant association between any further factors and time to progression.

Figure 26. Kaplan-Meier plot of progression free survival above and below median baseline SUVmean (p=0.12)
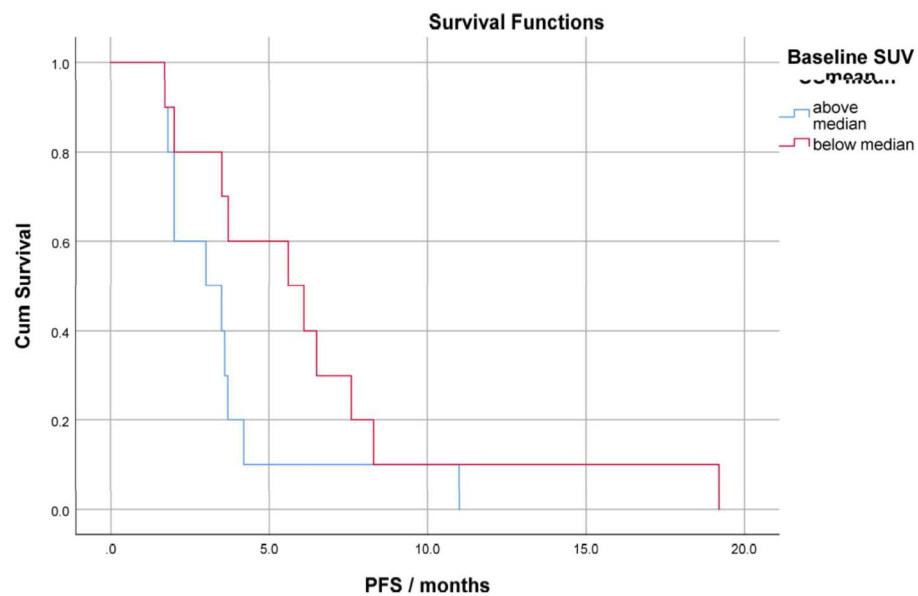
Figure 27. Kaplan -Meier plot of progression free survival above and below median kurtosis change from baseline to 4 weeks (p=0.14)
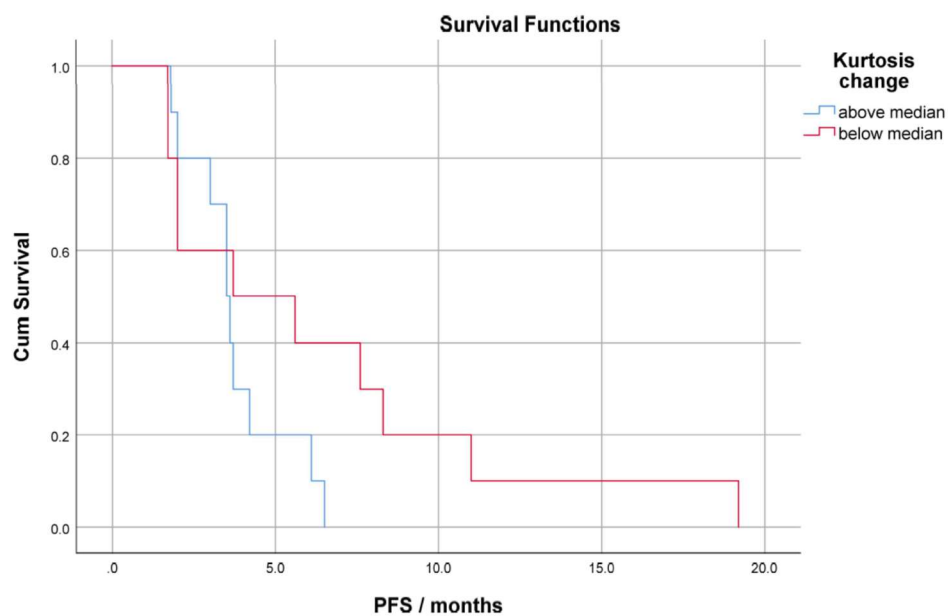
3.2.5 Association with overall survival

Median OS was 18.9 months (mean 20.2 months), with no survivors at the time of analysis. The length of time to progression is shown graphically by the Kaplan-Meier plot in Figure 28 and differences in OS in Figure 29. Looking at participants who progressed on RECIST (with median OS 18.5 months) and participants who did not progress on RECIST (with median OS 20.8 months), there was no statistically significant difference in OS (p=0.334).

Figure 28. Kaplan-Meier plot of overall survival in all patients

Figure 29. Kaplan-Meier plot of overall survival on RECIST in participants who progressed and did not progress. (p=0.33)

The association between texture variables and overall survival times was examined. Initially the separate association between each texture variable at baseline, 4-week percentage change and the outcome were examined separately in a series of univariable analyses. The analysis results are summarised in Table 24. As with PFS, the hazard ratios are reported for a one SD increase in each of the texture variables.
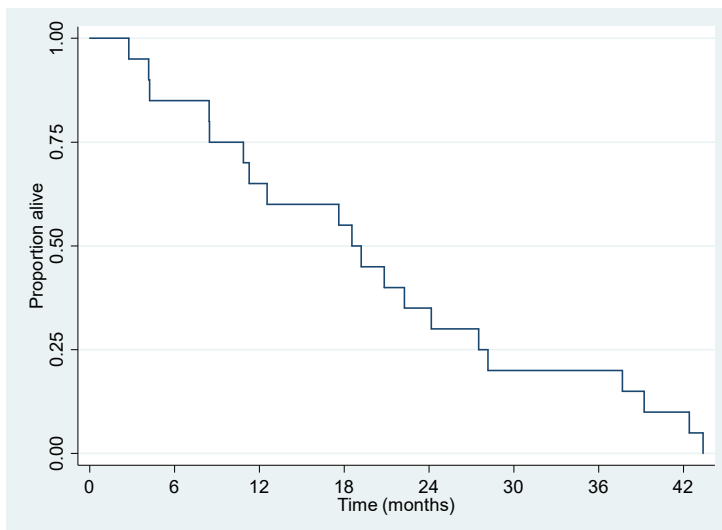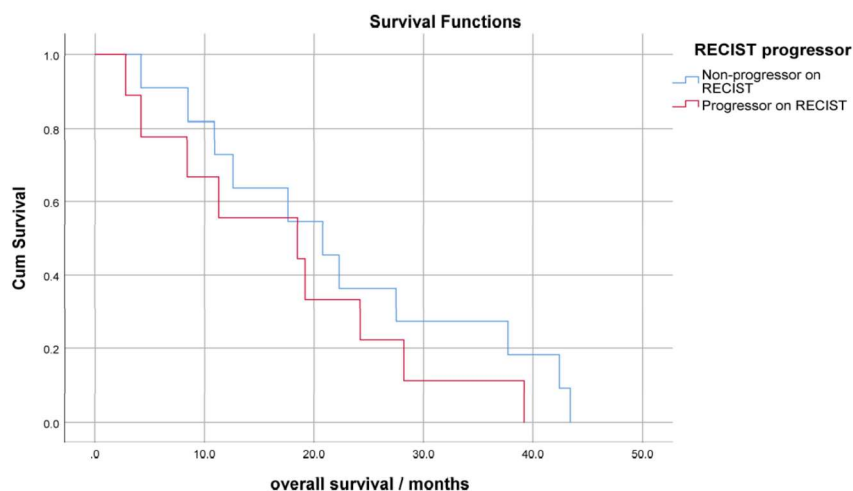
Univariable analysis suggested that a number of the texture variables at baseline were significantly associated with OS times (unlike PFS which was not affected). Baseline SUVmean, SUVpeak, MTV and TLG were all found to be significantly associated with OS. Additionally, there was some evidence that baseline SUVmax, SD and entropy could predict OS, however, the results for these variables were not quite statistically significant. Higher values of all these variables were associated with an increased risk of death at any time. The largest effect was for TLG, where a one SD increase was associated with a 2.5-fold increase in the risk of death at any time.

Of the texture variables at 4 weeks, only MTV and TLG were significantly associated with OS. Large values of both these variables were associated with an increased risk of death with a one SD increase in MTV associated with a 1.9-fold increase in risk and a 1 SD increase in TLG associated with a 2.2-fold increased risk in death.

There was no evidence that the percentage change in any of the texture variables was significant associated with survival times, again suggesting that drug effect does not impact OS significantly.

Table 24. Univariable analyses for overall survival

Timepoint	Parameter	Hazard Ratio (95% CI) [*]	P-value
Baseline	SUVmax	1.58 (0.92, 2.72)	0.10
	SUVmean	1.90 (1.08, 3.36)	**0.03**
	SUVpeak	1.84 (1.04, 3.26)	**0.04**
	MTV	2.01 (1.16, 3.48)	**0.01**
	TLG	2.58 (1.41, 4.70)	**0.002**
	Standard deviation	1.74 (0.98, 3.11)	0.06
	Skewness	0.66 (0.37, 1.19)	0.17
	Kurtosis	0.82 (0.46, 1.47)	0.51
	Entropy	1.69 (0.94, 3.06)	0.08
	Uniformity	0.88 (0.50, 1.57)	0.69
	Contrast	1.18 (0.67, 2.09)	0.56
	Coarseness	0.91 (0.54, 1.53)	0.73
	Busyness	1.39 (0.84, 2.31)	0.20
	Complexity	1.06 (0.62, 1.83)	0.83
4 weeks	SUVmax	1.54 (0.86, 2.74)	0.15
	SUVmean	1.61 (0.90, 2.86)	0.11
	SUVpeak	1.49 (0.84, 2.63)	0.17
	MTV	1.86 (1.10, 3.15)	**0.02**
	TLG	2.21 (1.26, 3.86)	**0.005**
	Standard deviation	1.34 (0.80, 2.24)	0.27
	Skewness	0.74 (0.41, 1.33)	0.32
	Kurtosis	0.95 (0.54, 1.67)	0.86
	Entropy	1.29 (0.75, 2.22)	0.36
	Uniformity	1.08 (0.66, 1.76)	0.76
	Contrast	0.85 (0.54, 1.32)	0.47
	Coarseness	0.81 (0.49,1.32)	0.40
	Busyness	1.20 (0.74, 1.96)	0.45
	Complexity	0.88 (0.53, 1.45)	0.61
% change baseline to 4 weeks	SUVmax	0.93 (0.56, 1.56)	0.79
	SUVmean	0.74 (0.43, 1.26)	0.27
	SUVpeak	0.76 (0.48, 1.23)	0.26
	MTV	1.22 (0.78, 1.90)	0.39
	TLG	1.09 (0.64, 1.87)	0.74
	Standard deviation	0.76 (0.48, 1.21)	0.25
Change baseline to 4 week	Skewness	1.34 (0.81, 2.22)	0.25
Change baseline to 4 week	Kurtosis	1.28 (0.76, 2.16)	0.36
% change baseline to 4 weeks	Entropy	0.79 (0.52, 1.21)	0.28
	Uniformity	1.44 (0.86, 2.40)	0.16
	Contrast	0.71 (0.37, 1.34)	0.29
	Coarseness	0.79 (0.45, 1.38)	0.41
	Busyness	0.92 (0.45, 1.89)	0.83
	Complexity	0.72 (0.38, 1.36)	0.31

Multi-variable analysis revealed collinearity between all of SUVmax, SUVmean, SUVpeak, SD and entropy at baseline, with all variables strongly positively correlated. SUVmax and entropy were included in the multivariable analyses, as these were clinically important factors with supportive evidence from previous literature. There was also found to be evidence of collinearity between MTV and TLG at baseline and 4 weeks, which is not surprising as TLG = MTV x SUVmean. TLG was found to be the strongest predictor in the univariable analysis, so was retained in the multi-variable analysis, with MTV omitted.

A backwards selection procedure (fitting regression model) of the remaining variables was performed. This found that only TLG at baseline was independently significantly associated with OS times (p=0.002). After adjusting for this variable, no further variables were found to be statistically significant. As this was the only variable in the final model, the size of the relationship between this variable and survival times was equivalent to that observed in the univariable analysis. A Kaplan-Meier plot of the dichotomised data around the median TLG value reveals p=0.006 (Figure 30), hence significant (and better than CT RECIST as this was not significant). Those with larger tumours with higher uptake (> median) had median survival of 11 month; those with smaller tumours with low uptake (< median) had median survival of 27 months.

Figure 30. Kaplan-Meier plot of overall survival above and below median TLG at baseline (p=0.006)
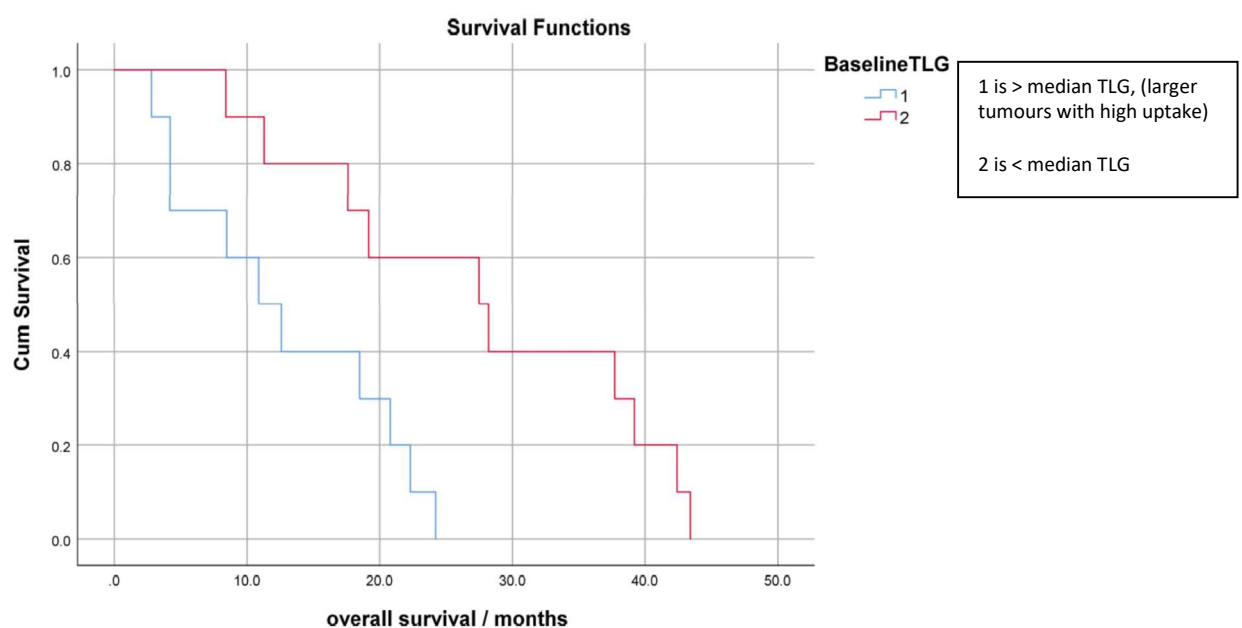
3.2.6 Texture parameter association with MTV

The mean MTV of the primary tumours was 627.7 ml at baseline (+/- 398.2 ml) and 565.4 ml at 4 weeks (+/- 381.3 ml). SUV parameters were associated with MTV (Table 25) as large tumours tend to demonstrate high SUVs. A minimum volume of 10mls needs to be reached before texture is affected (114). In this study the tumour volumes were large and above the minimum threshold, hence the partial volume effect is unlikely to be a factor here.

Table 25. Texture parameter associations with MTV

Parameter	Baseline		% change baseline to 4 wks	
	Correlation (r)	P-value	Correlation (r)	P-value
SUVmax	0.41	0.08	0.42	0.06
SUVmean	0.55	**0.01**	0.22	0.36
SUVpeak	0.51	**0.02**	0.34	0.14
Standard	0.37	0.11	0.34	0.14
Entropy	0.46	**0.04**	0.41	0.07
Uniformity	-0.3	0.2	0.09	0.69
Coarseness	-0.51	**0.02**	-0.65	**0.002**
Contrast	-0.11	0.63	-0.52	**0.02**
Busyness	0.84	**<0.001**	0.66	**0.002**
Complexity	0.17	0.48	-0.03	0.91
TLG	0.92	**<0.001**	0.82	**<0.001**
Skewness [*]	-0.53	**0.02**	0.16	0.5
Kurtosis [*]	-0.4	0.08	0.27	0.26

(*) Figures for raw change, not percentage change

The results suggested that a number of the texture variables at baseline were significantly associated with baseline MTV, including SUVmean (Figure 31) and SUVpeak, entropy, coarseness and notably busyness (r=0.84, p<0.001, Figure 32); so large tumours are more heterogeneous, more metabolically active and less coarse. Additionally, the percentage change in MTV was also significantly associated with the changes in high order variables including contrast, coarseness and busyness (r=0.66, p=0.002, Figure 33).

At baseline and change from baseline to 4 weeks, the strongest association with MTV was with

TLG (r=0.92 and r=0.82, respectively), which is irrelevant as TLG= MTV x SUVmean.

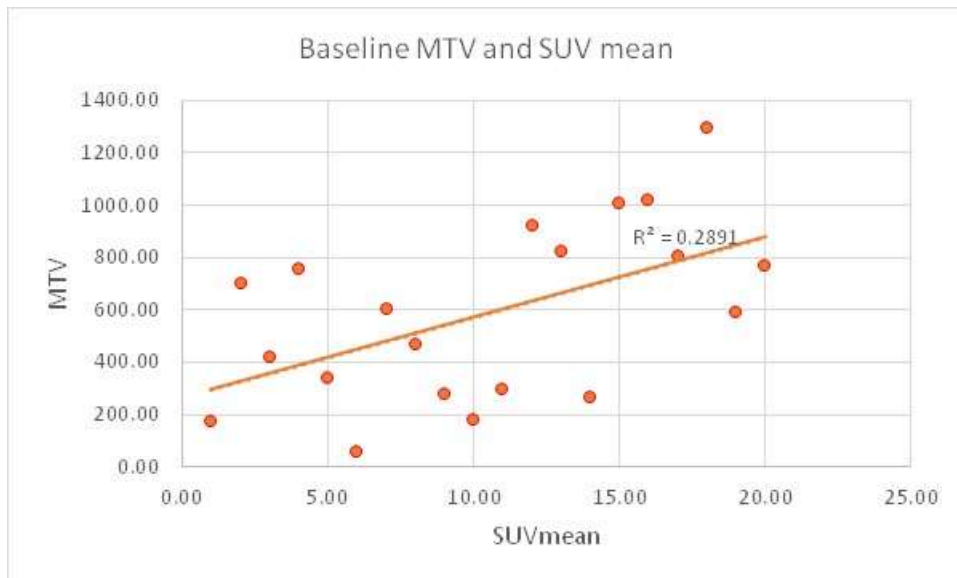Figure 31. Correlation of baseline SUV mean and MTV (p=0.01) (r=0.55; r^2=0.29)

Figure 32. Correlation of baseline busyness and MTV (p<0.001) (r=0.84; r^2=0.70)
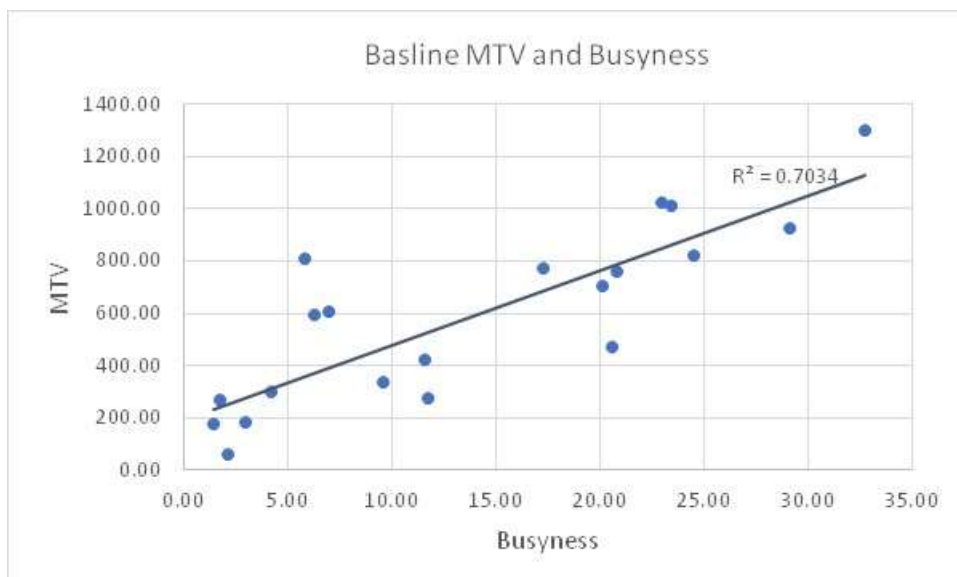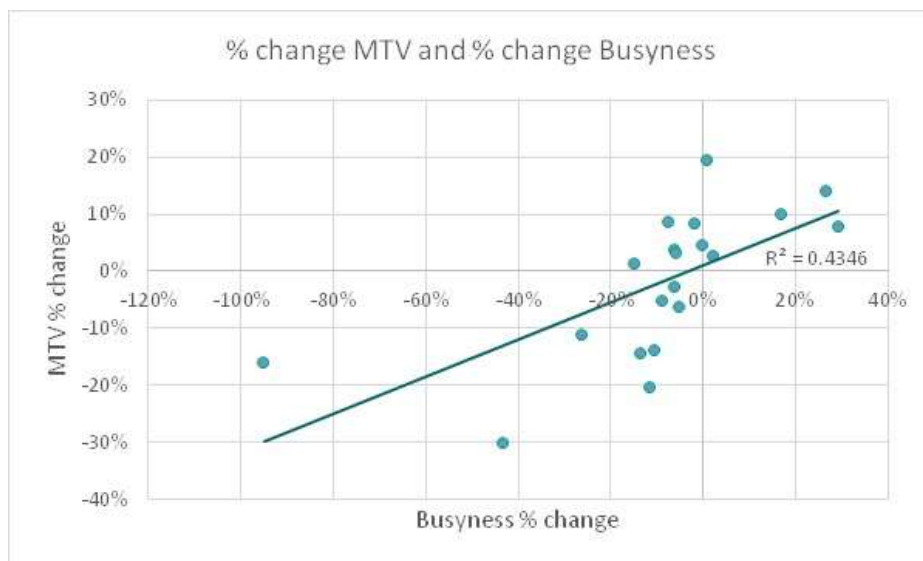
Figure 33. Correlation of percentage change busyness and MTV (p=0.002) (r=0.66; r^2=0.43)

3.2.7 Summary of results

From baseline to 4 weeks post therapy, there was decrease in skewness (mean 0.15 units, p=0.002) and kurtosis (median 0.2 units, p=0.03). None of the parameters at baseline or post therapy were associated with progression according to RECIST criteria (modified RECIST response at 2 months).

The median PFS in all participants was 3.6 months. PFS (which reflects treatment effect) differed between progressors (n=9) on RECIST (median PFS 2 months) and non-progressors (n=11) on RECIST (median PFS 4.2 months), p=0.015; although OS did not.

In terms of PFS, on univariable analysis, an increase in uniformity (or lesser decrease) was associated with progression (hazard ratio 2.3, p=0.02); similarly an increase in standard deviation was associated with decreased risk of progression (hazard ratio 0.56, p=0.03); hence that texture features become more homogeneous after ADI therapy, but patients have reduced PFS (which is contrary to previously published literature with other treatments in other tumour types). On multivariable analysis a greater percentage increase in SUVpeak from baseline to 4 weeks was associated with a decreased risk of progression (hazard ratio 0.51, p=0.03).

The median OS in all participants was 18.9 months. Baseline SUVmean (p=0.03), SUVpeak (p=0.04), metabolic tumour volume (MTV) (p=0.01) and total lesion glycolysis (TLG) (0.002) were all associated with OS (hence these predict nature of the tumour but not drug/therapy effect).

At four weeks, only MTV and TLG were significantly associated with OS with 1.9 and 2.2-fold increased risk in death, respectively. On multi-variable analysis, TLG at baseline was independently significantly associated with OS (p=0.002) and better than RECIST (p=0.334)

Associations with MTV include busyness (r=0.84) and SUVmean and peak, entropy, coarseness at baseline (large tumours are more heterogeneous, hotter and less coarse); whereas high order features such as contrast, coarseness and busyness were associated with change in MTV from baseline to 4 weeks.

Arginine deprivation therapy shows some increased homogeneity in texture features, but this does not translate to improved survival.

3.3 Discussion

Between baseline and 4 weeks, there is a significant decrease in skewness in the distribution of FDG uptake in mesotheliomas treated with arginine deprivation therapy. Skewness reflects asymmetry of histogram distribution. In our study, skewness is positive at baseline, hence most values are concentrated on the left of the mean, with extreme values to the right; whereas at 4 weeks the skewness reduces (but remains positive), so the histogram of SUV values is more symmetrically distributed.

Kurtosis reflects the sharpness/peakedness/pointedness of histogram distribution, the wider the histogram, the lower/negative the kurtosis. It is also a measure of how outlier-prone a distribution is. The kurtosis of the normal distribution is 3. In this study kurtosis was 0.11 at baseline, hence <3 and in keeping with a platykurtic distribution (flatter than a normal distribution with a wider peak). This decreases further post therapy a hence further flattening of the peak (as shown in the results section). However, kurtosis post therapy also becomes negative, so it is considered to be a "light-tailed" dataset with as much data in each tail as it does in the peak (and therefore less extreme values).

The published literature does not describe changes in kurtosis and skewness post treatment, but has described changes in SUVmean, SUVmax, SD and entropy, in NSCLC post treatment (102). We also saw a borderline decrease in SUVmax from mean 8.5 to 8.0, however this change is too small to suggest a definite therapy effect.

In our study, no PET texture parameters at baseline, 4 weeks post treatment or percentage change from baseline to 4 weeks predicted progression according to RECIST data. In a study by Cook et al.(102), none of the PET parameters at baseline or in that study at 6 weeks post treatment, were associated with RECIST response at 12 weeks either, however, percentage changes in SUVmax, SD, entropy and uniformity were associated with response. In this study, therapy was with erlotinib, which is a tyrosine kinase inhibitor and the study looked at NSCLC whereas ADAM looked at arginine deprivation therapy in MPM. Entropy is a statistical measure of randomness that can characterize the heterogeneity of the tumour, hence a treatment

response was associated with a decrease in heterogeneity, as one would expect. In the same study, increase in uniformity was associated with response.

In patients with NSCLC receiving either conventional radiation therapy or stereotactic body radiation therapy (SBRT), a number of first-order features on FDG PET-CT were able to predict for local and locoregional control with a model of combined PET and CT features as predictors (101). However, radiation therapy has a very different effect than arginine deprivation therapy. SBRT uses very focused beams of high dose radiation (with fewer treatments) aimed at the tumour from different angles to damages the cancer cells by breaking the DNA.

In our study, median and mean PFS were 3.6 and 5 months, respectively with no survivors at the time of analysis. PFS differed between those who progressed (n=9) on RECIST (median PFS 2 months) and those who did not progress (n=11) on RECIST (median PFS 4.2 months), although OS did not.

In terms of PFS, on univariate analysis, a decrease in SD was associated with increased risk of progression. Increase in uniformity (or lesser decrease) was significantly associated with progression, hence that texture features become more homogeneous after ADI therapy, but patients have reduced PFS. This is contrary to previously published literature in NSCLC (102) where uniformity at 6 weeks was associated with increased survival, albeit OS rather than PFS.

Multi-variable analysis of PFS found that uniformity was no longer significant. Now, a greater percentage reduction in SUVpeak from baseline to 4 weeks was associated with a greater risk of progression in terms of PFS (one SD reduction in this variable was associated with a doubling of the risk of progression, p=0.03) suggesting the treatment was having a pharmacological effect, but this does not translate into improved survival, which is an unexpected finding. Possible explanations for this include false positives from talc pleurodesis (present in 11/20 of the patients); calcified plaques (present in 5/20); variation in outlining the lesions (however this is unlikely as would affect all groups); or a real finding (although this is not easily explained biologically with reference to FDG distribution within a tumour). The effect of talc pleurodesis on texture features is unknown, but this is not expected to have an effect. It may be that the

patients had significant co-morbidity, as they had exhausted all other available treatment options, before commencing on the ADAM trial.

Most studies in the published literature deal with OS rather than PFS. In our study, median and mean OS was 18.9 months and 20.2 months, respectively and showed that a number of the texture variables at baseline were significantly associated with survival including SUVmean (p=0.03), SUVpeak (p=0.04), MTV (p=0.01) and TLG (p=0.002). Additionally, there was some evidence that SUVmax (p=0.1), SD (p=0.06) and entropy (p=0.08) were also prognostic, although not quite statistically significant. The largest effects were for TLG where a one SD increase was associated with a 2.5-fold increase in the risk of death and MTV with doubling risk of death. At 4 weeks, MTV and TLG were also significantly associated with OS with 1.9 and 2.2-fold increased risk in death, respectively. On multi-variable analysis, TLG at baseline was independently significantly associated with OS (p=0.002) and better than RECIST (p=0.334). This is consistent with the published data from Klabatsa et al. (105) which showed that FDG parameters which take account of MTV and TLG show significant associations with OS in patients with MPM. Cook et al. also found that a 10% increase in entropy was associated in a 14% increased risk of death (this was of borderline significance in our study) and a high-order feature, contrast, was associated with an 80% risk of death (102). Other studies have also shown that other high-order features, in particular, coarseness, have shown predictive and prognostic capability in NSCLC patients who underwent chemoradiation therapy, namely that patients with PET images showing relatively uniform tracer distribution (high contrast, low coarseness) were more likely to respond to treatment (100).

A retrospective study of 26 patients with stage 1 NSCLC tested standard metrics and texture parameters in pretherapy (SBRT) PET-CT scans for the prediction of progression-free and OS (115). Only SUVmax was predictive for progression-free survival (p=0.03), with no PET parameters found for OS on univariate analysis. A larger study of 63 patients with NSCLC who underwent SBRT tested standard metrics and 13 texture features in FDG PET-CT for disease specific and OS (116). On multi-variable analysis, only dissimilarity, a second-order feature was associated with disease-specific and disease-free survival (hazard ratio 0.822, P =0 .037; hazard ratio 0.834, P < 0.01, respectively).

The literature has suggested the possible dependence of certain texture features on tumour volume. In our study, the median MTV of the primary tumours was 596.5 ml at baseline (range: 55.6 -1296.7) and 633.0 ml at 4 weeks (range: 49.3 – 1355.1). SUV parameters are associated with MTV as large tumours demonstrate high SUV. Brooks and Grigsby, using probability theory, calculated that local (second) order entropy from cervical tumour volumes of <45 cm^3 can be very sensitive to size, and may reflect size rather than underlying heterogeneity (117) and also reported that second-order entropy is 5 times more sensitive to changes in volumes below 45cm^3. Hatt et al. (114) found second-order entropy showed high correlation in volumes of <10 cm^3 but much less at volumes >10 cm^3. The minimal volume to consider may therefore be closer to 10 cm^3 than 45 cm^3. In our study the tumour volumes are large and above the minimum threshold, hence the partial volume effect is unlikely to be a factor.

Our study found that associations with MTV include busyness (r=0.84) and SUVmean and peak, entropy, coarseness at baseline; so large tumours are more heterogeneous, hotter and less coarse. Larger tumours are known to exhibit higher hypoxia, necrosis, or anatomic and physiologic complexity at the microscopic and macroscopic scales, which translates to higher complexity in the spatial distribution of FDG uptake and consequently associated heterogeneity quantification (114). The association with entropy has been highlighted in the literature (as above), but was not shown by Cook et al. in NSCLC (102). However, they also describe associations between MTV and high-order features including busyness and coarseness (but also contrast). Our study also found that high-order features such as contrast, coarseness and busyness were associated with change in MTV from baseline to 4 weeks, which is consistent with published literature.

3.3.1 Limitations

Texture analysis methodology varies between manually drawn regions of interest (which are subject to the greatest inter- and intra-observer variability) to automatic or semiautomatic methods, such as using a fixed percentage threshold of SUVmax, commonly 40%, to more sophisticated methods such as fuzzy locally adaptive Bayesian methods(114) . Analysis in our study was all with manually drawn regions of interest, which risks associated error from possibly including "normal" lung, pleura or rib, rather than just disease. However, it was not possible to use automated methods due to the extensive volume of disease and difficulty in separating from uptake in ribs. The ROIs were also only drawn by one clinician, so there are no interobserver measurements. Also, the numbers were small, with only 20 patients. There is no published literature to date of FDG PET-CT texture features in mesothelioma treatment response for comparison.

A major limitation in this substudy is that we only had 20 participants and thus the study is too small a population for radiomics evaluation as the number of parameters may be exceeding the number of participants – which will increase the false discovery rate. In addition, no correction was applied to correct for multiple comparisons and "control" the false discovery rate (neither the Bonferroni correction, or the more conservative Benjamini Hockberg correction).

3.3.2 Conclusion

By 4 weeks, no first-order PET parameters predict CT RECIST response at 2 months, however, MTV and TLG are prognostic for OS (with 1.9 and 2.2-fold increased risk of death, respectively). Increase in uniformity was associated with progression (hazard ratio 2.3, $p=0.02$) and increase in standard deviation was associated with decreased risk of progression (hazard ratio 0.56, $p=0.03$); hence that texture features become more homogeneous after ADI therapy, but patients have reduced PFS Arginine deprivation therapy is having a pharmacological effect, with some increased homogeneity in texture features, but this does not translate into improved survival.

Summary

The TRAP substudy revealed that tumour proliferation imaging (using FLT PET-CT) undertaken within 12 hours of arginine deprivation therapy in thoracic malignancy can predict end of treatment CT (RECIST) response in nearly 2/3 cases, hence it is a marker of treatment response. However, ANOVA analysis reveals no significant evidence that a decrease in proliferation (measured as SUVmax on FLT PET-CT) precedes a decrease is size RECIST length, hence it is not a reliable marker of early treatment response and offers no real advantage over conventional CT imaging. Interestingly, when using end of treatment CT as the gold standard, the response to ADIPEMCIS therapy as demonstrated on FLT PET-CT is greater than on end of treatment CT (mean decrease of 36.5% in SUVmax compared to 21.9% decrease in RECIST length).

The TRAP phase 1 trial overall revealed a 94% disease control rate in non-epithelioid (biphasic and sarcomatoid) MPM subtypes characterized by a 75% rate of ASS1 loss. This has led to the ATOMIC-Meso, a phase 2/3 study looking at the role of targeted arginine deprivation again in combination with cisplatin and pemetrexed in aggressive subtypes of mesothelioma, with patients assessed every 6 weeks on CT imaging using modified RECIST criteria to assess treatment response (118).

Tumour heterogeneity, as assessed using texture features on FDG PET-CT at baseline and 4 weeks, did not predict CT RECIST response at 2 months to arginine deprivation treatment (ADAM trial). However, MTV and TLG are prognostic for OS (with 1.9 and 2.2-fold increased risk of death, respectively) indicating that arginine deprivation therapy is having a pharmacological effect, with some increased homogeneity in texture features, but this does not translate into improved survival.

Radiomics allow us to extract multiple 'unseen' features from images, which can provide additional information that allows better tumour characterization, treatment prediction and prognostication. However, the requirement for dealing with increasingly large amounts of data from medical images has led to the increasing interest in artificial intelligence (AI), which is related to improvements in computing power and advances in machine learning (ML). ML is a

powerful and flexible tool that has wide medical imaging applications beyond the assessment of tumour heterogeneity and biology. Use of AI for automated tumour detection, segmentation, biological assessment, automated interpretation of findings and clinical decision support through an integrated pathway is not far away from clinical reality (119).

References

1.   Mountain CF. Revisions in the International System for Staging Lung Cancer. Chest 1997 Jun 1;111(6):1710–7

2.   Buccheri G, Ferrigno D. Lung cancer : clinical presentation and specialist referral time. 2004;898–904.

3.   American Cancer Society. Cancer Facts & Figures 2008. Cancer. 2008;

4.   Purandare N, Rangarajan V. Imaging of lung cancer: Implications on staging and management. Indian J Radiol Imaging. 2015;25(2):109.

5.   Goldstraw P, Chansky K, Crowley J, Rami-Porta R, Asamura H, Eberhardt WEE, et al. The IASLC lung cancer staging project: Proposals for revision of the TNM stage groupings in the forthcoming (eighth) edition of the TNM Classification for lung cancer. J Thorac Oncol. 2016;11(1):39–51.

6.   Quint LE, Francis IR. Radiologic staging of lung cancer. J Thorac Imaging 1999 Oct;14(4):235—246.

7.   Dales RE, Stark RM, Raman S. Computed tomography to stage lung cancer. Approaching a controversy using meta-analysis. Am Rev Respir Dis. 1990 May;141(5 Pt 1):1096–101.

8.   Dwamena BA, Sonnad SS, Angobaldo JO, Wahl RL. Metastases from non-small cell lung cancer- mediastinal staging in the 1990s-meta-analytic comparison of PET and CT. Radiology 1999: 213:530-36.

9.   Padovani B, Mouroux J, Seksik L, Chanalet S, Sedat J, Rotomondo C, et al. Chest wall invasion by bronchogenic carcinoma: evaluation with MR imaging. Radiology. 2014;187(1):33–8.

10.   Suzuki K, Yamamoto M, Hasegawa Y, Ando M, Shima K, Sako C, et al. Magnetic resonance imaging and computed tomography in the diagnoses of brain metastases of lung cancer. Lung Cancer. 2004;46(3):357–60.

11.   Price B. Analysis of Current Trends in United States Mesothelioma Incidence. 2000;145(3):211–8.

12.   Aisner J. Current Approach to Malignant Mesothelioma of the Pleura. Chest 1995;107(6):332S-344S.

13.   Rusch V. A Proposed New International TNM Staging System for Malignant Pleural Mesothelioma Chest. 108(4):1122–8.

14.   Berzenji L, Schil PE Van, Carp L. The eighth TNM classification for malignant pleural mesothelioma. Transl Lung Cancer Res. 2018 Oct; 7(5): 543–549.

15.   Wang ZJ, Reddy GP, Gotway M, Higgins CB, Jablons DM, Ramaswamy M, Hawkins RA, Webb R. Malignant Pleural Mesothelioma: Evaluation with CT, MR Imaging, and PET. 2004;105–19.

16.   Heelan RT, Rusch VW, Begg CB, Panicek M, Caravelli JF, Eisen C. Staging of malignant pleural mesothelioma: comparison of CT and MR imaging. 1999;(April):1039–47.

17.   Delage B, Fennell DA, Nicholson L, McNeish I, Lemoine NR, Crook T, et al. Arginine deprivation and argininosuccinate synthetase expression in the treatment of cancer. Int J Cancer. 2010;126(12):2762–72.

18.   Tytell AA, Neuman RE. Growth response of stable and primary cell cultures to L-ornithine, L-citrulline, and L-arginine. Exp Cell Res. 1960 Jun;20:84–91.

19.   Sugimura K, Ohno T, Kusuyama T, Azuma I. High sensitivity of human melanoma cell lines to the growth inhibitory activity of mycoplasmal arginine deiminase in vitro. Melanoma Res. 1992 Sep;2(3):191–6.

20.   Ensor CM, Holtsberg FW, Bomalaski JS, Clark MA. Pegylated Arginine Deiminase (ADI-Pegylated arginine deiminase (ADI-SS PEG20,000 mw) inhibits human melanomas and hepatocellular carcinomas in vitro and in vivo. Cancer Res. 2002 Oct 1;62(19):5443-50SS

21.   Dillon BJ, Prieto VG, Curley SA, Ensor CM, Holtsberg FW, Bomalaski JS, et al. Incidence and Distribution of Argininosuccinate Synthetase Deficiency in Human Cancers: A Method for Identifying Cancers Sensitive to Arginine Deprivation. Cancer. 2004;100(4):826–33.

22.   Szlosarek PW, Klabatsa A, Pallaska A, Sheaff M, Smith P, Crook T, et al. In vivo loss of expression of argininosuccinate synthetase in malignant pleural mesothelioma is a biomarker for susceptibility to arginine depletion. Clin Cancer Res. 2006;12(23):7126–31.

23.   Nicholson LJ, Smith PR, Hiller L, Szlosarek PW, Kimberley C, Sehouli J, et al. Epigenetic silencing of argininosuccinate synthetase confers resistance to platinum-induced cell death but collateral sensitivity to arginine auxotrophy in ovarian cancer. Int J Cancer. 2009;125(6):1454–63.

24.   Delage B, Luong P, Maharaj L, O'Riain C, Syed N, Crook T, et al. Promoter methylation of argininosuccinate synthetase-1 sensitises lymphomas to arginine deiminase treatment, autophagy and caspase-dependent apoptosis. Cell Death Dis. 2012;3(7):1–9.

25.   Bowles TL, Kim R, Galante J, Parsons CM, Virudachalam S, Kung HJ, et al. Pancreatic cancer cell lines deficient in argininosuccinate synthetase are sensitive to arginine deprivation by arginine deiminase. Int J Cancer. 2008;123(8):1950–5.

26.   Khadeir R, Szyszko T, Szlosarek PW. Optimizing arginine deprivation for hard-to-treat cancers. Oncotarget. 2017;8(57):96468–9.

27.   Syed N, Langer J, Janczar K, Singh P, Lo Nigro C, Lattanzio L, et al. Epigenetic status of argininosuccinate synthetase and argininosuccinate lyase modulates autophagy and cell death in glioblastoma. Cell Death Dis. 2013;4(1):1–11.

28.   Kobayashi E, Masuda M, Nakayama R, Ichikawa H, Satow R, Shitashige M, et al. Reduced Argininosuccinate Synthetase Is a Predictive Biomarker for the Development of Pulmonary Metastasis in Patients with Osteosarcoma. Mol Cancer Ther. 2010;9(3):535–44.

29.   Huang H-L, Hsu H-P, Shieh S-C, Chang Y-S, Chen W-C, Cho C-Y, et al. Attenuation of Argininosuccinate Lyase Inhibits Cancer Growth via Cyclin A2 and Nitric Oxide. Mol Cancer Ther. 2013;12(11):2505–16.

30.   Allen MD, Luong P, Hudson C, Leyton J, Delage B, Ghazaly E, et al. Prognostic and Therapeutic Impact of Argininosuccinate Synthetase 1 Control in Bladder Cancer as Monitored Longitudinally by PET Imaging. 2014;74(3):896–908.

31.   Brin E, Wu K, Lu H-T, He Y, Dai Z, He W. PEGylated arginine deiminase can modulate tumor immune microenvironment by affecting immune checkpoint expression, decreasing regulatory T cell accumulation and inducing tumor T cell infiltration. Oncotarget. 2017;8(35):58948–63.

32.   Kraemer PM. Interaction of mycoplasma (PPLO) and murine lymphoma cell cultures: prevention of cell lysis by arginine. Proc Soc Exp Biol Med. 1964 Jan;115:206–12.

33.   KraemerPM. Mycoplasma (PPLO) from covertly contaminated tissue cultures: differences in arginine degradation between strains. Proc Soc Exp Biol Med. 1964 Dec;117:910–8.

34.   Schimke RT, Berlin CM, Sweeney EW, Carroll WR. The generation of energy by the arginine dihydrolase pathway in Mycoplasma hominis 07. J Biol Chem. 1966;241(10):2228–36.

35.   Takaku H, Takase M, Abe S, Hayashi H, Miyazaki K. In vivo anti-tumor activity of arginine deiminase purified from Mycoplasma arginini. Int J Cancer. 1992 May8;51(2):244-9.

36.   Holtsberg FW, Ensor CM, Steiner MR, Bomalaski JS, Clark MA. Poly(ethylene glycol) (PEG) conjugated arginine deiminase: Effects of PEG formulations on its pharmacological properties. J Control Release. 2002;80(1–3):259–71.

37.   Ascierto PA, Scala S, Castello G, Daponte A, Simeone E, Ottaiano A, et al Pegylated arginine deiminase treatment of patients with metastatic melanoma: results from phase I and II studies. J Clin Oncol. 2005 Oct 20;23(30):7660-8

38.   Glazer ES, Piccirillo M, Albino V, Di Giacomo R, Palaia R, Mastro AA, et al. Phase II Study of Pegylated Arginine Deiminase for Nonresectable and Metastatic Hepatocellular Carcinoma. J Clin Oncol. 2010;28(13):2220–6.

39.   Abou-Alfa GK, Qin S, Ryoo BY, Lu SN, Yen CJ, Feng YH, et al. Phase III randomized study of second line ADI-PEG 20 plus best supportive care versus placebo plus best supportive care in patients with advanced hepatocellular carcinoma. Ann Oncol. 2018;29(6):1402–8.

40.   Szlosarek PW, Steele JP, Nolan L, Gilligan D, Taylor P, Spicer J, et al. Arginine Deprivation With Pegylated Arginine Deiminase in Patients With Argininosuccinate Synthetase 1–Deficient Malignant Pleural Mesothelioma A Randomized Clinical Trial. JAMA Oncol. 2017;

41.   Lowery MA, Yu KH, Kelsen DP, Harding JJ, Bomalaski JS, Glassman DC, et al. A phase 1/1B trial of ADI-PEG 20 plus nab-paclitaxel and gemcitabine in patients with advanced pancreatic adenocarcinoma. Cancer. 2017;123(23):4556–65.

42.   Beddowes E, Spicer J, Chan PY, Khadeir R, Garcia Corbacho J, Repana D, et al. Phase 1 dose-escalation study of pegylated arginine deiminase, cisplatin, and pemetrexed in patients with argininosuccinate synthetase 1–deficient thoracic cancers. J Clin Oncol.

43.   AL-Jahdali H, Khan AN, Loutfi S, Al-Harbi AS. Guidelines for the role of FDG-PET/CT in lung cancer management. J Infect Public Health 2012;5(5 SUPPL.1):S35–40.

44.   Kapoor V, McCook BM, Torok FS. An Introduction to PET-CT Imaging. RadioGraphics. 2004;24(2):523–43.

45.   Conti M, Pet TOF. State of the art and challenges of time-of-flight PET. Phys Medica 2009;25(1):1–11.

46.   Kinahan PE, Townsend DW, Beyer T, Sashin D. Attenuation correction for a combined 3D PET / CT scanner. 1998;(October 1997):2046–53.

47.   Matthews J, Bailey D, Price P, Meikle SR, Matthews JC, Cunningham VJ, et al. Physics in Medicine & Biology Related content Parametric image reconstruction using spectral analysis of PET projection data Parametric image reconstruction using spectral analysis of PET projection data. 1998;

48.   Ambrosini V, Nicolini S, Caroli P, Nanni C, Massaro A, Marzola MC, et al. PET/CT imaging in different types of lung cancer: An overview. Eur J Radiol [Internet]. 2012;81(5):988–1001.

49.   Cronin P, Dwamena BA, Kelly AM, Carlos RC. Solitary Pulmonary Nodules: Meta-analytic Comparison of Cross-sectional Imaging Modalities for Diagnosis of Malignancy. Radiology. 2008;246(3):772–82.

50.   Matthies A, Hickeson M, Cuchiara A, Alavi A. Dual time point 18F-FDG PET for the evaluation of pulmonary nodules. J Nucl Med . 2002;43(7):871–5.

51.   Herder GJ, Golding RP, Hoekstra OS, Comans EF, Teule GJ, Postmus PE, et al. The performance of 18F-fluorodeoxyglucose positron emission tomography in small solitary pulmonary nodules. Eur J Nucl Med Mol Imaging. 2004;31(9):1231–6.

52.   Gould MK, C MC, Kuschner WG, Rydzak CE, Owens DK. Accuracy of Positron Emission Tomography for Diagnosis of Pulmonary Nodules. JAMA. 2001;285(7).

53.   Bryant AS, Cerfolio RJ. The Maximum Standardized Uptake Values on Integrated FDG-PET/CT Is Useful in Differentiating Benign From Malignant Pulmonary Nodules. Ann Thorac Surg. 2006;82(3):1016–20.

54.   Lardinois D, Weder W, Hany TF, Kamel EM, Korom S, Seifert B et al Staging of Non–Small-Cell Lung Cancer with Integrated Positron-Emission Tomography and Computed Tomography. J Bronchol. 2003;10(3):238–9.

55.   Wu Y, Li P, Zhang H, Shi Y, Wu H, Zhang J, et al. Diagnostic value of fluorine 18 fluorodeoxyglucose positron emission tomography/computed tomography for the detection of metastases in non-small-cell lung cancer patients. Int J Cancer. 2013;132(2).

56.   Silvestri GA, Gonzalez A V., Jantz MA, Margolis ML, Gould MK, Tanoue LT, et al. Methods for staging non-small cell lung cancer: Diagnosis and management of lung cancer, 3rd ed: American college of chest physicians evidence-based clinical practice guidelines. Chest 2013;143(5 SUPPL):e211S-e250S.

57.   Sun Y, Yu H, Ma J, Lu P. The role of 18F-FDG PET/CT integrated imaging in distinguishing malignant from benign pleural effusion. PLoS One. 2016;11(8):1–12.

58.   Qu X, Huang X, Yan W, Wu L, Dai K. A meta-analysis of 18FDG-PET-CT, 18FDG-PET, MRI and bone scintigraphy for diagnosis of bone metastases in patients with lung cancer. Eur J Radiol. 2012;81(5):1007–15.

59.   Fischer B, Lassen U, Mortensen J, Larsen S, Loft A, Bertelsen A, et al. Preoperative staging of lung cancer with combined PET-CT. N Engl J Med. 2009 Jul 2;361(1):32-9

60.   Hicks RJ, Kalff V, MacManus MP, Ware RE, Hogg A, McKenzie AF, et al. F-18-FDG PET provides high-impact and powerful prognostic stratification in staging newly diagnosed non-small cell lung cancer. J Nucl Med. 2001;42(11):1596–604.

61.   Sachs S, Bilfinger T V. The impact of positron emission tomography on clinical decision making in a university-based multidisciplinary lung cancer practice. Chest. 2005;128(2):698–703.

62.   Higashi K, Ueda Y, Seki H, Yuasa K, Oguchi M, Noguchi T, et al. Fluorine-18-FDG PET imaging is negative in bronchioloalveolar lung carcinoma. J Nucl Med 1998;39(6):1016–20.

63.   Wachsmann JW, Gerbaudo VH. Thorax: Normal and Benign Pathologic Patterns in FDG-PET/CT Imaging. PET Clin. 2014 Apr 1;9(2):147–68.

64.   Benard F, Sterman D, Smith R. Metabolic Imaging of Malignant Pleural Mesothelioma With Fluorodeoxyglucose Positron Emission Tomography 1998;713–22.

65.   Schneider DB, Clary-Macy C, Challa S, Sasse KC, Merrick SH, Hawkins R, et al. Positron emission tomography with f18-fluorodeoxyglucose in the staging and preoperative evaluation of malignant pleural mesothelioma. J Thorac Cardiovasc Surg. 2000 Jul;120(1):128-33..

66.   Benard F, Sterman D, Smith RJ, Kaiser LR, Albelda SM, Alavi A. Prognostic value of FDG PET imaging in malignant pleural mesothelioma. J Nucl Med. 1999 Aug;40(8):1241-5.

67.   Elliott HS, Metser U, de Perrot M, Cho J, Bradbury P, Veit-Haibach P, et al. [18] F-FDG PET/CT in the management of patients with malignant pleural mesothelioma being considered for multimodality therapy: experience of a tertiary referral center. Br J Radiol. 2018;(October 2017):20170814.

68.   Murphy DJ, Gill RR. Volumetric assessment in malignant pleural mesothelioma. Ann Transl Med. 2017;5(11):241–241.

69.   Greco C, Rosenzweig K, Cascini GL, Tamburrini O. Current status of PET/CT for tumour volume definition in radiotherapy treatment planning for non-small cell lung cancer (NSCLC). Lung Cancer. 2007;57(2):125–34.

70.   Eisenhauer EA, Therasse P, Bogaerts J, Schwartz LH, Sargent D, Ford R, et al. New response evaluation criteria in solid tumours : Revised RECIST guideline (version 1 . 1). Eur J Cancer 2008;45(2):228–47

71.   Young H, Baum R, Cremerius U, Herholz K, Hoekstra O, Lammertsma AA, et al. Measurement of clinical and subclinical tumour response using [18F]- fluorodeoxyglucose and positron emission tomography: Review and 1999 EORTC recommendations. Eur J Cancer. 1999;35(13):1773–82.

72. Wahl RL, Jacene H, Kasamon Y, Lodge MA. From RECIST to PERCIST: Evolving Considerations for PET Response Criteria in Solid Tumors. J Nucl Med. 2009;50(Suppl_1):122S-150S.

73. Min SJ, Jang HJ, Kim JH. Comparison of the RECIST and PERCIST criteria in solid tumors: a pooled analysis and review. Oncotarget. 2016;7(19).

74. Decoster L, Schallier D, Everaert H, Nieboer K, Meysman M, Neyns B, et al. Complete metabolic tumour response, assessed by 18-fluorodeoxyglucose positron emission tomography (18FDG-PET), after induction chemotherapy predicts a favourable outcome in patients with locally advanced non-small cell lung cancer (NSCLC). Lung Cancer. 2008;62(1):55–61.

75. Pöttgen C, Levegrün S, Theegarten D, Marnitz S, Grehl S, Pink R, et al. Value of 18F-fluoro-2-deoxy-D-glucose-positron emission tomography/computed tomography in non-small-cell lung cancer for prediction of pathologic response and times to relapse after neoadjuvant chemoradiotherapy. Clin Cancer Res. 2006;12(1):97–106.

76. Weber WA, Petersen V, Schmidt B, Tyndale-Hines L, Link T, Peschel C, et al. Positron emission tomography in non-small-cell lung cancer: Prediction of response to chemotherapy by quantitative assessment of glucose use. J Clin Oncol. 2003;21(14):2651–7.

77. De Geus-Oei LF, Van Der Heijden HFM, Corstens FHM, Oyen WJG. Predictive and prognostic value of FDG-PET in nonsmall-cell lung cancer. A systematic review. Cancer. 2007;110(8):1654–64.

78. Huang W, Zhou T, Ma L, Sun H, Gong H, Wang J, et al. Standard uptake value and metabolic tumor volume of 18F-FDG PET/CT predict short-term outcome early in the course of chemoradiotherapy in advanced non-small cell lung cancer. Eur J Nucl Med Mol Imaging. 2011 Sep;38(9):1628–35.

79. Kanemura S, Kuribayashi K, Funaguchi N, Shibata E, Mikami K, Doi H, et al. Metabolic response assessment with 18F-FDG-PET/CT is superior to modified RECIST for the evaluation of response to platinum-based doublet chemotherapy in malignant pleural mesothelioma. Eur J Radiol 2017;86:92–8.

80. Ceresoli GL, Zucali PA, Favaretto AG, Grossi F, Bidoli P, Del Conte G, et al. Phase II study of pemetrexed plus carboplatin in malignant pleural mesothelioma. J Clin Oncol. 2006;24(9):1443–8.

81.   Veit-Haibach P, Schaefer NG, Steinert HC, Soyka JD, Seifert B, Stahel RA. Combined FDG-PET/CT in response evaluation of malignant pleural mesothelioma. Lung Cancer 2010;67(3):311–7.

82.   Crandall JP, Tahari AK, Juergens RA, Brahmer JR, Rudin CM, Esposito G, et al. A comparison of FLT to FDG PET/CT in the early assessment of chemotherapy response in stages IB–IIIA resectable NSCLC. EJNMMI Res 2017;7(1):1–10.

83.   Barwick T, Bencherif B, Mountz JM, Avril N. Molecular PET and PET / CT imaging of tumour cell proliferation using F-18 fluoro- L -thymidine : a comprehensive evaluation Nucl Med Commun. 2009 Dec;30(12):908-17 1998;

84.   Sherley JL, Kelly TJ. Regulation of human thymidine kinase during the cell cycle. J Biol Chem. 1988;263(17):8350–8.

85.   Buck AK, Schirrmeister H, Hetzel M, Von Der Heide M, Halter G, Glatting G, et al. 3-Deoxy-3-[18F]fluorothymidine-positron emission tomography for noninvasive assessment of proliferation in pulmonary nodules. Cancer Res. 2002;62(12):3331–4.

86.   Buck AK, Hetzel M, Schirrmeister H, Halter G, Moller P, Kratochwil C, et al. Clinical relevance of imaging proliferative activity in lung nodules. Eur J Nucl Med Mol Imaging. 2005 May;32(5):525–33.

87.   Szyszko TA, Yip C, Szlosarek P, Goh V, Cook GJR. The role of new PET tracers for lung cancer. Lung Cancer 2016;94:7–14.

88.   Buck AK, Halter G, Schirrmeister H, Kotzerke J, Wurziger I, Glatting G, et al. Imaging proliferation in lung tumors with PET: 18F-FLT versus 18F-FDG. J Nucl Med 2003;44(9):1426–31.

89.   Yang W, Zhang Y, Fu Z, Yu J, Sun X, Mu D, et al. Imaging of proliferation with 18F-FLT PET/CT versus 18F-FDG PET/CT in non-small-cell lung cancer. Eur J Nucl Med Mol Imaging. 2010 Jul;37(7):1291–9.

90.   Tian J, Yang X, Yu L, Chen P, Xin J, Ma L, et al. A Multicenter Clinical Trial on the Diagnostic Value of Dual-Tracer PET/CT in Pulmonary Lesions Using 3'-Deoxy-3'-18F-Fluorothymidine and 18F-FDG. J Nucl Med 2008;49(2):186–94.

91.   Sohn HJ, Yang YJ, Ryu JS, Seung JO, Ki CI, Dae HM, et al. [18 F]fluorothymidine positron emission tomography before and 7 days after gefitinib treatment predicts response in patients with advanced adenocarcinoma of the lung. Clin Cancer Res. 2008;14(22):7423–9.

92.   Trigonis I, Koh PK, Taylor B, Tamal M, Ryder D, Earl M, et al. Early reduction in tumour [18F]fluorothymidine (FLT) uptake in patients with non-small cell lung cancer (NSCLC) treated with radiotherapy alone. Eur J Nucl Med Mol Imaging. 2014;41(4):682–93.

93.   Stelter L, Evans MJ, Jungbluth AA, Zanzonico P, Ritter G, Ku T, et al. Novel Mechanistic Insights into Arginine Deiminase Pharmacology Suggest 18F-FDG Is Not Suitable to Evaluate Clinical Response in Melanoma. J Nucl Med. 2012;53(2):281–6.

94.   Stelter L, Fuchs S, Jungbluth AA, Ritter G, Longo VA, Zanzonico P, et al Evaluation of arginine deiminase treatment in melanoma xenografts using (18)F-FLT PET. Mol Imaging Biol. 2013 Dec;15(6):768-75..

95.   Scrivener M, de Jong EEC, van Timmeren JE, Pieters T, Ghaye B, Geets X. Radiomics applied to lung cancer: a review. Transl Cancer Res. 2016;5(4):398–409.

96.   Al-Kadi OS, Watson D. Texture analysis of aggressive and nonaggressive lung tumor CE CT images. IEEE Trans Biomed Eng. 2008;55(7):1822–30.

97.   Chicklore S, Goh V, Siddique M, Roy A, Marsden PK, Cook GJR, et al. Quantifying tumour heterogeneity in imaging by texture analysis. Eur J Nucl Med Mol Imaging 2013;133–40.

98.   Cook GJR, Siddique M, Taylor BP, Yip C, Chicklore S, Goh V. Radiomics in PET: Principles and applications. Clin Transl Imaging. 2014;2(3):269–76.

99.   Gatenby RA, Grove O, Gillies RJ. Quantitative Imaging in Cancer Evolution and Ecology. Radiology. 2013;269(1):8–14.

100.   Cook GJR, Yip C, Siddique M, Goh V, Chicklore S, Roy A, et al. Are Pretreatment 18F-FDG PET Tumor Textural Features in Non-Small Cell Lung Cancer Associated with Response and Survival After Chemoradiotherapy? J Nucl Med. 2013;54(1):19–26.

101.   Vaidya M, Creach KM, Frye J, Dehdashti F, Bradley JD, El Naqa I. Combined PET/CT image characteristics for radiotherapy tumor response in lung cancer. Radiother Oncol 2012 Feb 1;102(2):239–45

102.   Cook GJR, O'Brien ME, Siddique M, Chicklore S, Loi HY, Sharma B, et al. Non–Small Cell Lung Cancer Treated with Erlotinib: Heterogeneity of 18 F-FDG Uptake at PET-Association with Treatment Response and Prognosis . Radiology. 2015;276(3):883–93.

103.   Bashir U, Foot O, Wise O, Siddique MM, Mclean E, Bille A, et al. Investigating the histopathologic correlates of 18F-FDG PET heterogeneity in non-small-cell lung cancer. Nucl Med Commun. 2018 Dec;39(12):1197–206.

104.	Bianconi F, Palumbo I, Fravolini ML, Chiari R, Minestrini M, Brunese L, et al. Texture Analysis on [18 F]FDG PET/CT in Non-Small-Cell Lung Cancer: Correlations Between PET Features, CT Features, and Histological Types. Mol Imaging Biol. 2019;

105.	Klabatsa A, Chicklore S, Barrington SF, Goh V, Lang-lazdunski L, Cook GJR. The association of 18 F-FDG PET / CT parameters with survival in malignant pleural mesothelioma. 2014;276–82.

106.	Byrne MJ, Nowak AK. Original article Modified RECIST criteria for assessment of response in malignant pleural mesothelioma. Ann Oncol . 2004;15(2):257–60.

107.	Gambhir SS. Molecular imaging of cancer with positron emission tomography. Nat Rev Cancer. 2002 Sep;2(9):683–93.

108.	Scheffler M, Kobe C, Zander T, Nogova L, Kahraman D, Thomas R, et al. Monitoring reversible and irreversible EGFR inhibition with erlotinib and afatinib in a patient with EGFR-mutated non-small cell lung cancer (NSCLC) using sequential [18F]fluorothymidine (FLT-)PET. Lung Cancer 2012;77(3):617–20.

109.	Bhoil A, Singh B, Singh N, Kashyap R, Watts A, Sarika S, et al. Can 3'-deoxy-3'-(18)F-fluorothymidine or 2'-deoxy-2'-(18)F-fluoro-d-glucose PET/CT better assess response after 3-weeks treatment by epidermal growth factor receptor kinase inhibitor, in non-small lung cancer patients? Preliminary results. Hell J Nucl Med. 2014;17(2):90–6.

110.	Everitt SJ, Ball DL, Hicks RJ, Callahan J, Plumridge N, Collins M, et al. Imaging Before and During Definitive Chemoradiation for. :1069–75.

111.	Frings V, Veldt AAM Van Der, Boellaard R, Herder GJM, Giovannetti E, Honeywell R, et al. Pemetrexed Induced Thymidylate Synthase Inhibition in Non-Small Cell Lung Cancer Patients : A Pilot Study with 3 9 -Deoxy-3 9 - [18 F] fluorothymidine Positron Emission Tomography. 2013;8(5).

112.	Kairemo K, Álvarez De Arriba C, Santos EB, Macapinlac HA, Subbiah V. Early Response Assessment to Targeted Therapy PET / CT in Lung Cancer. 2020;(18):1–7.

113.	Kenny L, Coombes RC, Aboagye EO. Imaging early changes in proliferation at 1 week post chemotherapy : a pilot study in breast cancer patients with 3 ' -deoxy-3 ' - [18 F] fluorothymidine positron emission tomography. 2007;1339–47.

114.	Hatt M, Majdoub M, Valli M, Tixier F, Cheze C, Rest L, et al. PET Uptake Characterization Through Texture Analysis : Investigating the Complementary Nature of Heterogeneity and Functional Tumor Volume in a Multi – Cancer Site Patient Cohort. 2015;56(1):38–45.

115.   Takeda K, Takanami K, Shirata Y, Yamamoto T, Takahashi N, Ito K, et al. Clinical utility of texture analysis of 18F-FDG PET / CT in patients with Stage I lung cancer treated with stereotactic body radiotherapy. 2017;58(6):862–9.

116.   Lovinfosse P, Janvary ZL, Coucke P, Jodogne S, Bernard C, Hatt M, et al. FDG PET / CT texture analysis for predicting the outcome of lung cancer treated by stereotactic body radiation therapy. 2016;1453–60.

117.   Brooks FJ, Grigsby PW. The Effect of Small Tumor Volumes on Studies of Intratumoral Heterogeneity of Tracer Uptake. :37–43

118.   Szlosarek PW, Baas P, Ceresoli GL, Fennell DA, Gilligan D, Johnston A, et al ATOMIC-Meso: A randomized phase 2/3 trial of ADI-PEG20 or placebo with pemetrexed and cisplatin in patients with argininosuccinate synthetase 1-deficient non-epithelioid mesothelioma. Journal of Clinical Oncology 2017 35:15_suppl, TPS8582-TPS8582

119.   Cook GJR, Goh V. What can artificial intelligence teach us about the molecular mechanisms underlying disease? Eur J Nucl Med Mol Imaging. 2019 Dec;46(13):2715-2721.

Appendix A

Scanner stability and background checks in TRAP substudy

QC data using SUV mean phantom measurement for March 2015-mid July 2016 (Figure34) demonstrated good PET-CT camera stability. SUVmean used rather than SUVmax thought to be more consistent for large area phantom measurements. The SUVmean was 1.006 (±0.004). The majority of FLT PET/CT scans were undertaken in this time period.

Figure 34. Camera stability
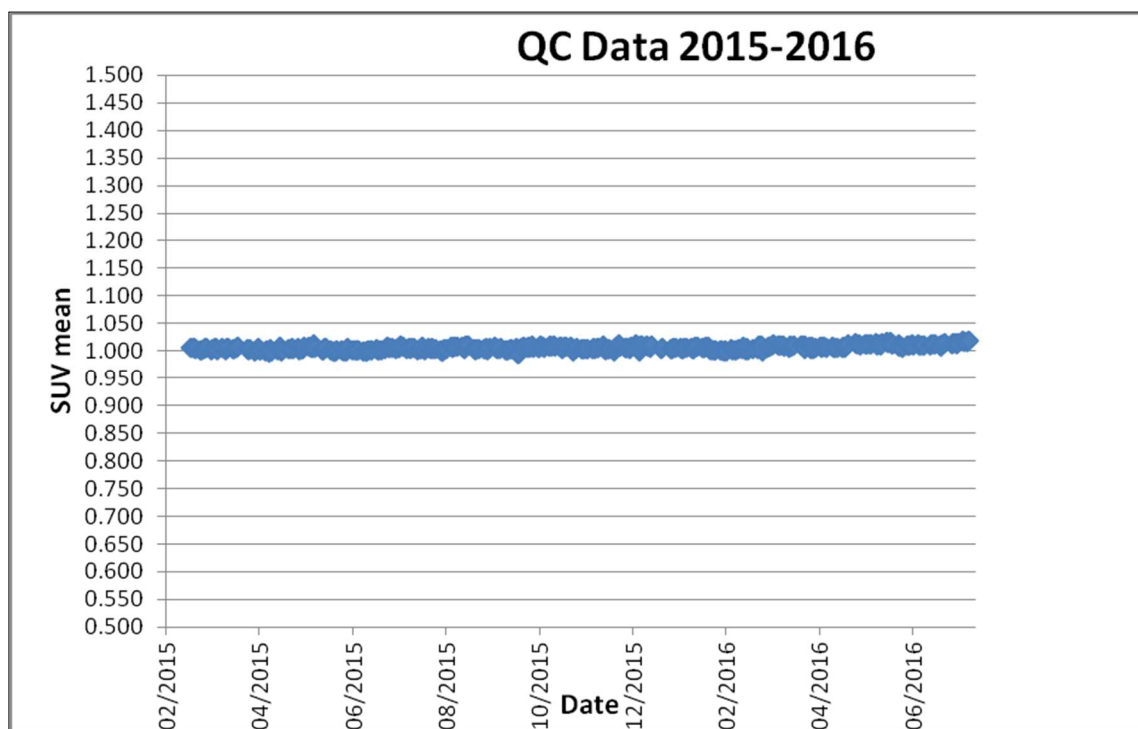
Background FLT variation on PET/CT

Measurements of background FLT uptake (using SUVmax) in bone marrow (BM) in the L1 vertebral body (Figure 35) and other background regions including liver (Figure 36); mediastinal blood pool (MBP) (Figure 37); and muscle (Figure 38). These provide a measure of biological variability (which may or may not be affected by the therapy) and were obtained for all the cases of MPM and the first four cases of NSCLCs.

We also calculated ratios of BM/MBP, and BM/liver, but this did not provide any additional useful data.

The results confirm that there is only small biological variability.

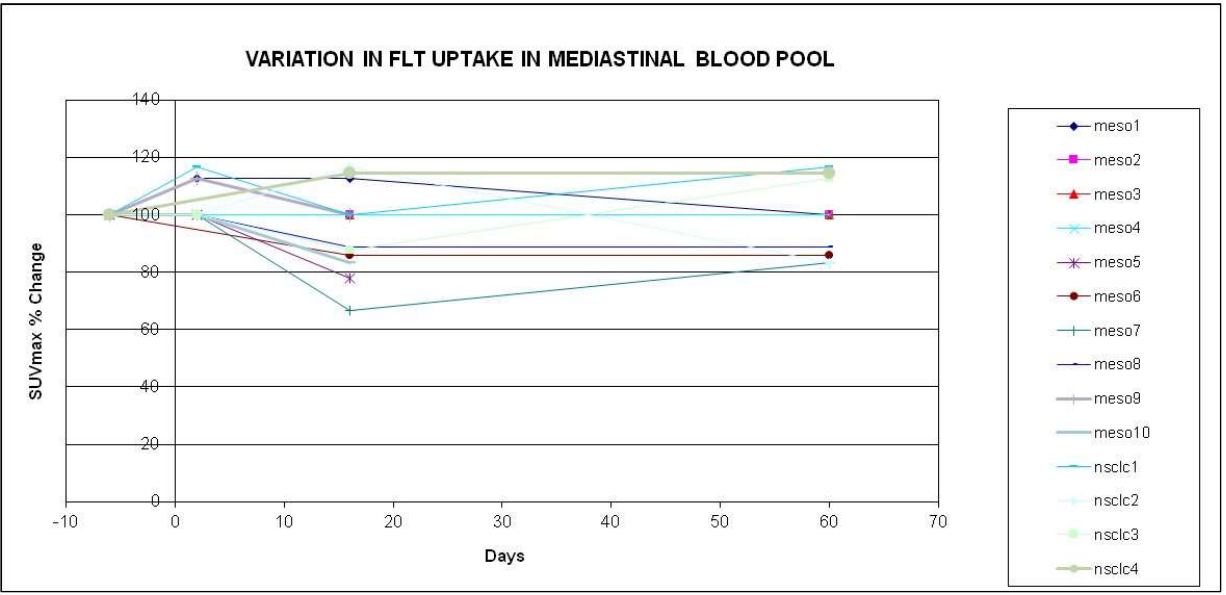## Figure 35. Proliferation imaging in bone marrow
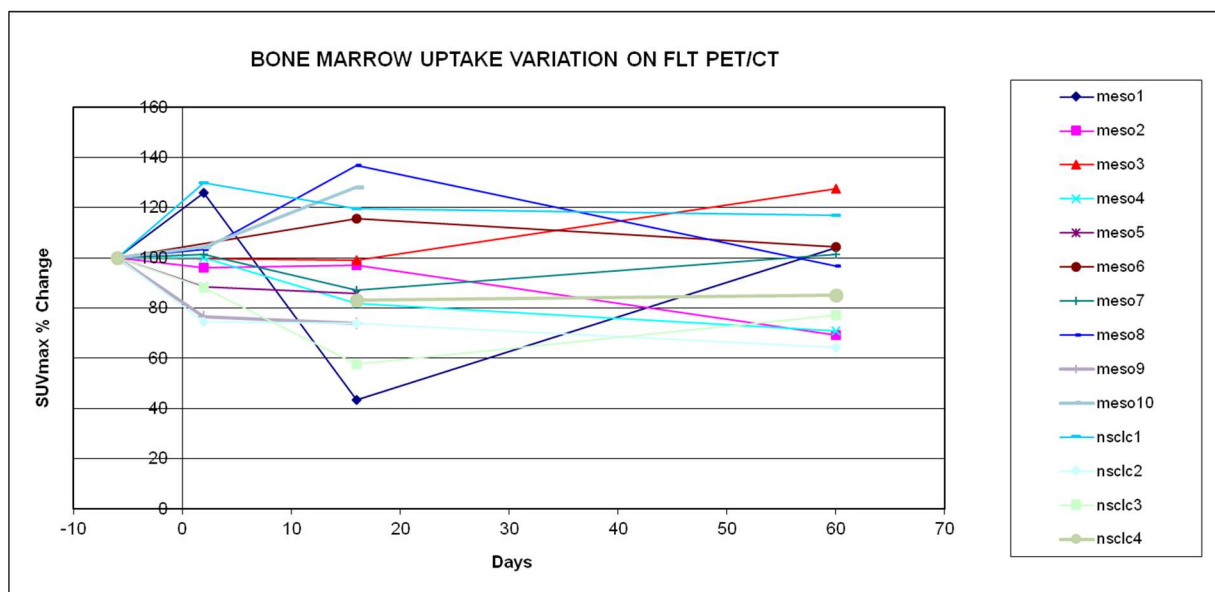
Bone marrow (BM) uptake demonstrated considerable variation, although the majority of values lay between 75% and 125 % of baseline. There is intense FLT accumulation in BM, this variation could relate to noise or biological variation, but ADI may also have an effect.

Figure 36. Proliferation imaging in liver
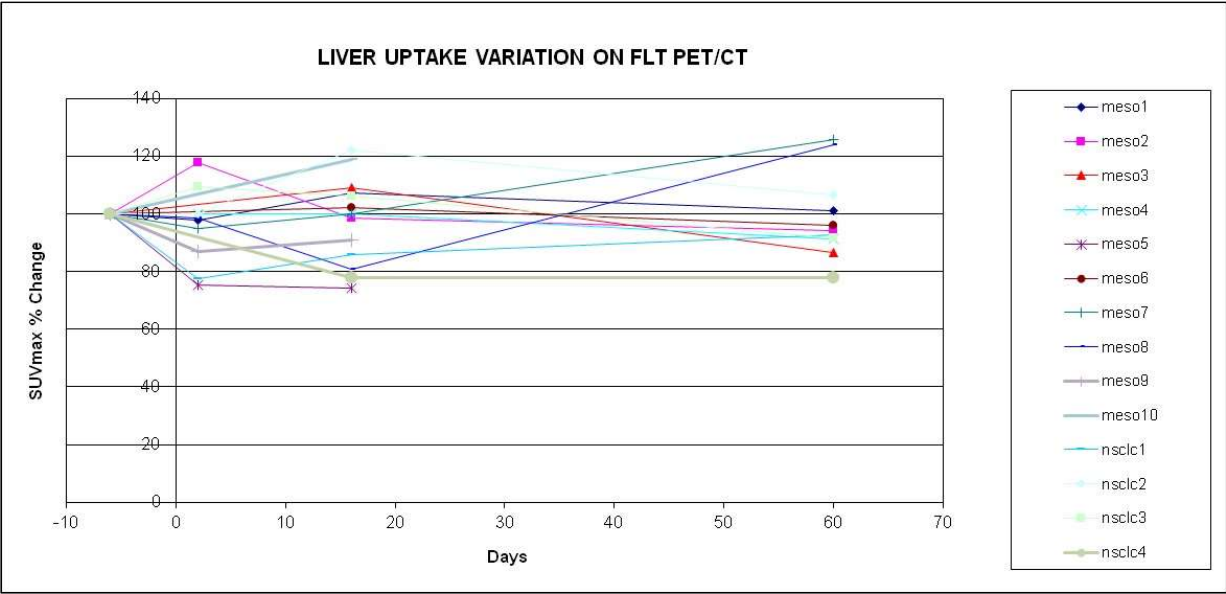
Liver uptake also demonstrated variation, although less than BM and the majority of values lay between 80% and 120%. As there is usually intense hepatic uptake with FLT, this variation could relate to measurement error, noise, biological variation, or a combination.

Figure 37. Proliferation imaging in MBP

MBP uptake was generally low grade (SUVmax <1) and again demonstrated variation, with values lying between 80% and 120%. This is almost certainly related to noise (statistical variation).

Figure 38. Proliferation imaging in muscle

VARIATION IN FLT UPTAKE IN MUSCLE
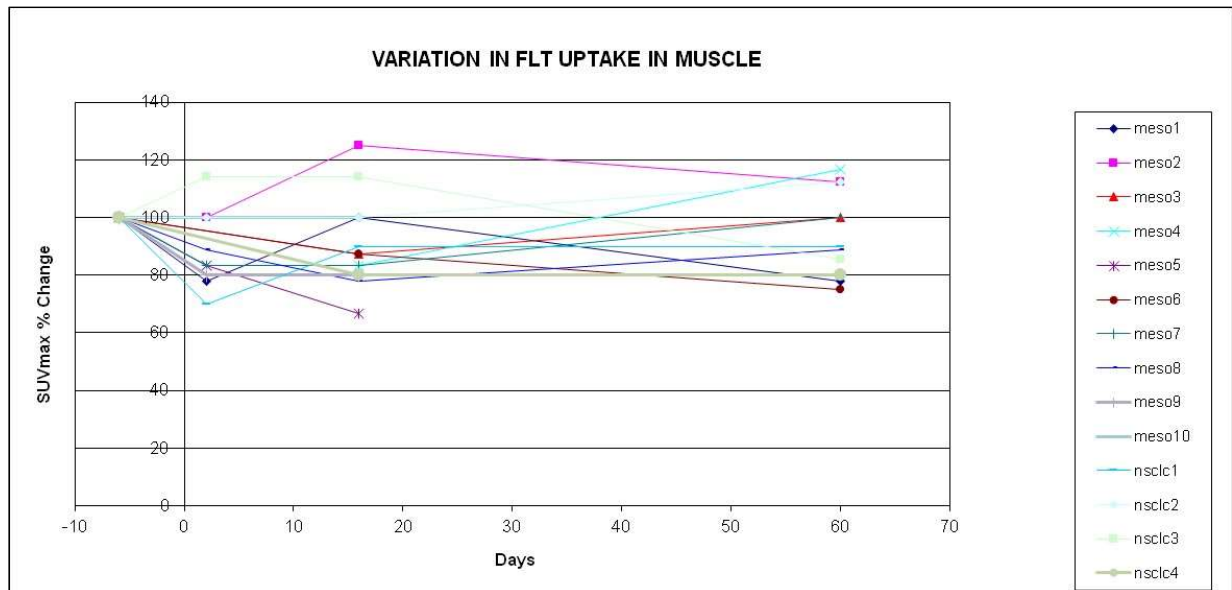
Muscle uptake was also generally low grade (SUVmax <1) with values lying between 80% and 120%. Again, this is likely related to background noise (statistical variation).

Appendix B

Radiation exposure in the TRAP substudy

The effective Dose (ED) of radiation per FLT PET scan was approximately 8.5 mSv per FLT PET (as calculated by L.P, senior clinical scientist). Patients who received a total of 4 FLT PETs had a cumulative exposure from this dose of approximately 34 mSv. The low dose CT of the neck, chest and abdomen used for attenuation correction and anatomical correlation results in additional radiation exposure of 9 mSv per CT scan and the cumulative exposure from 4 low dose CTs was 36 mSv. Hence, the total ED for the 4 FLT PET-CT scans was 70 mSv.